Electrochemistry of stainless steel colonized by manganese-oxidizing bacteria
by Wayne Harold Dickinson

A thesis submitted in partial fulfillment of the requirements for the degree of Doctor of Philosophy in Chemistry
Montana State University

Abstract:
Microbial colonization of stainless steel (SS) surfaces can modify the electrochemical properties of the metal and increase the risk of corrosion damage. Two dominant effects of colonization -a several hundred millivolt noble shift in electrical potential and a two to three decade increase in cathodic current density- are implicated in the corrosion processes. These effects, collectively known as Ennoblement, are attributed to the metabolic activity of attached microorganisms, however the mechanism by which microbial activity modifies cathodic reactions at the metal surface remains unclear. The present dissertation investigates the role of microbially generated oxidants in Ennoblement and demonstrates that Ennoblement is caused by manganic oxide biomineralization.

Microelectrode measurements of dissolved oxidants within biofilms on SS indicated that redox potential in the bulk biofilm did not change during Ennoblement. A proposed mechanism involving oxygen electroreduction was also eliminated by showing that cathodic rates were independent of oxygen concentration. The findings directed attention to microbial production of surface-bound oxidants. Quantification of metal capacitance and surface-bound reactants suggested that metal oxides were involved in Ennoblement and led to the hypothesis that Ennoblement is caused by manganic oxide biodeposition.

Epifluorescence microscopy and bacterial culture methods confirmed the presence of manganese-oxidizing bacteria on Ennobled SS. Manganese-rich surface deposits were confirmed by wet chemical and energy-dispersive x-ray analysis. SS coated with Mn02 paste exhibited electrochemical properties that closely matched those of Ennobled SS and elevated electrical potential decayed to pre-exposure values when bisulfite ion was used to reductively dissolve the surface manganese deposits. The biological mechanism of Ennoblement was validated by inducing the effect using pure cultures of the manganese-oxidizing bacterium Leptothrix discophora. Coulometric titration and wet chemical analysis demonstrated that 15-75 nmoles cm^'2 of manganic oxide surface deposit shifts the potential of SS to a value near +350 mV versus the saturated calomel electrode.

Manganese-oxidizing bacteria have been widely reported at sites of SS corrosion. The present dissertation unifies this observation with the separate issue of Ennoblement by linking both issues to a common cause, manganic oxide biomineralization. The finding provides a plausible explanation for the corrosive effects of manganese-oxidizing bacteria on SS.

ELECTROCHEMISTRY OF STAINLESS STEEL COLONIZED BY MANGANESE-OXIDIZING BACTERIA

by

Wayne Harold Dickinson

A thesis submitted in partial fulfillment
of the requirements for the degree

of

Doctor of Philosophy

in

Chemistry

MONTANA STATE UNIVERSITY-BOZEMAN
Bozeman, Montana

November 1996

APPROVAL

of a thesis submitted by

Wayne Harold Dickinson

This thesis has been read by each member of the thesis committee and has been found to be satisfactory regarding content, English usage, format, citations, bibliographic style, and consistency, and is ready for submission to the College of Graduate Studies.

Richard D. Geer _____ 11/8/96
Date

Approved for the Department of Chemistry

David M. Dooley _____ 11/8/96
Date

Approved for the College of Graduate Studies

Robert Brown _____ 12/3/96
Date

STATEMENT OF PERMISSION TO USE

In presenting this thesis in partial fulfillment of the requirements for a doctoral degree at Montana State University-Bozeman, I agree that the Library shall make it available to borrowers under rules of the Library. I further agree that copying of this thesis is allowable only for scholarly purposes, consistent with "fair use" as prescribed in the U.S. Copyright Law. Requests for extensive copying or reproduction of this thesis should be referred to University Microfilms International, 300 North Zeeb Road, Ann Arbor, Michigan 48106, to whom I have granted "the exclusive right to reproduce and distribute my dissertation in and from microform along with the non-exclusive right to reproduce and distribute my abstract in any format in whole or in part."

Signature Wayne Harold Dickinson

Date 8 November 1996

TABLE OF CONTENTS

LIST OF TABLES

LIST OF FIGURES

NOTATION

i_{meas} = measurable current, the sum of anodic and cathodic currents for all half-reactions

i_{net} = the sum of anodic and cathodic currents for a single half-reaction

i_a = anodic current

i_c = cathodic current

i_{corr} = corrosion current

i_o = exchange current

i_{pass} = passivation current

k^o = standard rate constant for electrode reactions; (cm sec^{-1})

k^o_c = standard rate constant for cathodic electrode reaction

k^o_a = standard rate constant for anodic electrode reaction

n_a = number of electrons transferred in rate determining step

n = number of electrons transferred in net reaction

A = electrode area; (cm^2)

C = capacitance; (coul $volt^{-1}$)

C^*_{ox} = concentration of oxidized specie at the electrode surface; (moles cm^{-3})

C^*_{red} = concentration of reduced specie at the electrode surface

C^*_c = concentration of cathodic reactant at the electrode surface

C^*_a = concentration of anodic reactant at the electrode surface

DO = dissolved oxygen

E = electrode potential

$E^{o'}$ = formal half-cell potential

$E^{o'}_c$ = formal half-cell potential for cathodic reactant

$E^{o'}_a$ = formal half-cell potential for anodic reactant

E_{corr} = equilibrium electrode mixed potential

F = Faraday constant, 96485 coulombs $equivalent^{-1}$

I_{app} = externally applied current

M = molecular weight

MOB = manganese-oxidizing bacteria

MFOB = manganese- and iron-oxidizing bacteria

Q = charge; (coulombs)

R = gas constant; (8.31414 volt-coulombs $mole^{-1}$ -deg^{-1} (K))

R_p = polarization resistance; (ohm cm^2)

SS = stainless steel

SCE = saturated calomel electrode

SRB = sulfate-reducing bacteria

T = temperature; (degrees, K)

α_a = anodic transfer coefficient

α_c = cathodic transfer coefficient

β_a = anodic Tafel slope; (Volts per decade of current)

β_c = cathodic Tafel slope; (Volts per decade of current)

γ = roughness factor

ρ = density; (g cm^{-3})

ABSTRACT

Microbial colonization of stainless steel (SS) surfaces can modify the electrochemical properties of the metal and increase the risk of corrosion damage. Two dominant effects of colonization -a several hundred millivolt noble shift in electrical potential and a two to three decade increase in cathodic current density- are implicated in the corrosion processes. These effects, collectively known as Ennoblement, are attributed to the metabolic activity of attached microorganisms, however the mechanism by which microbial activity modifies cathodic reactions at the metal surface remains unclear. The present dissertation investigates the role of microbially generated oxidants in Ennoblement and demonstrates that Ennoblement is caused by manganic oxide biomineralization.

Microelectrode measurements of dissolved oxidants within biofilms on SS indicated that redox potential in the bulk biofilm did not change during Ennoblement. A proposed mechanism involving oxygen electroreduction was also eliminated by showing that cathodic rates were independent of oxygen concentration. The findings directed attention to microbial production of surface-bound oxidants. Quantification of metal capacitance and surface-bound reactants suggested that metal oxides were involved in Ennoblement and led to the hypothesis that Ennoblement is caused by manganic oxide biodeposition.

Epifluorescence microscopy and bacterial culture methods confirmed the presence of manganese-oxidizing bacteria on Ennobled SS. Manganese-rich surface deposits were confirmed by wet chemical and energy-dispersive x-ray analysis. SS coated with MnO_2 paste exhibited electrochemical properties that closely matched those of Ennobled SS and elevated electrical potential decayed to pre-exposure values when bisulfite ion was used to reductively dissolve the surface manganese deposits. The biological mechanism of Ennoblement was validated by inducing the effect using pure cultures of the manganese-oxidizing bacterium *Leptothrix discophora*. Coulometric titration and wet chemical analysis demonstrated that 15-75 nmoles cm^{-2} of manganic oxide surface deposit shifts the potential of SS to a value near +350 mV versus the saturated calomel electrode.

Manganese-oxidizing bacteria have been widely reported at sites of SS corrosion. The present dissertation unifies this observation with the separate issue of Ennoblement by linking both issues to a common cause, manganic oxide biomineralization. The finding provides a plausible explanation for the corrosive effects of manganese-oxidizing bacteria on SS.

CHAPTER 1

PROBLEM STATEMENT AND RESEARCH OVERVIEW

Microbially Influenced Corrosion

Microbial colonization of metal surfaces can accelerate the corrosion of a variety of metals and metal alloys including aluminum, copper, nickel, iron, and steel. This effect, known as microbially-influenced corrosion (MIC), is widely implicated in the failure of metals exposed to aqueous systems and is the focus of worldwide research efforts. Such studies link MIC to the metabolic activities of microorganisms that modify the electrochemical environment near the metal surface; however, the complex chemistry of corrosion in the presence of microorganisms has made identification of exact mechanisms difficult. At present, the true nature of MIC is poorly understood.

One of the most puzzling aspects of MIC is the change in electrochemical properties of stainless steel that occurs as the metal surface is colonized by microorganisms. Microbial colonization in natural waters causes the corrosion potential (E_{corr}) of stainless steel to shift several-hundred millivolts in the positive or noble direction and produces an accompanying two to three decade increase in cathodic current density. These phenomena, collectively known as Ennoblement, increase the risk of localized corrosion of the metal. Concern over accelerated

stainless steel corrosion has stimulated research on Ennoblement for more than three decades, and has led to a thorough characterization of the phenomenon; nevertheless, no progress in establishing the mechanism of Ennoblement has been made.

Stainless Steel Corrosion

Stainless steel provides the corrosion resistance, strength, and temperature stability required for use in a variety of harsh environments. Typical applications include boiler and condenser tubing, containment vessels, and fluid pumps used in the steam electric, water and wastewater, food processing, and pulp and paper industries. Resistance to corrosion is imparted by formation of a thin surface oxide layer, or passive film, that inhibits the rate of metal dissolution. Oxidation of the principal alloying elements of stainless steel -iron, chromium, and nickel- is thermodynamically favored in aqueous media, and as a consequence, the protective passive film must be cohesive and contiguous to prevent sites of localized corrosion from developing.

Passive film breakdown can occur when elevated metal potential raises the metal-solution potential difference above an empirical value known as the critical pitting potential, E_{pit}. As damage to the oxide layer develops, oxidation and hydrolysis of the underlying metal can occur, producing an acidic environment and causing migration of charge-neutralizing counter ions to the metal surface. Surface acidification and counter-anion accumulation combine to prevent the protective oxide layer from reforming and generate an autocatalytic condition in which corrosion products stabilize the site of metal dissolution.

Rapid penetration of the metal can result, leading to perforation failures and costly repair or replacement of stainless steel tubing and containment vessels. Industries affected by this type of failure include the steam-electric power utilities, pulp and paper mills, petrochemical plants, wastewater-treatment facilities and the maritime industry.

In dilute chloride media, the positive shift in potential that develops during Ennoblement can exceed E_{pit}, enhancing the frequency of pit nucleation. Elevated current density supports the high local corrosion rate required to acidify and stablilize the nucleated site. Thus the two principal characteristics of Ennoblement, elevated E_{corr} and elevated current density, work in concert to aggravate the risk of localized corrosion and perforation failure of stainless steel.

Microbial activities that enhance the oxidizing power of the environment near the metal surface can be expected to elevate both E_{corr} and cathodic current density. Oxidizing power may increase due to microbial production of oxidizing chemicals, including both dissolved and solid-phase constituents, or due to acceleration of principal cathodic reactions, such as the reduction of dissolved oxygen, that occur even in the absence of microorganisms. Investigation of the role these factors play in Ennoblement is the primary research focus of this thesis.

Research Goal

The goal of the present research is to establish the mechanism by which microbial colonization induces the electrochemical phenomenon of Ennoblement. Table 1.1 provides an overview of the research objectives that were developed to achieve this goal.

Table 1.1 Overview of Research Leading to Elucidation of the Ennoblement Mechanism

Working Hypothesis	Experimental Approach	Outcome	Chapter
Ennoblement is caused by dissolved oxidants	Measure concentrations of specific oxidants (H_2O_2, dissolved oxygen) and local E_{corr} within biofilms on Ennobled stainless steel	Dissolved oxidants do not cause Ennoblement	4
Ennoblement is caused by acceleration of the oxygen reduction reaction	Measure cathodic reaction rate for Ennobled stainless steel in the presence and absence of dissolved oxygen	Ennoblement is not caused by acceleration of the oxygen reduction reaction	5
Metal surface properties change during Ennoblement	Measure metal capacitance as a broad indicator of electrical double-layer and surface film properties	Ennoblement is correlated with changes in metal capacitance	4
The abundance of reducible surface-bound material increases during Ennoblement	Electrochemically titrate reducible surface material	A new oxidizing surface phase develops during Ennoblement	4 & 6
Ennoblement is caused by manganic oxide biofouling	1) Analyze biofilms for Mn-rich deposits and manganese-oxidizing bacteria. 2) Measure E_{corr} as Mn-rich deposits are chemically dissolved from the surface 3) Compare electrochemical characteristics of Ennoblement with those of stainless steel coated with pure MnO_2 paste	Manganic oxide mineralization causes Ennoblement	5
Ennoblement is caused by the activity of manganese-oxidizing bacteria	Assess Ennoblement of stainless steel exposed to pure cultures of *Leptothrix discophora*	Manganese-oxidizing bacteria can induce Ennoblement	7

CHAPTER 2

THE LITERATURE OF ENNOBLEMENT

Ennoblement Characteristics

The electrochemical phenomenon known as Ennoblement, was first observed in the mid-1960's[1], and has remained a controversial issue for the past three decades. The dominant characteristics of Ennoblement are a several-hundred millivolt increase in E_{corr} to values near +350 mV verses the saturated calomel electrode (SCE) and a two to three decade increase in cathodic current density at potentials between approximately -300 and +300 mV_{SCE}. These two defining electrochemical characteristics are depicted in figures 2.1 and 2.2. Studies have confirmed both effects for a variety of inert or passive metals including stainless steel, titanium, and platinum exposed to marine, estuarine, and fresh waters worldwide and have sought to demonstrate the biological nature of the phenomenon by showing that the shift in E_{corr} correlates with biofilm formation. A variety of mechanisms have been suggested to explain Ennoblement, but none has been supported by convincing experimental evidence.

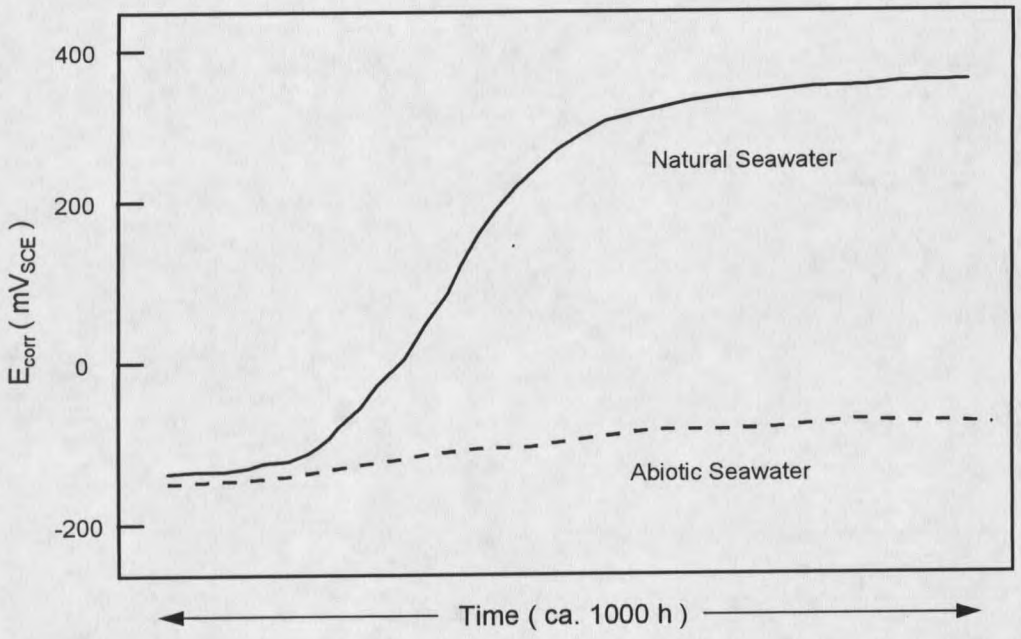

Figure 2.1. Schematic shift in E_{corr} with exposure time in natural and abiotic seawater

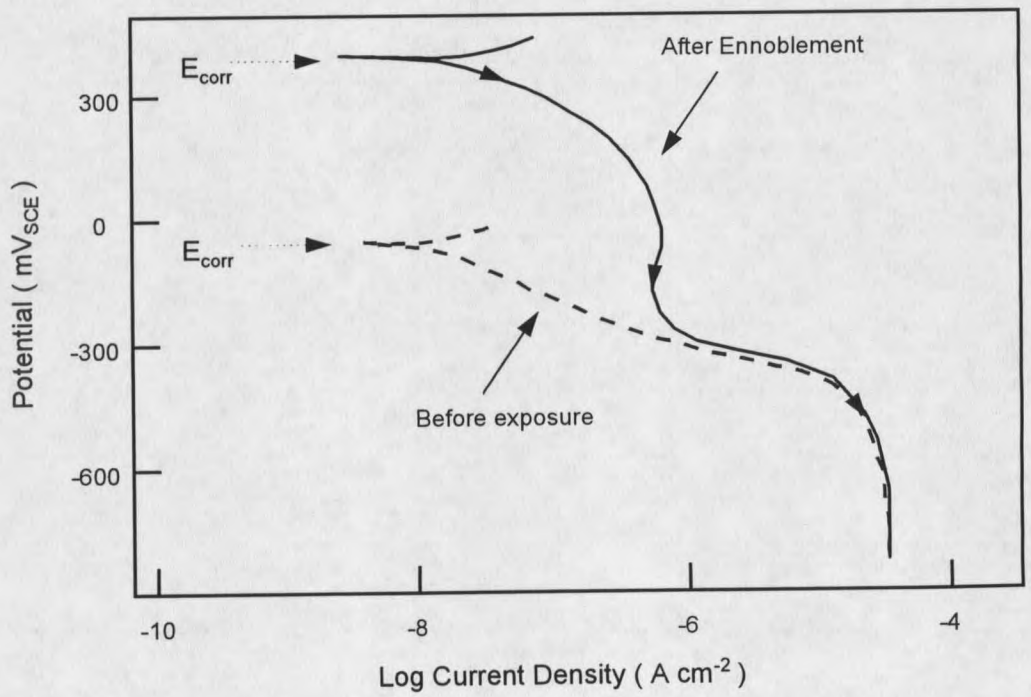

Figure 2.2 Schematic diagram of cathodic polarization behavior before and after Ennoblement

Ennobled E_{corr}

On initial exposure to seawater, E_{corr} for passive metals such as stainless steel and titanium lies in the range $-200\ mV_{SCE} < E_{corr} < -50\ mV_{SCE}$ [2]. Within a few days of exposure, E_{corr} typically begins to shift in the positive or noble direction reaching steady-state values between +300 and +400 mV_{SCE} within a few weeks. This shift is a defining characteristic of Ennoblement. Scotto et al.[3] observed an initial increase in E_{corr} of approximately 20 mV d^{-1} for 22 Cr - 3 Mo - 0.6 Ti (wt. %) steel beginning within one day of exposure to seawater and increasing asymptotically towards +375 mV_{SCE} over 65 days. Mollica[4] observed similar rates of increase towards the same limiting potential for a 17.5 Cr - 2.4 Mo - 0.6 Ti steel exposed to seawater, however the increase began only after ten days of exposure. Motoda et al.[5] reported that E_{corr} reached +400 mV_{SCE} within 10 days for 18 different stainless alloys exposed to seawater near Shizuoka, Japan, and that E_{corr} for commercially pure Ti reached +350 mV_{SCE} during the same exposure. Chandrasekaran and Dexter[6] found that E_{corr} for platinum became fixed at a value of +400 mV_{SCE} after 12 days exposure to saline water from the Delaware Bay near Lewes, DE. Dexter and Zhang[7] reported E_{corr} values slightly over +400 mV_{SCE} for a series of stainless steels with molybdenum content between 0.2 and 6 wt % after 3 to 6 weeks exposure to fresh-water from a lake in Lewes, DE. Steady-state E_{corr} for replicate Ti samples varied between +200 and +400 mV_{SCE} during the same exposure. A collaboration of six European research centers[8] confirmed steady-state E_{corr} of +320 mV_{SCE} for 24 Cr - 22 Ni - 7 Mo stainless steel exposed at coastal sites in the Norwegian sea, North sea, Mediterranean sea, and Eastern Atlantic. Time to reach steady-state varied from 6 to 19 days at the different

sites. Holthe et al.[9] reported E_{corr} of +300 mV_{SCE} for Pt and 24 Cr - 22 Ni - 7 Mo stainless steel and E_{corr} of +260 mV_{SCE} for Ti after 30 days exposure to water from the Norwegian sea, however, E_{corr} for a 90 Cu - 10 Ni alloy remained nearly unchanged at -240 +/-30 mV_{SCE} during the same exposure.

Clearly, a noble shift in E_{corr} can occur for a variety of passive metals exposed to natural waters. Nevertheless, some authors[10,11] have found that E_{corr} changes little during exposure, indicating that the effect is not universal. As an example, E_{corr} for stainless steel and titanium coupons remained less than +50 mV_{SCE} throughout a 4 month exposure to eastern coastal Pacific Ocean water[10], and three types of stainless steel exposed to seawater from the Gulf of Mexico under continuous illumination showed steady-state E_{corr} of only +125 mV_{SCE}, less than 70 mV higher than E_{corr} for sterile controls[11]. In the latter study, samples exposed under exclusively dark conditions showed a brief (1-2 day) noble excursion of E_{corr}, followed by a decay to a constant value of -100 mV_{SCE}. Anaerobic conditions were confirmed near the metal surface for this exposure, while dissolved oxygen levels of 2-3 ppm persisted at the surface for samples exposed under illuminated conditions. Results of this study suggested that anaerobic conditions are inconsistent with Ennoblement.

The foregoing indicates that metals with very low corrosion currents such as stainless steel, platinum, and titanium can attain E_{corr} values between +300 and +400 mV_{SCE} during exposure to waters at diverse geographic locations. This limiting range, independent of metal composition, implies that E_{corr} is influenced by processes external to the metal rather than by changes in the metallurgy that occur during exposure. The similarity in steady-state E_{corr} for different locations suggests that a common process is occurring at the different sites, although

the rate of development of the process appears to vary with location. The failure of the Cu-Ni alloy to become Ennobled may indicate that corrosion current is an important factor since Cu-Ni has a considerably higher corrosion rate than the other metals[9]. This explanation is consistent with the fact that Ennoblement has never been reported for mild steel or other actively corroding metals. A relationship between corrosion current and Ennoblement could reflect a balance between the rate of formation of a new oxidizing chemical specie and the rate of discharge of this specie through the corrosion current.

Elevated Cathodic Current

A second defining electrochemical characteristic that develops for passive metals exposed to natural waters is an increase in cathodic current density (i_c). A shift toward greater cathodic current indicates an increase in the rate at which reduction reactions occur at the metal surface. Mollica[4], investigating the electrochemical behavior of 17.5 Cr - 2.4 Mo - 0.6 Ti steel in seawater, observed an increase in i_c over the potential range -250 to +300 mV_{SCE}. After 30 days exposure, i_c had increased by 0.8 decades at -200 mV_{SCE} and 3.2 decades at +250 mV_{SCE}. Below -250 mV_{SCE} the current before and after exposure was identical. Motoda et al.[5] observed an increase in i_c over exactly the same potential range for type 316 stainless steel. After 14 days exposure to seawater, i_c had increased by 2 decades at +300 mV. Unlike Mollica's findings, however, where i_c increased steadily with decreasing potential, the increase in i_c showed a maximum of 2.3 decades at 0 mV_{SCE} for Motoda's work. Ijsseling[12] examined the cathodic behavior of a 24 Cr - 22 Ni - 7 Mo stainless steel in seawater for

exposure periods up to 160 days. Cathodic current density increased over the same range of potentials as noted above. The increase at -200 mV_{SCE} varied from 0.8 decades after 15 days to 1.2 decades after 133 days. At +250 mV_{SCE}, the increase was 2.2 decades after 15 days and 3.0 decades after 133 days. Ijsseling also examined the influence of polarization scan rate (0.9 0.09, and 0.009 mV s^{-1}) on cathodic current. Throughout the range +250 to -200 mV_{SCE}, i_c increased with increasing scan rate and was 3 to 8 times greater at a scan rate of 0.9 mV s^{-1} than at a rate of .009 mV s^{-1}. A well resolved maximum occurred in the log i_c vs. potential (E) curves at 0 mV_{SCE} and -200 mV_{SCE} for the 0.09 and 0.9 mV s^{-1} sweep rates respectively. Only a very slight maximum at +140 mV_{SCE} was identifiable for the 0.009 mV s^{-1} sweep. At 0.009 mV s^{-1}, i_c at -600 mV_{SCE} was 20 $\mu A\ cm^{-2}$ before and after 150 days exposure. In contrast after 150 days, i_c at -600 mV_{SCE} was 70 and 130 $\mu A\ cm^{-2}$ for scan rates of 0.09 and 0.9 mV s^{-1} respectively.

It is apparent that i_c increases up to 2-3 decades in the potential range -250 to +300 mV_{SCE} for stainless alloys exposed to seawater. A maximum in the log i_c vs. E curves also develops, and this may indicate that a mass transfer limitation or depletion of a reducible specie occurs during the scan. The former could occur if a new electrode process decreases the oxygen reduction overvoltage, whereas the latter condition would result if a finite amount of a new reducible specie is formed near the electrode surface since cathodic current furnished by this specie would decrease as the specie becomes depleted by reduction. Either of these possibilities could explain the increase in cathodic current density observed during Ennoblement, and both are consistent with the scan rate dependence of i_c that was observed

(i.e. i_c may be higher at faster scan rates due to less depletion of the new reducible specie or due to establishment of a smaller diffusion field).

Biological Origin

Several approaches have been used to determine if Ennoblement is caused by microbial colonization of the metal surface. These can be roughly classified as controlled biotic experiments and experiments designed to correlate Ennoblement with biological parameters such as biomass and respiratory activity.

Filtration and Other Control Measures

The effect of filtration and pasteurization on the development of Ennoblement was investigated by Dexter[7,13] for a variety of stainless alloys exposed to seawater and to estuarine waters from the Delaware Bay. Control experiments were carried out by exposing the alloys to the same waters treated by low temperature pasteurization (75°C) and filtration through 0.2 μm membranes. Ennobled E_{corr} and a 30-160 μm thick biofilm developed within 20 days for coupons exposed to untreated water, while E_{corr} remained less than 0 mV_{SCE} and negligible biofilm developed for the control coupons. Scotto[3] observed similar results for control experiments involving only filter sterilization. Johnsen and Bardal[14] compared E_{corr} for stainless steel exposed to natural seawater and to abiotic synthetic seawater. E_{corr} increased to +300 mV_{SCE} after 12 days exposure to seawater and remained stable at that potential

throughout the ensuing 6 weeks of exposure. In contrast, E_{corr} did not exceed +130 mV_{SCE} for the coupon exposed to synthetic seawater. These studies demonstrated a correlation between Ennoblement and attached bacterial cell density, however, neither filtration nor filtration plus pasteurization produced entirely abiotic controls. As a consequence, a purely biological basis for Ennoblement could not be inferred.

Mollica[4] investigated the effect of flow rate on Ennoblement. The rate of increase in E_{corr} shifted from 20 to 7 mV d^{-1} as flow rate was increased from 1 to 5 m s^{-1}. It was shown that the rate of increase in E_{corr} correlated with dried weight of biofilm on the metal surface, and that the biofilm mass decreased with increasing flow rate.

Holthe et al.[9] investigated the relationship between Ennoblement and temperature by exposing stainless steel to seawater in a heated recirculation loop. For temperatures less than 32°C, E_{corr} shifted to +300 mV_{SCE} during a 24 day exposure. At 32°C, E_{corr} remained less than +100 mV_{SCE} throughout the exposure. Mollica[15] found a similar effect with a transition temperature of 35-40 °C, above which Ennoblement did not occur. The results were attributed to a decrease in microbial viability at the higher temperatures as indicated by a low ATP content in the surface deposits formed at temperatures greater than 35°C. A relationship between cathodic current and temperature was observed for stainless steels exposed to seawater in the Mediterranean, eastern coastal Atlantic, and North Sea[8]. The exposure time required for elevated cathodic current to develop decreased with increasing water temperature over the range 2 - 21°C. The correlation is consistent with the temperature dependence of biological growth although the effect of other seasonal and chemical parameters on the rate of cathodic current increase could not be evaluated.

Correlation with Indices of Biological Activity

Scotto et al.[16] compared E_{corr} with the respiratory activity of biofilms -measured as oxygen uptake- on a 20 Cr - 18 Ni - 6 Mo stainless steel exposed to seawater. E_{corr} covaried with the logarithm of respiratory activity. E_{corr} and cathodic current density also correlated with the logarithm of the amount of extracellular polymeric substances (EPS) -measured as polysaccharide content- in the biofilms. The onset of increased cathodic current occurred when approximately 150 ng cm^{-2} of EPS had been deposited on the coupon surface. In a related experiment[3], the same authors showed that attached bacterial cell density and E_{corr} evolved towards limiting values according to an equation of the form

$$X = X_{\infty}(1-e^{-kt})$$

Where X is the value at time, t, X_{∞} is the value at infinite time and k is a constant with the empirical value 2.5 x 10^{-2} d^{-1}. Mollica[15] observed that Ennobled E_{corr} developed only when the ATP content in the biofilm was greater than approximately 1 ng cm^{-2}. Gundersen et al.[17] investigated the effect of hypochlorite on Ennoblement, using a lipid hydrolysis technique to assess bacterial activity. Hypochlorite applied at 1 ppm for 30 minutes daily was effective in eliminating bioactivity and prevented Ennoblement from developing.

Another study of the biological nature of Ennoblement used sodium azide to poison biofilms on Ennobled metals[3]. Azide addition caused E_{corr} for a stainless alloy to drop from +375 to +125 mV_{SCE} over a five day period. Dexter[13] observed similar effects for Ennobled platinum. Since azide inhibits respiration without causing biofilm detachment, it was concluded that active metabolism rather than the mere physical presence of the biofilm was

responsible for Ennoblement. Dexter pointed out, however, that azide produces a significant drop in E_{corr} even for abiotic controls, although the magnitude of such decrease is much smaller than that observed for the azide treatment of Ennobled samples.

Mechanisms of Ennoblement

Oxygen Reduction

Oxygen reduction is the dominant cathodic reaction on stainless steel under aerated conditions, and much attention has been focused on the relationship between oxygen reduction and Ennoblement.

Oxygen concentration can be influenced by photosynthetic activity within biofilms and this consideration has been used to interpret data from Ennoblement experiments. Little[11] attributed the absence of Ennoblement for coupons exposed under dark conditions to a lack of photosynthesis that allowed anaerobic conditions to develop. Motoda[5] found high numbers of attached diatoms on Ennobled stainless steel and argued that Ennoblement was caused by a metabolite of the diatoms. Scotto[16] however, found no correlation between Ennoblement and chlorophyll-a content in the biofilms and Mollica[15] observed that Ennoblement occurred even when chlorophyll-a was negligible. Dexter[7] found that sunlight had a deleterious effect on the development of Ennoblement, and argued that this was caused by a decrease in the thermodynamic potential for oxygen reduction brought about by algal consumption of CO_2 that increased pH near the metal surface. Eashwar et al.[18] reported that exposure to direct

sunlight prevented Ennoblement from occurring in waters that otherwise caused a 250 mV increase in E_{corr}.

Many authors have suggested that acceleration of the oxygen reduction reaction -possibly by metallo-organic catalysts produced during microbial respiration- is the cause of Ennoblement[15,16,19]. This idea has become quite well entrenched, although no direct evidence of accelerated oxygen reduction has been presented. As indicated by studies on the effects of photosynthesis, a coherent picture of the role of oxygen in Ennoblement is missing.

Other Cathodic Reactants

Dexter[13] attribute the finding that Ennobled E_{corr} decreased during daylight hours to an increase in pH, implying that Ennoblement was associated with acidification at the metal surface. Protons are a dominant cathodic reactant in dearated media and in aerated media, pH causes a thermodynamic shift in the oxygen reduction potential of -60 mV pH^{-1}. Thus a pH drop of 5-6 units from a seawater pH near 8.0 could explain Ennoblement. Dexter suggested that pH 3 could be reached within biofilms containing acid producing bacteria and Chandresekaran and Dexter[6] argued that at pH 3, 8 mM hydrogen peroxide could account for the electrochemical characteristics of Ennobled platinum. Their conclusion was based in part on detection of several mM hydrogen peroxide in the biofilm. Mollica[20] however, found that seawater acidified to pH 7.5 caused little change in E_{corr} while the same seawater left untreated caused E_{corr} to shift to +300 mV_{SCE}. From this and other data, he concluded that Ennoblement was prevented by acidification. Mansfeld et al.[10] pointed out that acidification lowers the

pitting potential of low molybdenum stainless steels below the value of Ennobled E_{corr}, thus making Ennoblement and acidification mutually exclusive.

Status of the Ennoblement Mechanism

Although several hypotheses have been suggested, most investigators acknowledge that the mechanism underlying Ennoblement remains unexplained[5,9,10,13,16,18,21]. Research undertaken in the present thesis was designed to establish the mechanism of Ennoblement, and was initiated by testing several of the Ennoblement hypotheses. Careful analysis and interpretation of the results of these experiments led to a new hypothesis involving manganese-oxidizing bacteria and to the confirmation of this hypothesis. The following paragraph briefly summarizes how this finding fits into previous knowledge concerning manganese-oxidizing bacteria and corrosion.

The occurrence of manganese and manganese-oxidizing bacteria at sites of stainless steel corrosion has been widely observed and is commonly thought to result from differential aeration caused by mineral occlusion of the metal surface[22-25]. Several authors[23,26,27] have noted, however, that microbial production of ferric and manganic chlorides would be corrosive to stainless steel, and Duquette and Ricker[28] suggested that these species would act to fix the metal potential above the pitting potential. Linhardt[29] demonstrated that manganese containing deposits from a severely pitted stainless steel turbine blade, when applied to a platinum electrode, could shift the metal potential above +300 mV_{SCE}. This potential was above the stainless steel pitting potential for water of approximately 100 ppm chloride, and

was thought to be the cause of the corrosion failure. These observations taken together with a mechanism of Ennoblement involving manganese-oxidizing bacteria, serve to unify the previously separate issues of Ennoblement and manganese-related corrosion by linking them to a common cause, biomineralization of manganese dioxide. Direct electrochemical reduction of the manganese dioxide, operating independently or in conjunction with surface occlusion processes, appears to be a significant factor in the corrosion mechanism.

References Cited

1. Crolet, J.-L. (1991). From Biology and Corrosion to Biocorrosion, in: Microbial Corrosion: Proceedings of the 2nd EFC Workshop. Sequeira, C.A.C., and A. K. Tiller eds., (Sesimbra, Portugal, 3-6 March 1991, The Institute of Materials, London), pp. 50-60.

2. Lula, R. (1986). Stainless Steel. (American Society of Metals, Metals Park, OH), 173 pp.

3. Scotto, V., R. DiCintio and G. Marcenaro, (1985). The Influence of Marine Aerobic Microbial Film on Stainless Steel Corrosion Behaviour. Corr. Sci. **25**:185-194.

4. Mollica, A. (1976). The Influence of the Microbiological Film on Stainless Steels in Natural Seawater, in: The 4th International Congress on Marine Corrosion and Fouling (Antibes, France), pp. 351-365.

5. Motoda, S., Y. Suzuki, T. Shinohara and S. Tsujikawa, (1990). The Effect of Marine Fouling on the Ennoblement of Electrode Potential for Stainless Steels. Corr. Sci. **31**:515-520.

6. Chandrasekaran, P. and S. C. Dexter, (1993). Mechanism of Potential Ennoblement on Passive Metals by Seawater Biofilms, CORROSION/93 paper no. 493 (NACE, Houston, TX).

7. Dexter, S. C. and H.-J. Zhang, (1990). Effect of Biofilms on Corrosion Potential of Stainless Steel Alloys in Estuarine Waters, in: The 11th International Corrosion Congress (Associazione Italiana di Metallurgia, Florence, Italy) pp. 333-340.

8. Audouard, J., *et al.*, (1994). Effect of Marine Biofilm on High Performance Stainless Steels Exposed in European Coastal Waters. in: The Third European Federation of Corrosion Workshop on Microbial Corrosion. Tiller, A.K. and C.A.C Sequeira, eds., (Estoril, Portugal, 13-16 March 1994, The Institute of Materials, London) pp. 198-210.

9. Holthe, R., E. Bardal and P. Gartland, (1989). Time Dependence of Cathodic Properties of Materials in Seawater. Mat. Perform. **28**:16-23.

10. Mansfeld, F., *et al.*, (1992). An Electrochemical and Surface Analytical Study of Stainless Steels and Titanium Exposed to Seawater. Corr. Sci. **33**:445-456.

11. Little, B.J., *et.al.*, (1991). Impact of Biofouling on the Electrochemical Behaviour of 304 Stainless Steel in Natural Seawater. Biofouling **3**:45-49.

12. Ijsseling, F., (1993). Improved Method for Measuring Polarisation Curves of Alloys during Prolonged Times of Exposure. in: Marine Corrosion of Stainless Steels: Chlorination and Microbial Effects. Ijsseling, F.P., ed. (The Institute of Materials, London), pp. 100-107.

13. Dexter, S., (1995). Effect of Biofilms on Marine Corrosion of Passive Alloys. in: Bioextraction and Biodeterioration of Metals. Gaylarde, C. and H. Videla eds., (Cambridge University Press, Cambridge, UK); pp. 129-168.

14. Johnsen, R. and E. Bardal, (1986). Effect of a Microbiological Slime Layer on Stainless Steels in Seawater. CORROSION/86 paper no. 227 (NACE, Houston, TX).

15. Mollica, A., *et al.*, (1989). Cathodic Performance of Stainless Steels in Natural Seawater as a Function of Microorganism Settlement and Temperature. Corrosion **45**:48-56 .

16. Scotto, V., M. Beggiato, G. Marcenaro and R. Dellepiane, (1993). Microbial and Biochemical Factors Affecting the Corrosion Behaviour of Stainless Steels in Seawater. in: Marine Corrosion of Stainless Steels: Chlorination and Microbial Effects. Ijsseling, F.P., ed. (The Institute of Materials, London), pp. 21-33.

17. Gundersen, R., *et al.*, (1991). The Effect of Sodium Hypochlorite on the Electrochemical Properties of Stainless Steels in Seawater with and without Bacterial Films. Corrosion **47**:800-807.

18. Eashwar, M., S. Maruthamuthu, S. Palanichamy and K. Balakrishnan, (1995). Sunlight Irradiation of Seawater Eliminates Ennoblement-Causation by Biofilms. Biofouling **8**:215-221.

19. Dexter, S. C. and G. Y. Gao, (1988). Effect of Seawater Biofilms on Corrosion Potential and Oxygen Reduction of Stainless Steel. Corrosion **44**:717-723.

20. Mollica, A., (1992). Biofilm and Corrosion on Active-Passive Alloys in Seawater. Internat. Biodeterio. Biodegrad. **29**:213-229.

21. Dowling, N., J. Guezennec, J. Bullen, B. Little and D. White, (1992). Effect of Photosynthetic Biofilms on the Open-Circuit Potential of Stainless Steel. Biofouling **5**:315-322.

22. Tatnall, R.E., (1981). Case histories: Bacteria Induced Corrosion. Mat. Perform. **20**:41-48.

23. Kobrin, G., (1986). Reflections on Microbiologically Induced Corrosion of Stainless Steels. in: Biologically Induced Corrosion. Dexter. S .C. ed., (NACE, Houston,TX) pp. 33-46.

24. Tverberg, J., K. Pinnow and L. Redmerski, (1990). The Role of Manganese Fixing Bacteria on the Corrosion of Stainless Steel. CORROSION/90 paper no. 151 (NACE, Houston, TX).

25. Tuthill, A., R. Avery, J. Musich, K. Pinnow and R. Lutey, (1995). Corrosion of Stainless Steel Piping in a High Manganese Fresh Water. in: 1995 International Conference on Microbially Influenced Corrosion. Angell, P. *et al.* eds., (New Orleans, 8-10 May, 1995, NACE, Houston, TX), pp. 54/1-54/7.

26. Tatnall, R., (1990). Case Histories: Biocorrosion. in: Biofouling and Biocorrosion in Industrial Water Systems. Flemming, H-C. and G. Geesey, eds., (Springer-Verlag, New York) pp. 165-185.

27. Videla, H. A. and W.G. Characklis, (1992). Biofouling and Microbially Influenced Corrosion. Internat. Biodeterio. Biodegrad. **29**:195-207.

28 Duquette, D., and R. Ricker (1986). Electrochemical Aspects of Microbially Induced Corrosion. in: Biologically Induced Corrosion. Dexter, S.C. ed., (NACE, Houston,TX), pp. 121-130.

29. Linhardt, P.,(1994). Manganese Oxidizing Bacteria and Pitting of Turbine Components Made of CrNi Steel in a Hydroelectric Power Plant. Werkst. Korros. **45**:79-83.

CHAPTER 3

THEORY AND EXPERIMENTAL APPROACH

Mixed Potential Theory

The potential of an electrode in solution reflects relative rates of anodic (oxidation) and cathodic (reduction) reactions occurring at the electrode surface. At equilibrium, the net rates of anodic and cathodic reactions are equal, and the electrode potential is constant. For inert or noble metals, such as platinum and gold, the electrode itself does not undergo reaction and serves only to facilitate charge transfer between external redox species. In contrast, electrodes of active metals such as iron do undergo oxidation and this process contributes to the net anodic rate. Metal oxidation is typically the dominant anodic process for freely corroding materials. In aerated solution, the dominant cathodic reactions are reduction of dissolved oxygen (DO) and reduction of water[1]. Equations 3.1-3.6 show relevant half-reactions and the corresponding net reaction for the corrosion of iron in aerated aqueous media[2,3].

$$Fe \Rightarrow Fe^{2+} + 2e^{-} \qquad \textit{anodic} \qquad (3.1)$$

$$2H_2O + 2e^{-} \Rightarrow H_2 + 2OH^{-} \qquad \textit{cathodic} \qquad (3.2)$$

$$2H_2O + Fe \Rightarrow Fe(OH)_2 + H_2 \qquad \textit{net} \qquad (3.3)$$

$$4OH^- + 4Fe(OH)_2 \Leftrightarrow 4Fe(OH)_3 + 4e^- \qquad \textit{anodic} \qquad (3.4)$$

$$O_2 + 2H_2O + 4e^- \Rightarrow 4OH^- \qquad \textit{cathodic} \qquad (3.5)$$

$$4Fe(OH)_2 + O_2 + 2H_2O \Leftrightarrow 4Fe(OH)_3 \qquad \textit{net} \qquad (3.6)$$

Eqs. 3.1-3.6 indicate that the anodic and cathodic processes occurring on the metal surface correspond to different half-reactions. The term 'mixed potential' is used to describe this condition, and to distinguish it from a reduction potential in which the anodic and cathodic reactions are simply the forward and reverse parts of a single half-reaction. A mixed-potential in which the anodic reaction is metal oxidation is termed the corrosion potential, E_{corr}.

Influence of Cathodic Rate on E_{corr}

The net rate for each half-reaction occurring on the metal surface is given by Butler-Volmer kinetics[1,4] as:

$$i_{net} = nFAk^o \left\{ C^*_{ox} \exp\left[-2.3 \frac{(E - E^{o'})}{B_c} \right] - C^*_{red} \exp\left[2.3 \frac{(E - E^{o'})}{B_a} \right] \right\} \qquad (3.7)$$

$$B_c = \frac{2.3\,RT}{\alpha_c n_c F} \qquad B_a = \frac{2.3\,RT}{\alpha_a n_a F}$$

where cathodic and anodic rates for each half-reaction are described by the first and second exponential terms in eq. 3.7 respectively, E refers to the electrode potential, and C^*_{ox} and C^*_{red} refer to concentrations of the oxidized and reduced species at the electrode surface. Other symbols are as defined in the Notation section. Measureable current across the

electrode-solution interface is the sum of the net currents for each half-reaction and at equilibrium, must equal zero. For n separate half-reactions:

$$i_{meas} = \sum_{j=1}^{n} i_{net}^{j} \tag{3.8}$$

Bearing in mind that only a single value of E can exist for a conductive surface, and setting the sum of currents described by eq. 3.8 to zero, E can be expressed in terms of the reactant concentrations, formal half-cell potentials ($E^{o'}$), and kinetic parameters associated with each half-reaction. If as is often the case, the anodic and cathodic rates are dominated by single half-reactions (e.g. reactions 3.1 and 3.2), and further, if the intrinsic rates for these half-reactions under the concentration conditions of the system are similar, E will acquire a value intermediate between the standard potentials of the dominant anodic and cathodic reactions. Equation 3.7 shows that in so doing, the cathodic rate for half-reactions possessing a formal potential more positive than E, and the anodic rate for half-reactions possessing a formal potential more negative than E, will increase. At the same time, rates of the reverse reactions decrease. Expressed in another way, for $C^{*}_{ox} = C^{*}_{red}$ and $E << E^{o'}$, the first exponential term in equation 3.7 dominates and the equation becomes:

$$i_c = nFAk_c^{o}\, C_c^{*}\, \exp\left[-2.3\frac{(E - E_c^{o'})}{B_c}\right] \tag{3.9}$$

Where i_{net} has been changed to i_c, to indicate that the net current for the half-reaction with the more positive reduction potential is cathodic. The subscript *c* has been added to indicate that this equation describes the current supplied by the cathodic half-reaction.

Taking the logarithm of equation 3.9 shows that a plot of E vs. natural log of current density will be a straight line, and that the position of this line will shift positively along the abscissa as the intrinsic rate constant or concentration of the cathodic reactant increase.

$$\ln\frac{i_c}{A} = D + \ln k_c^o + \ln C_c^* - \frac{2.3}{B_c}E$$
$$D = \left(\ln(nF) + \frac{2.3}{B_c}E_c^{o'}\right) \tag{3.10}$$

Equation 3.10 pertains for each half-reaction, j, that satifies the condition $E << (E^{o'})_j$. Net cathodic current is then:

$$(i_c)_{net} = \sum_{j=1}^{n} i_c^j \tag{3.11}$$

In a similar manner, for $C^*_{ox} = C^*_{red}$ and $E >> E^{o'}$, the second exponential term in equation 3.7 dominates and the equation becomes:

$$i_a = -nFAk_a^o\ C_a^*\ \exp\left[2.3\frac{(E - E_a^{o'})}{B_a}\right] \tag{3.12}$$

Where i_{net} has been changed to i_a, to indicate that the net current for the half-reaction with the more negative reduction potential is anodic. The subscript *a* has been added to indicate that this equation describes the current supplied by the anodic half-reaction.

Measureable current across the electrode-solution interface is the difference between the net anodic and cathodic rates, so that $i_{meas} = i_c - i_a$ and:

$$i_{meas} = nFA\left(k_c^o\ C_c^*\ \exp\left[-2.3\frac{(E - E_c^{o'})}{B_c}\right] - k_a^o\ C_a^*\ \exp\left[2.3\frac{(E - E_a^{o'})}{B_a}\right]\right) \tag{3.13}$$

For an electrode at equilibrium, $i_c = i_a$ and for the special case of a corroding metal, the current at equilibrium is termed the corrosion current, i_{corr}. As noted above, under these conditions $E = E_{corr}$. At equilibrium, $i_c = i_a = i_{corr}$, and either equation 3.9 or 3.12 can be used to express i_{corr} as a function of E_{corr}. In terms of the cathodic reaction:

$$i_{corr} = nFAk_c^o \, C_c^* \, \exp\left[-2.3\frac{(E_{corr} - E_c^{o'})}{B_c}\right] \tag{3.14}$$

Dividing equation 3.9 by equation 3.14 yields the expression:

$$i_c = i_{corr} \exp\left[-2.3\frac{(E - E_{corr})}{B_c}\right] \tag{3.15}$$

Similarly:

$$i_a = i_{corr} \exp\left[2.3\frac{(E - E_{corr})}{B_a}\right] \tag{3.16}$$

Again noting that $i_{meas} = i_c - i_a$:

$$i_{meas} = i_{corr}\left(\exp\left[-2.3\frac{(E - E_{corr})}{B_c}\right] - \exp\left[2.3\frac{(E - E_{corr})}{B_a}\right]\right) \tag{3.17}$$

It can be seen, that for $E << E_{corr}$, or for $E >> E_{corr}$, equation 3.17 reduces to equations 3.15 or 3.16 respectively. Equation 3.17 relates measureable current to the displacement of E from E_{corr} and is an important expression used to experimentally determine i_{corr}. The current-voltage characteristics given by equations 3.7 and 3.17 are shown graphically in figure 3.1.

Figure 3.1 and equation 3.17 serve to define E_{corr} and i_{corr}, and correctly relate these quantities for a freely corroding metal, however, anodic current for metals in the passive state

is controlled by oxide film dissolution and/or cation transport through the passive film[5,6], and is nearly independent of E. Under these conditions, anodic current is equal to the passivation current, i_{pass}, and can be taken as roughly constant[1]. For a passive metal at equilibrium, i_{corr} then equals the constant value i_{pass}. From equation 3.14, it can be seen that an increase in the intrinsic rate constant or concentration of any cathodic species must shift E_{corr} in the positive direction in order to maintain a constant value of i_{corr}. Equation 3.9 shows that for a constant value of E, an increase in these same quantities will increase cathodic current. These relationships are shown schematically in figure 3.1 assuming eq. 3.5 as the sole cathodic reaction. Curve 'P' shows the current-voltage behavior for a metal in the passive state. An increase in the intrinsic rate constant from $k_c^{o,1}$ to $k_c^{o,2}$ shifts E_{corr} from E^1_{corr} to E^2_{corr}. An increase in the concentration of cathodic reactant would qualitatively produce the same effects.

Based on the foregoing, the noble shift in E_{corr} and elevated cathodic current density that define Ennoblement may be related to processes that increase the concentration or the intrinsic rate constant of cathodic reactants. To understand Ennoblement, possible increases in rate constants and cathodic reactant concentrations, and their influence on the electrochemical behavior of the metal need to be investigated. The following sections describe several processes by which microbial colonization may alter the electrochemical environment at metal surfaces, and discuss techniques used to study these processes. The order of presentation corresponds roughly to the order in which these techniques and related experiments were carried out, and reflects evolution of the overall experimental design used to elucidate the mechanism of Ennoblement.

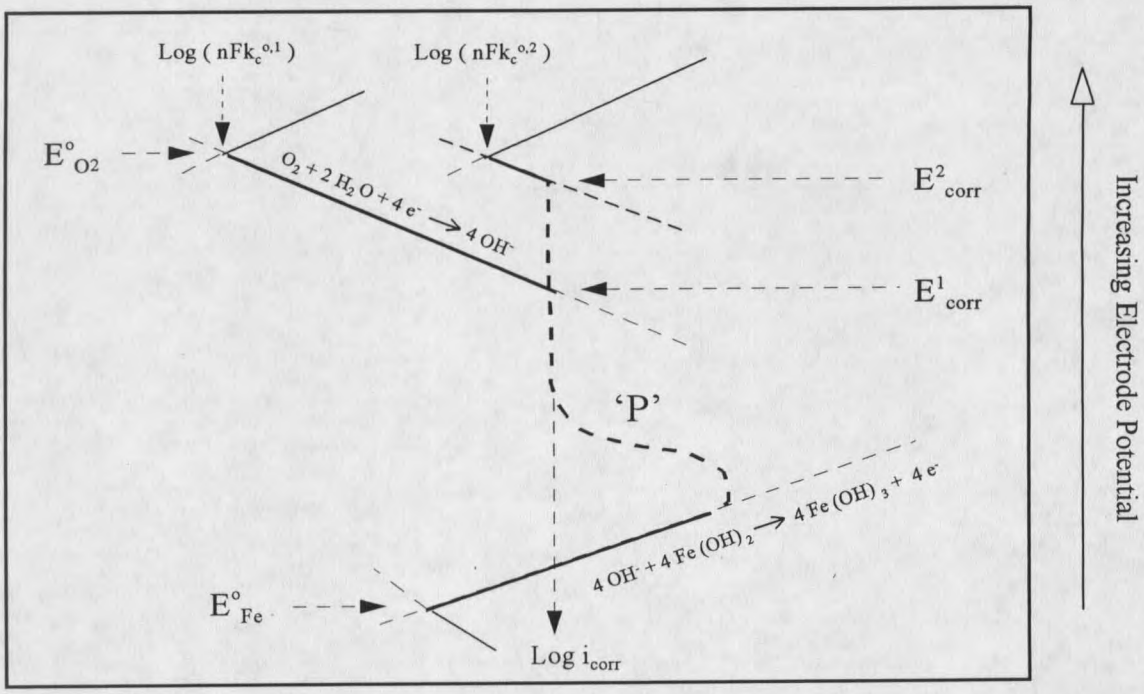

Figure 3.1 Schematic diagram showing current-voltage relationships according to eq. 3.7 and 3.17. Curve 'P' illustrates behavior for a metal in the passive state. E_{corr} shifts from E^1_{corr} to E^2_{corr} as the equilibrium rate for the cathodic reaction increases.

Ecorr Measurements

As defined in chapter 2, the dominant characteristic of Ennoblement is a several hundred mV, noble shift in E_{corr}. This noble shift has been used throughout the present work to monitor the development of Ennoblement. E_{corr} appears as the voltage difference between a metal specimen and a known reference voltage, and is easily measured using a voltmeter or A/D converter. To avoid polarizing the sample specimen, these measurements are made using high impedance ($>10^9\ \Omega$) equipment. In a typical experiment, circular metal specimens or

coupons were exposed to a test environment and E_{corr} was measured periodically against the saturated calomel reference electrode (SCE).

Many experiments required frequent measurement intervals on ten or more coupons. To simplify data collection, a 64 channel, multiplexed, A/D converter connected to a computer was used to automatically record E_{corr}. The data collection interface was custom built for this application using eight CD4051 CMOS multiplexers controlled by a commercial, eight channel, A/D interface card (DAS-8PGA, Keithley Metrabyte Corporation, Taunton, MA). The interface was operated in single-ended mode, so that all coupons were directly referenced to a single SCE. Software to control the interface and record data was written specifically for these experiments.

Potentiodynamic Polarization

Cathodic polarization behavior is the second defining characteristic of Ennoblement. To ensure that noble shifts in E_{corr} observed in the present work were characteristic of the changes observed elsewhere in the literature, potentiodynamic polarization measurements were carried out and an increase in cathodic current density was confirmed. These experiments are described in chapters 4 and 5. The measurements were made using a conventional three-electrode system by applying current between the stainless steel specimen (the working electrode) and a graphite or platinum counter electrode, and measuring the potential difference between the working electrode and an SCE reference electrode located within a few mm of the metal surface. A computer controlled, model 273A potentiostat and

352 SoftCorr™ software (EG&G Instruments, Princeton, NJ) were used to generate the polarization curves. For a single reaction taking place at potentials where charge transfer is the rate determing step, a plot of electrode potential vs. log current density generates a straight line according to equation 3.10. Shifts in the slope or position of this line are an indication that changes in reaction kinetics, identity, or concentration of the reacting specie(s) have occurred as described above.

Redox Environment within Biofilms

Microbial activity may influence the redox environment near metal surfaces in a number of ways. Photosynthesis by algae and cyanobacteria produces oxygen and could increase the concentration of this cathodic reactant. Extracellular hydrogen peroxide, is known to be produced by a variety of microorganisms[7], and as a strong oxidant can significantly elevate E_{corr} for stainless steel. Extracellular production of superoxide and other active oxygen species that can be expected to elevate E_{corr} has also been demonstrated[8]. A variety of redox active species are produced during microbial metabolism including organic acids from the citric acid cycle and constituents such as NAD^+, FAD, and quinones that are part of the electron transport system. These species may accumulate within biofilms during cell death and lysis and may be reduced at the metal surface if they possess a reduction potential greater than E_{corr}.

Microbial metabolites may influence the intrinsic rate constant for oxygen reduction. Metallo-porphyrins and analogues of other respiratory macrocycles have been investigated

widely as electrocatalysts[9-11], and the enzyme laccase has been shown to produce a forty-fold increase in the rate of oxygen reduction on platinum[12]. Metabolic electron-transfer mediators such as menadione can couple extracellular oxygen reduction to oxidation of membrane bound species of the electron transport system, producing superoxide[8]. Superoxide formation has been established as the rate determining step in oxygen reduction on iron at neutral pH[13], consequently, overall oxygen reduction rate may increase if superoxide is catalytically produced near the metal surface. Alternatively, extracellular levels of electrocatalytic enzymes may reach sufficiently high levels within biofilms to directly increase oxygen reduction rate.

A final example of microbially mediated redox processes that can effect the electrochemistry of metals involves heterotrophic respiration. Aerobic respiration within biofilms consumes oxygen and can lead to development of anaerobic conditions suitable for the growth of sulfate-reducing bacteria (SRB). Sulfide production by SRB sharply lowers redox potential and further scrubs oxygen from the system. These effects modify E_{corr} and can degrade the oxide films on passive metals. The process is common in MIC, and while not a direct cause, may aggravate the corrosive effects of Ennoblement. Chapter 8 discusses possible relationships between Ennoblement and SRB.

Microelectrode Measurements

Microelectrodes were used to directly evaluate the redox environment within biofilms on Ennobled stainless steel. Hydrogen peroxide and dissolved oxygen were measured using amperometric microelectrodes, and E_{corr} for a stainless steel microelectrode was used as a

general measure of the oxidizing power within the biofilm. The latter measurement was based on the idea that if unspecified oxidants shift E_{corr} for the metal substratum in the noble direction they should produce a similar shift for a stainless steel microelectrode placed in the same environment. The experimental details and results of microelectrode measurements are described in chapter 4.

Oxygen Reduction Rate

According to equation 3.9, cathodic current should be directly proportional to oxygen concentration if oxygen is the dominant cathodic reactant. To determine the influence of oxygen on the cathodic reaction that develops during Ennoblement, coupons that had previously been Ennobled by exposure to natural water were cathodically polarized in the presence and absence of oxygen. The region of elevated cathodic current density between approximately -200 to +400 mV_{SCE} characteristic of Ennoblement was examined to determine if oxygen concentration influenced net current. This experiment is described in chapter 5.

Surface Metal Oxide Abundance

The state of the surface can directly influence the rates of chemical and electrochemical reactions occurring on metals. Metal oxide properties are known to influence intrinsic oxygen reduction rates on iron[13,14], and it has been shown that oxygen reduction proceeds more rapidly on γ-FeOOH than on Fe_3O_4 in the potential range -0.55 to -0.1 V_{SCE}[15]. Surface films on stainless steel contain varying amounts of reducible iron oxides depending on surface

treatment[16] that can in some instances produce a slight break in the cathodic polarization curve for uncolonized metal samples coincident with the break observed in Ennoblement. This behavior is illustrated by the lower curve in figure 2.2. Polarization curves generated immediately following cathodic polarization at -500 mV_{SCE}, or generated by scanning in the positive direction from cathodic potentials do not show the break in slope; however the feature reappears for scans made a few hours after cathodic polarization. This behavior is characteristic of reversible oxide formation as typically observed for iron[15,17]. Coincidence of the break in polarization slope for unexposed and Ennobled coupons, with the later break being much more pronounced, suggests that Ennoblement may involve enrichment in oxide abundance at the metal surface. As noted above, such changes may potentially enhance oxygen reduction kinetics.

In addition to influencing the reduction rates of dissolved species, the foregoing suggests that metal-oxides can themselves be reduced. The reactions:

$$FeOOH + H_2O + e^- \Rightarrow Fe^{2+} + 3OH^- \tag{3.18}$$

$$3Fe_2O_3 + H_2O + 2e^- \Leftrightarrow 2Fe_3O_4 + 2OH^- \tag{3.19}$$

are implicated in the reduction of the passive film on stainless steel[16] and may participate as cathodic reactions in the atmospheric rusting of iron[18]. Reduction of iron oxides occurs in the same potential region as oxygen reduction[19], suggesting that reduction of surface oxides could contribute to the increase in cathodic current observed in Ennoblement.

Two approaches were taken to investigate the possibility that Ennoblement correlated with changes in surface oxide properties of the metal: 1) capacitance was measured during the

course of Ennoblement, and 2) the abundance of reducible surface material was assessed before and after Ennoblement.

Capacitance Studies

Capacitance is a broad measure of the thickness, area, and dielectric properties of phases present at the metal surface. Therefore, if surface changes occur during Ennoblement, they may produce changes in capacitance. The passive film on stainless steel is generally considered to have a complex oxide composition, with magnetite (Fe_3O_4), chromium oxides, and ferric oxides present in different proportions depending on conditions of surface treatment[16,20]. The capacitance of these oxides differ, consequently changes in oxide composition that may develop during Ennoblement should produce changes in capacitance. Conversely, capacitance that remains invariant would provide evidence that surface oxide composition does not change during Ennoblement.

Capacitance measurements were carried-out using the galvanostatic transient method[1]. This technique utilizes a constant current to polarize the metal and determines capacitance by fitting polarization vs. time data to the equation

$$\eta_{act} = I_{app} R_p \left(1 - e^{-\frac{t}{R_p C}} \right) \tag{3.20}$$

where η_{act} is the polarization or activation overvoltage, R_p is the polarization resistance which reflects the Faradaic reaction rate at the metal surface, and C is the net capacitance.

Application of this technique to determine capacitance changes during Ennoblement is described in chapter 4.

A special constant current source and differential amplifier were designed and constructed to supply the nanoampere currents and detect the millivolt changes associated with the capacitance measurements. Appendix A describes the design of the current source and amplifier and provides the derivation of equation 3.20.

Coulometric Titration

The abundance of cathodically active material bound to a metal can be determined by coulometric titration of the metal surface. This measurement, also known as the galvanostatic reduction technique, is performed by applying constant cathodic current to a specimen in an oxidant free electrolyte and observing the polarization versus time response. In the absence of dissolved reducible species, the applied current charges the electrode capacitively according to the relationship:

$$\frac{dE}{dt} = \frac{1}{C} I_{app} \tag{3.21}$$

As E becomes more negative the cathodic reaction rate for surface bound species increases exponentially according to equation 3.9. If the cathodic rate becomes equal to the applied current, a steady-state is attained and E remains constant. This condition persists as long as surface bound material is available to react and results in a potential lag or plateau. Duration of the plateau corresponds to coulombs of reducible surface material (current x time = coulombs), and the plateau potential is related to the reduction potential of the surface phase.

In principle, the plateau occurs when the electrode reaches the reduction potential for the oxide, however, this is dependent on the applied current since excessively high currents will require significant overvoltage to attain steady-state (cf. equation 3.9). By choosing a suitable value for I_{app}, the plateau and reduction potentials can agree closely. As an example, reaction 3.19, which has a formal reduction potential of -529 mV_{SCE} at pH 8.5, appears to correspond to the plateau potential near -550 mV_{SCE} frequently observed during reduction of oxide films on iron and stainless steel[16,17]. In coulometric titrations, the occurrence of different plateaus indicates the presence of more than one reducible phase. The technique has been used to investigate the nature and abundance of oxide phases on crystalline iron oxides[21] and on mild and stainless steels[16,22]. In the present work, it was used to determine if new reducible surface phases developed during Ennoblement, and to quantify the abundance of these phases. These experiments are described in chapters 4 and 6.

Metal-oxide Depositing Bacteria

Micro-electrode, capacitance, and coulometric titration experiments provided strong evidence that Ennoblement correlated with development of a new reducible surface phase. The nature of this phase was not known, however as noted in the Surface Metal-Oxide Section above, the coincidence of the break in cathodic polarization behavior seen before and after Ennoblement suggested that an enrichment in surface oxide abundance may have occurred. A variety of iron- and manganese-oxidizing microorganisms exist in nature, and the possibility that microbial metal-oxide deposition produced the new reducible phase and the

modified electrochemical parameters observed in Ennoblement became the final focus of the present research.

Anodic Polarization by Metal-Oxides

Equation 3.19 exemplifies surface metal-oxide reactivity. Interconversion between surface-bound oxide phases has the effect of fixing a redox couple at the metal surface. Depending on the uniformity of the lattice structure between the oxidized and reduced phases these reactions can be electrochemically reversible. If both phases are present, and the reaction is the sole significant electrochemical reaction occurring at the surface (i.e an inert electrode), the metal electrode will acquire the reduction potential of the oxide half-cell. In cases where only one phase is present (e.g. only the oxidized phase), the electrode will polarize positively in the manner described for dissolved oxidants, as reduction of the oxide increases cathodic current. This anodic polarization will continue until re-oxidation of the accumulated reduced products, or development of other anodic reactions (e.g. oxidation of water), balance the cathodic current.

The value of E_{corr} determines whether a particular oxide will be reactive, where E_{corr} is the equilibrium mixed-potential of the metal electrode. Oxides with reduction potentials more positive than the electrode potential will behave as cathodes when galvanically coupled to the metal, with oxidation of the metal serving as the anodic reaction. In this fashion, galvanically coupled manganic oxides have been used to inhibit corrosion in strongly acidic media by anodically polarizing stainless steel into the passive region[23]. In contrast, oxides with

reduction potentials more negative than E_{corr} will be stable with respect to reduction and will not contribute cathodic current.

E_{corr} for stainless steel in neutral aerated waters lies in the range -50 to -200 mV_{SCE}. Based on the above discussion, ferric oxide ($E^{o'}$ = -529 mV_{SCE}, cf. equation 3.19) should not anodically polarize the metal under these conditions. In the present research, this fact was confirmed by applying a synthetic ferric oxide paste to the surface of stainless steel. No shift in E_{corr} resulted. As a consequence, in evaluating the possible role of metal-oxide depositing bacteria in Ennoblement, attention was focused on more strongly oxidizing manganic rather than ferric-oxide deposition.

Manganese-oxidizing Bacteria

Manganese-oxidizing bacteria (MOB) are widely distributed in both fresh and marine waters and are considered to be "directly or indirectly, the major catalyst of manganese cycling in the natural environment" [24]. These bacteria catalyze oxidation of dissolved divalent manganese to form insoluble manganic oxides. The oxides are formed extracellularly and encrust the extracellular polymeric material (bacterial capsules) that surround individual cells or cell aggregates. The genera *Leptothrix* and *Siderocapsa* are particularly associated with formation of highly enriched manganic oxide deposits[25,26]. *Leptothrix* are typified by filamentous growth in tubelike polymeric sheaths with individual cell dimensions of 0.6-1.4 μm diameter x 1-10 μm length[27]. Sessile species of *Siderocapsa* grow as aggregates of a few to several dozen cells surrounded by a common ring-shaped polymeric capsule[28]. Manganese

deposits that form on the extracellular polymers of these genera can frequently be visualized without magnification. Such deposits are expected to be electroactive when formed in immediate proximity to metal surfaces and present a rational mechanism by which bacteria may alter the electrochemical behavior of metals leading to Ennoblement. To test whether biofouling by manganic oxides could account for Ennoblement, the following threefold approach was devised.

MOB and Manganese Deposition Microbiological and surface analytical techniques were used to test for accumulation of manganese and MOB within biofilms on Ennobled stainless steel. Reflected-light microscopy was used to determine the presence of mineral encrustations. Colorimetric spot tests and surface analysis by scanning electron microscopy with energy dispersive x-ray analysis (SEM/EDS) were used to confirm the presence of manganese. Leuco-crystal violet, the reduced, colorless form of the dye crystal violet, was chosen as the reagent for the spot test. On contact with manganic oxide, the reagent is rapidly oxidized to produce an intense violet color discernable by eye. In natural waters the reagent is highly specific for manganic oxides and is used both as a spot test and as a quantitative measure of MnO_2 abundance[29,30]. Epifluorescence microscopy at 400 - 1000x magnification was used to visualize the microbial composition of intact biofilms on stainless steel. Staining was carried out using the nucleic acid fluorochrome acridine-orange which is widely used to visualize and enumerate microorganisms[31,32]. Characteristic cell morphology, colonial habit, and the presence of distinctive structures such as bacterial sheaths were noted. The presence of MOB in the biofilms was assessed by streak plating inoculums from natural biofilms onto a

low manganese modification of the yeast-manganese medium of Pringsheim[33], and staining isolated colonies with leuco-crystal violet. Formation of the violet color confirmed that the colonies produced manganic oxides. Final composition of the modified Pringsheim medium was 50 ppm yeast and 0.5 ppm Mn(II), buffered at pH 8.1 by acid titration of 1.3 g L^{-1} HEPES buffer.

Reductive Dissolution of MnO_2 To confirm that Ennoblement was dependent on the presence of manganic oxides, biofilms on Ennobled coupons were treated with sodium sulfite to reductively dissolve MnO_2. Sulfite ion and SO_2 quantitatively reduce MnO_2 to Mn(II)[34] and are used under acidic conditions to leach manganese from low-grade ores. In the present work, sulfite solution was used at pH 8.4 to retain the pH value of the natural water exposure. E_{corr} was monitored as Ennobled coupons were exposed to sulfite and at the conclusion of the experiment, the electrolyte was analyzed for the presence of Mn(II) either by atomic absorption or colorimetrically using the formaldoxime method[35]. A decrease in E_{corr} to pre-Ennobled values and a corresponding release of Mn(II) into solution were taken as evidence that manganic oxides were essential for Ennoblement.

Electrochemical Changes Induced by MnO_2 Paste The sulfite experiment tested whether Ennoblement could be eliminated by removing MnO_2. To demonstrate the reverse, i.e. that MnO_2 could produce the electrochemical characteristics of Ennoblement, E_{corr} and cathodic polarization measurements were made on stainless steel coated with chemically prepared MnO_2 paste. Results of the measurements were compared with the electrochemical

behavior of Ennobled coupons. The paste -prepared by addition of permanganate ion to an alkaline solution of manganous ion[36]-, was also used to calibrate the potential of the plateau observed during coulometric titration of Ennobled coupons. Agreement between Ennobled and MnO_2 paste coated coupons with respect to E_{corr}, the potential of the coulometric titration plateau, and general cathodic curve shape and current density at specified potentials, were taken as evidence that MnO_2 was the cause of Ennoblement.

The experiments and results relating manganic oxide biofouling to Ennoblement are described in chapters 5 and 6.

Ennoblement by *Leptothrix discophora*

The relationship between manganic oxides and Ennoblement was firmly established by the foregoing experiments, but the relationship between MOB and Ennoblement remained circumstantial, i.e. both MOB and manganese were identified in the biofilms, but no strict causal relationship could be inferred. To demonstrate that Ennoblement could be induced by MOB, controlled experiments were carried out with pure cultures of the manganese-oxidizing bacterium *Leptothrix discophora*. Masses of sheathed cells characteristic of this species were among the bacteria present in biofilms on Ennobled coupons. A strain of *L. discophora* identified as SP-6 [37] was obtained from the American Type Culture Collection (Rockville, MD) and grown in a mineral salts-vitamin-pyruvate medium. In the presence of Mn(II), this organism formed copius manganic oxide deposits on all submerged surfaces. Experiments were performed by exposing stainless steel coupons in three identical reactors containing the

bacteria and dissolved Mn(II). For each reactor, measurements of E_{corr}, concentration of Mn(II) in solution, surface cell density on the coupons, and surface-bound Mn on the coupons were made. Solution Mn(II) was measured colorimetrically by the formaldoxime technique, surface cell density was determined by acridine-orange direct count, and surface-bound Mn was determined using both the sulfite dissolution and the coulometric titration techniques. Two control experiments were performed, one with bacteria but no added Mn(II), the other with Mn(II) but no bacteria. Ennoblement of E_{corr} in the first experiment and absence of Ennoblement in both control experiments was taken as confirmation that Ennoblement was caused by MOB. These experiments are described in chapter 7.

Outline of the Thesis

The experimental approach outlined in the foregoing chapter demonstrates the evolution and coherence of the work comprising this thesis. Chapters 4 through 7 describe individual experiments and can be read as independent articles. Chapter 4 presents preliminary findings concerning the redox environment on Ennobled coupons and the surface state of the metal that focus attention on manganic oxide biofouling; chapters 5-7 describe the experiments relating Ennoblement to MOB. The content of these chapters is summarized in Table 1.1. Chapter 8 is also self-contained and serves to summarize the preceeding experimental results and to discuss implications of the research.

References Cited

1. Jones, D.A., (1992). Principles and Prevention of Corrosion, (Macmillan Publishing Company, New York, NY) 568 pp.

2. Stumm, W. and F. Lee, (1961). Oxygenation of Ferrous Iron. Indust. and Engineer. Chem. **53**:143-146.

3. Greenwood, N. N. and A. Earnshaw, (1990). Chemistry of the Elements, (Pergamon Press, New York, NY), 1542 pp.

4. Bard, A. and L. R. Faulkner, (1980). Electrochemical Methods: Fundamentals and Applications, (John Wiley & Sons, New York, NY) 718 pp.

5. Huesler, K. (1990). Growth and Dissolution of Passivating Films. Corr. Sci. **31**:597-606.

6. Irhzo, A., Y. Segui, N. Bui, and F. Dabosi, (1986). On the Conduction Mechanisms of Passive Films on Molybdenum-Containing Stainless Steel. Corrosion **12**:141-147.

7. Glenn, J. K. and M. H. Gold, (1985). Purification and Characterization of an Extracellular Mn(II)-Dependent Peroxidase from the Lignin Degrading Basidiomycete Archiv. Biochem. Biophys. **242**:329-341.

8. Yamashoji, S., T. Ikeda, and K. Yamashoji, (1991). Extracellular Generation of Active Oxygen Species Catalyzed by Exogenous Menadione in Yeast Cell Suspension. Biochim. Biophys. Acta **1059**:99-105.

9. Anson, F. C., C.-L. Ni, and J.-M. Saveant, (1985). Electrocatalysis at Redox Polymer Electrodes with Separation of the Catalytic and Charge Propagation Roles. Reduction of O_2 to H_2O_2 as Catalyzed by Cobalt(II) Tetrakis(4-N-methyl pyridyl)porphyrin. J. Am. Chem. Soc. **107**:3442-3450.

10. Nagaoka, T., T. Saka, K. Ogura, and T. Yoshino, (1986). Oxygen Reduction at Electrochemically Treated Glassy Carbon Electrodes. Anal. Chem. **58**:1953-1955.

11. Su, Y., T. Huwana, and Chen.S-M., (1990). Electrocatalysis of Oxygen Reduction by Water-Soluble Iron Porphyrins. J. Electroanal. Chem. **288**:177-195.

12. Srinivasan, S., Y. A. Chizmadzhev, J. O. M. Bockris, B. E. Conway, and E. Yeager, (eds.), Bioelectrochemistry, Comprehensive Treatise of Electrochemistry, Vol. 10, (Plenum Press, New York, NY) 541 pp.

13. Jovancicevic, V., and J. O. M. Bockris, (1986). The Mechanism of Oxygen Reduction on Iron in Neutral Solutions. J. Electrochem. Soc. **133**:1797-1807.

14. Zecevic, S., D. M. Drazic, and S. Gojkovic, (1991). Oxygen Reduction on Iron-V. Processes in Boric Acid-Borate Buffer Solutions in the 7.4-9.8 pH Range. Corr. Sci. **32**:563-576.

15. Vago, E. R., E. J. Calvo, and M. Stratmann, (1994). Electrocatalysis of Oxygen Reduction at Well-Defined Iron Oxide Electrodes. Electrochim. Acta **39**:1655-1659.

16. Ramasubramanian, N., N. Preocanin, and R. D. Davidson, (1990). Analysis of Passive Films on Stainless Steel by Cyclic Voltammetry and Auger Spectroscopy. J. Electrochem. Soc. **132**:793-798.

17. Nagayama, M.-I. and M. Cohen, (1961). The Anodic Oxidation of Iron in a Neutral Solution I. The Nature and Composition of the Passive Film. J. Electrochem. Soc. **109**:781-790.

18. Evans, U., and C. Taylor, (1972). Mechanism of Atmospheric Rusting. Corr. Sci. **12**:227-246.

19. Vago, E., and E. Calvo, (1992). Electrocatalysis of Oxygen Reduction at Fe_3O_4 Oxide Electrodes in Alkaline Solutions. J. Electroanal. Chem. **339**:41-67.

20. Ferreira, M. G. S., and J. L. Dawson, (1985). Electrochemical Studies of the Passive Film on 316 Stainless Steel in Chloride Media. J. Electrochem. Soc. **132**:760-765.

21. Stockbridge, C., P. Sewell, and M. Cohen, (1961). Cathodic Behavior of Iron Single Crystals and the Oxides Fe_3O_4, Gamma- Fe_2O_3, and Alpha- Fe_2O_3. J. Electrochem. Soc. **108**:928-933.

22. Okada, H., Y. Hosoi, and H. Naito, (1970). Electrochemical Reduction of Thick Rust Layers Formed on Steel Surfaces. Corrosion **26**:429-430.

23. Tomashov, N. D. and G. P. Chernova, (1967). Passivity and Protection of Metals Against Corrosion, (Plenum Press, New York, NY) 208 pp.

24. Gounot, A.-M., (1994). Microbial Oxidation and Reduction of Manganese: Consequences in Groundwater and Applications. FEMS Microbiol. Rev. **14**:339-350.

25. Hanert, H., (1981). The Genus Siderocapsa (and Other Iron- or Manganese-Oxidizing Eubacteria, in: The Prokaryotes, A Handbook on Habitats, Isolation, and Identification of Bacteria. Starr, M., H. Truper, A. Balows, and H Schlegel eds., (Springer-Verlag, New York, NY) pp. 1049-1059.

26. Emerson, D., and W. Ghiorse, (1992). Isolation, Cultural Maintenance, and Taxonomy of a Sheath-Forming Strain of *Leptothrix discophora* and Characterization of Manganese-Oxidizing Activity Associated with the Sheath. Appl. Environ. Microbiol.

58:4001-4010.

27. Mulder, E., (1989). Genus Leptothrix Kutzing, 1843, in: Bergey's Manual of Systematic Bacteriology, Vol. 3, Staley, J. ed., (Williams and Wilkins, Baltimore), pp. 1998-2003.

28. Tuovinen, O., P. Hirsch, and G. Zavarzin, (1989). Family "Siderocapsaceae" Pribram, 1929, in: Bergey's Manual of Systematic Bacteriology, Vol. 3, Staley, J. ed., (Williams and Wilkins, Baltimore), pp. 1874-1878.

29. Spratt, H., E. Siekmann, and R. Hodson, (1994). Microbial Manganese Oxidation in Saltmarsh Surface Sediments Using a Leuco Crystal Violet Manganese Oxide Detection Technique. Estuar. Coast. Shelf Science **38**:91-112.

30. Kessick, M., J. Vuceta, and J. Morgan, (1972). Spectrometric Determination of Oxidized Manganese with Leuco Crystal Violet. Environ. Sci. Technol. **6**:642-644.

31. Bitton, G., B. Koopman, K. Jung, and G. Voiland, (1993). Modification of the Standard Epifluorescence Microscopic Method for Total Bacterial Counts in Environmental Samples. Wat. Res. **27**:1109-1112.

32. Hobbie, J., R. Daley, and S. Jasper, (1977). Use of Nucleopore Filters for Counting Bacteria by Fluorescence Microscopy. Appl. Environ. Microbiol. **33**:1225-1228.

33. Pringsheim, E., (1949). Iron Bacteria. Biol. Rev. Cambridge Philos. Soc. **24**:200-245.

34. Herring, A. and S. Ravitz, (1965). Rate of Dissolution of Manganese Dioxide in Sulfurous Acid. Trans. Soc. Mining Engineers **September**:191-196.

35. Brewer, P. and D. Spencer, (1971). Colorimetric Determination of Manganese in Anoxic Waters. Limnol. Oceangr. **16**:107-110.

36. Lovley, D., and E. Phillips, (1988). Novel Mode of Microbial Energy Metabolism: Organic Carbon Oxidation Coupled to Dissimilatory Reduction of Iron or Manganese. Appl. Environ. Microbiol. **54**:1472-1480.

37. Emerson, D. and W. Ghiorse, (1993). Ultrastructure and Chemical Composition of the Sheath of *Leptothrix discophora* SP-6. J. Bacteriol. **175**:7808-7818.

CHAPTER 4

REDOX AND CAPACITANCE MEASUREMENTS *

Overview

Ennobled open-circuit potential (E_{corr}) for Type 316L stainless steel (SS, UNS S31603) exposed to fresh river-water was investigated using microelectrodes to measure dissolved oxygen (DO), hydrogen peroxide (H_2O_2), and local E_{corr} within biofouling deposits, and using galvanostatic techniques to measure capacitance and to titrate reducible surface material. Results indicated that the deposits were uniformly aerobic and did not contain elevated levels of cathodic depolarizers. Development of Ennobled potential was related to E_{corr} near the beginning of exposure and occurred on surfaces having as little as 3-5% biofouling coverage. Galvanostatic measurements revealed a strong correlation between capacitance and E_{corr} as the latter increased during biofouling, and galvanostatic reduction measurements indicated an increased abundance of reducible surface-bound material during the same period. Results suggest an Ennoblement mechanism involving modifications of the metal-oxide surface.

---

* Published as: *Evidence for Surface Changes During the Ennoblement of Type 316L Stainless Steel: Dissolved Oxidant and Capacitance Measurements*, W. H. Dickinson, Z. Lewandowski, and R. D. Geer (1996), Corrosion **52**(12): in press.

Introduction

Microbial colonization of passive metals exposed to natural waters can shift the open-circuit potential (E_{corr}) several hundred millivolts (mV) in the noble direction[1-6]. Polarization behavior of the colonized metals shows an increase in cathodic current density at modest overpotentials[7-11], and reveals a break in cathodic Tafel[12] slope near -200 mV[1,7,9] (all potentials vs. the saturated calomel electrode, SCE.) These phenomena, collectively known as Ennoblement, are an expression of biofouling induced changes in the nature and/or kinetics of reactions occurring on the metal surface. From a technical perspective, Ennobled potentials can exceed critical pitting potentials for low molybdenum SS[(1)], increasing the risk of localized corrosion. Once initiated, localized attack may proceed rapidly due to the enhanced cathodic rate.

The principal electrochemical factors expected to contribute to Ennoblement are: 1) elevation of cathodic depolarizer concentration(s) and 2) acceleration of intrinsic oxygen reduction rate; either of which would increase cathodic current and anodically polarize the metal. Factor 1 may arise from localized changes in solution chemistry due to microbial activity and the presence of metabolic products, while factor 2 will be influenced by dissolved electrocatalysts and by the surface state of the metal. A third potential factor, diminished passivation current, would elevate E_{corr}, but would have little effect on cathodic current density and may be ignored.

---

[1] Critical pitting potential for type 304 SS (UNS S30400) in aqueous 0.5M chloride solution is -50 mV(SCE)[12].

Reduction of dissolved oxygen (DO) is the dominant cathodic reaction for unpolluted natural waters. In the presence of biofouling, metabolic production of active oxygen species (e.g. superoxide[13] and hydrogen peroxide (H_2O_2)[14]) or other unspecified oxidants, may raise concentrations sufficiently for these constituents to contribute to cathodic current. This has been reported for the Ennoblement of platinum[6]. In the absence of elevated oxidant concentrations, cathodic rate enhancement must arise from acceleration of the dominant cathodic reaction, reduction of DO. Although this prospect has been suggested repeatedly[5,8,10], no progress toward identifying a rate-enhancing mechanism for DO reduction has been made.

Surface metal-oxide properties are known to influence DO reduction rates on iron[15,16], and it was recently shown that DO is reduced more rapidly on maghemite (γ-FeOOH) than on magnetite (Fe_3O_4) in the potential range -0.55 to -0.1 V[17]. Surface films on SS contain varying amounts of reducible iron-oxides depending on surface treatment[18], and reduction of these oxides can in some instances produce a slight break in Tafel slope coincident with the break observed for Ennobled SS. The more pronounced break at -200 mV for Ennobled SS may reflect changes in the oxide film, and raises the possibility that Ennoblement is related to enhanced DO reduction rate caused by modification of surface-oxide mineralogy. This possibility is further suggested by the finding that metals with variable oxide stoichiometry such as titanium and platinum[19] display Ennoblement[3,6,9], while nickel, which has only a single well defined oxide state (NiO), does not Ennoble[20]. To date, the possible relationship between Ennoblement and changes in surface-oxide chemistry has not been studied.

In the present work, several proposed bases for Ennoblement were investigated. Microelectrodes were used to measure DO, H_2O_2, and local E_{corr} within biofouling deposits; capacitance was determined, as a broad measure of near surface changes that may reflect changes in the surface-oxides; and the quantity of reducible surface-bound material was measured before and after Ennoblement. To reduce the risk of localized corrosion, type 316L SS (UNS S31603) was used exclusively.

Experimental Procedure

Epoxy-embedded 316L SS coupons (1.59 cm diameter x 0.16 cm) from a single metallurgical heat were abraded on wet 600 grit silicon-carbide paper, swabbed with cotton under flowing distilled water, rinsed with 95% ethanol and air dried. Samples were exposed to flowing natural stream-water in once-through 2 cm x 60 cm polycarbonate reactors by either flush mounting in the reactor floor or suspending into the solution from above. Mounting was such that only a single face of each coupon was exposed to solution, and suspended samples were submersed 0.5 cm beneath the surface to fully immerse the exposed coupon face. Water from an aerated 20 L carboy was pumped through the reactor to maintain 1 cm fluid depth and a dilution rate of 3 h^{-1}. Chemical composition of influent water classified the source as a clean stream (DO > 6 ppm; pH 8.4; alkalinity 3 meq L^{-1}; nitrate ion (NO_3^-) 1.2 ppm; dissolved Fe 1.2 ppm; conductivity 4 x 10^{-4} ohm^{-1}-cm^{-1}; total organic carbon 110 ppm) with some seasonal variation.

Extent of biofouling coverage was evaluated using both reflected-light and epifluorescence microscopy. The biofouling deposits were patchy and were easily distinguished from the metal substratum, which allowed areal coverage to be estimated by measuring the dimensions of the biofouling patches. The dimensions of several different sized deposits were measured using a calibrated microscope graticule, from which estimates of the deposit cross-sections (foot-prints) were made. The number of deposits of each size within a microscope field (typically 500 x 500 μm) were then counted and a percent coverage was calculated. This was done for several fields, from which an overall percent coverage was estimated. Distribution of microorganisms within the biofouling deposits was determined by adding 10 ppm propidium-iodide solution to the attached deposits and examining by laser-confocal microscopy at 568 nm excitation wavelength. Bacterial cultures were obtained by streak-plating material from the biofouling deposits onto R2A agar and culturing at 25° C.

E_{corr} was measured hourly against the SCE by computer, using a high impedance ($>10^{11}$ Ω), multiplexed, analog-to-digital converter. With the exception of the galvanostatic reduction experiments, polarization measurements were made in the exposure reactor using a computer-controlled potentiostat/galvanostat. High-density graphite counter electrodes were used for all polarization measurements. Galvanostatic reduction of surface-bound material[18] was carried out in a 1 L corrosion-test flask in argon-deareated 0.1M Na_2SO_4 buffered with sodium carbonate at pH 8.4. Potential was recorded as the coupon was polarized by constant cathodic current (2.5 μA cm^{-2}) for periods of 30 to 60 minutes. In these experiments, lags in polarization rate signify reduction of surface-bound material, and coulombs of reducible material were calculated from the duration of the regions of potential lag.

Capacitance measurements were made by the galvanostatic transient method[21]. A 25 second, constant current pulse in the range 2 to 10 nA cm^{-2} was applied to the coupon producing an overvoltage-time response. Applied current was chosen to generate less than -10 mV cathodic overvoltage, and typical overvoltages were in the range -2 to -8 mV. After amplification through a high-impedance differential-amplifier, signals were recorded at 10 millisecond intervals by computer. Capacitance was determined by non-linear fitting to the equation:

$$\eta_{act} = I_{app} R_p \left(1 - e^{-\frac{t}{R_p C}} \right) \tag{4.1}$$

(η_{act}, overvoltage; I_{app}, applied current; R_p polarization resistance; C, capacitance; t, time) assuming a simple parallel combination of R_p and C as the model for the electrode-solution interface. In most cases this produced an acceptable fit, although for some measurements introduction of a second time constant was required to accurately fit the data. The procedure is described more fully in the Results and Discussion section. Close proximity of working and reference electrodes and the small applied currents made corrections for uncompensated resistance unnecessary.

DO microelectrode design has been previously described[22]. H_2O_2 microelectrodes were prepared by sheathing tapered platinum wire within glass in a fashion identical to that used to construct the DO probes. The sensing tip was coated by dipping in a solution of 1g cellulose-acetate dissolved in 20 ml acetone and air dried. Tip diameters were in the range 5 to 15 μm. DO and H_2O_2 microelectrodes were polarized to -0.8 and +0.8 V respectively

against the SCE and current proportional to analyte concentration was measured with a picoammeter. For DO, air-saturated and nitrogen-purged volumes of reactor water were used to give a two-point calibration. The H_2O_2 electrode was calibrated by adding known volumes of 30% H_2O_2 previously standardized by permanganate titration, to water from the reactor influent carboy. Separate calibrations performed over the pH range 2.2 to 9.6 showed an H_2O_2 detection limit < 2 μM at all pH.

SS microelectrodes were prepared by sheathing 100 μm diameter SS wire in glass. Tips were polished on a precision diamond wheel. Electrode response to variation in cathodic depolarizer concentration was confirmed by exposure to solution containing up to 6 mM H_2O_2. Increase in E_{corr} for the electrode was comparable to the change observed for sample coupons exposed to the same H_2O_2 concentrations. The electrode was conditioned by exposing to influent reactor solution for several hours prior to measuring E_{corr} within biofouling deposits.

Profiles of DO and H_2O_2 concentrations and microelectrode E_{corr} were measured within biofouling deposits on coupons mounted in the reactor floor. The microelectrodes, mounted in a commercial 3-axis micromanipulator, were positioned above a deposit by adjusting the x-y micromanipulator controls manually. Vertical positioning was then executed in 10 or 20 μm increments starting with the probe tip just above the deposit, and continuing until the tip was within about 10 μm of the metal substratum. Vertical movement was controlled by a computer-driven stepper motor attached to the micromanipulator z-axis, and probe position was determined by viewing the tip at 70x magnification through a stereo

microscope. Positioning accuracy from bulk solution to the substratum was 5 μm. Stable measurements were usually attained within 30 seconds after incrementing the probe position.

Results and Discussion

Biofouling

Visible brown slime began to accumulate on coupons mounted in the reactor floor after two to three days exposure. Examination of the slime by reflected-light microscopy showed an assemblage of microorganisms and debris within gelatinous, cottony-shaped deposits. After 35 days exposure, roughly 50% of the coupon surface was covered with patchy deposits 200 μm^2 to 0.2 mm^2 in cross-sectional area (foot-print) and from 20 to 400 μm thick. Between the deposits, only the uncolonized metal substratum was visible. Laser-confocal microscopy of propidium-iodide stained coupons confirmed that bacterial cells were present, and that the cells were constrained to the area within the gelatinous deposits, a finding in accord with current models of biofilm structure[23]. Coupons exposed by suspending into solution from above accumulated a morphologically similar brown slime, which typically covered less than 20% of the coupon and did not exceed 60 μm thickness. The diminished coverage for these coupons compared with those mounted in the reactor floor was thought to reflect lesser sedimentation fouling. Material from the biofouling deposits, when cultured on agar, exhibited seven colony types distinguished by color and morphology.

The presence of unspecified debris together with bacterial cells, suggested that the brown slime material should be described as biofouling, to indicate a complex inorganic, organic, and biotic composition, rather than as a biofilm. In accord with this, the term biofouling is used hereafter to refer to the brown slime.

E_{corr} Measurements

E_{corr} for a set of 12 coupons (Set #1) mounted in the reactor floor was monitored during a 35 day exposure. Results for 10 samples from the Set are shown in figure 4.1. E_{corr} for the remaining two coupons exhibited marked instability and was not plotted. After one hour exposure, E_{corr} varied from -41 to -212 mV for the 10 coupons and decreased to minimum values after 10 hours. For five coupons, E_{corr} increased uniformly at about 30 mV/day between days two and nine, and approached a steady-state value near +350 mV after 17 days. E_{corr} for the remaining five coupons increased more slowly, showed greater variability between coupons, and did not exceed +110 mV during the experiment.

A second set of 12 coupons (Set #2) mounted in the reactor floor were treated by periodically removing biofouling with a cotton swab. Throughout the exposure, the biofouling was easily dislodged by wiping, and microscopic examination confirmed that biofouling deposits did not develop. Stable values of E_{corr} did not exceed +70 mV for any sample from this Set, and for nine samples, E_{corr} did not exceed 0 mV. E_{corr} for four samples representative of the Set are shown as a function of time in figure 4.2. Episodes of increasing E_{corr} were apparent for two samples. For each episode, removal of the biofouling re-

established the E_{corr} value observed prior to the event. In the absence of increased potential, swabbing had no effect on E_{corr} as is evident from the lower two curves in figure 4.2, which implied that the treatment did not disturb the native passive film on the metal.

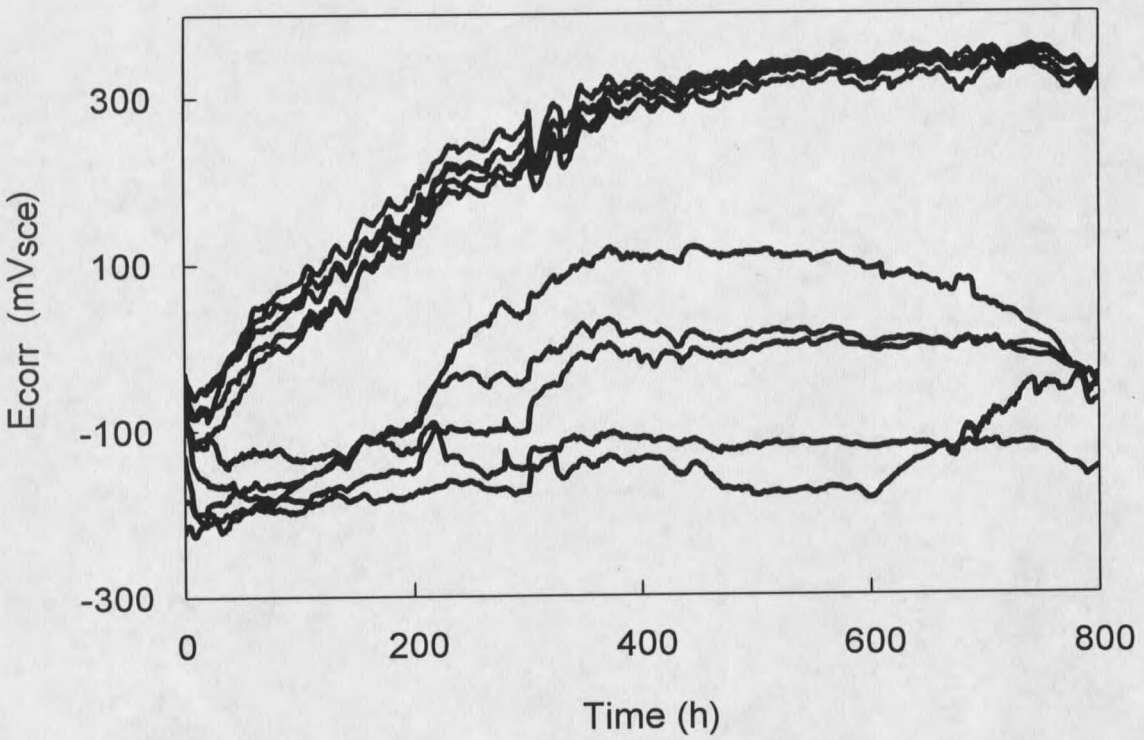

Figure 4.1. E_{corr} for ten 316L stainless steel coupons during biofouling in fresh river water.

Information relating biofouling thickness to Ennobled potential was obtained by monitoring E_{corr} as biofouling was progressively wiped from an Ennobled coupon surface. The procedure was viewed under magnification to allow estimation of biofouling thickness, and the range of initial thickness was between 20 and 400 μm. E_{corr} decreased less than 12 mV as all but a 20 μm thick adherent film was removed. This film was brown and was morphologically similar to regions of thicker biofouling, but could only be removed by

rubbing, which then exposed the SS substratum. Removal of the adherent film covering only 10% of the coupon surface caused a 20 mV decrease in E_{corr}. Substantially greater pressure was required to markedly shift E_{corr} to more active potentials, which suggested that the pressure required to remove the adherent film did not perturb the native passive film.

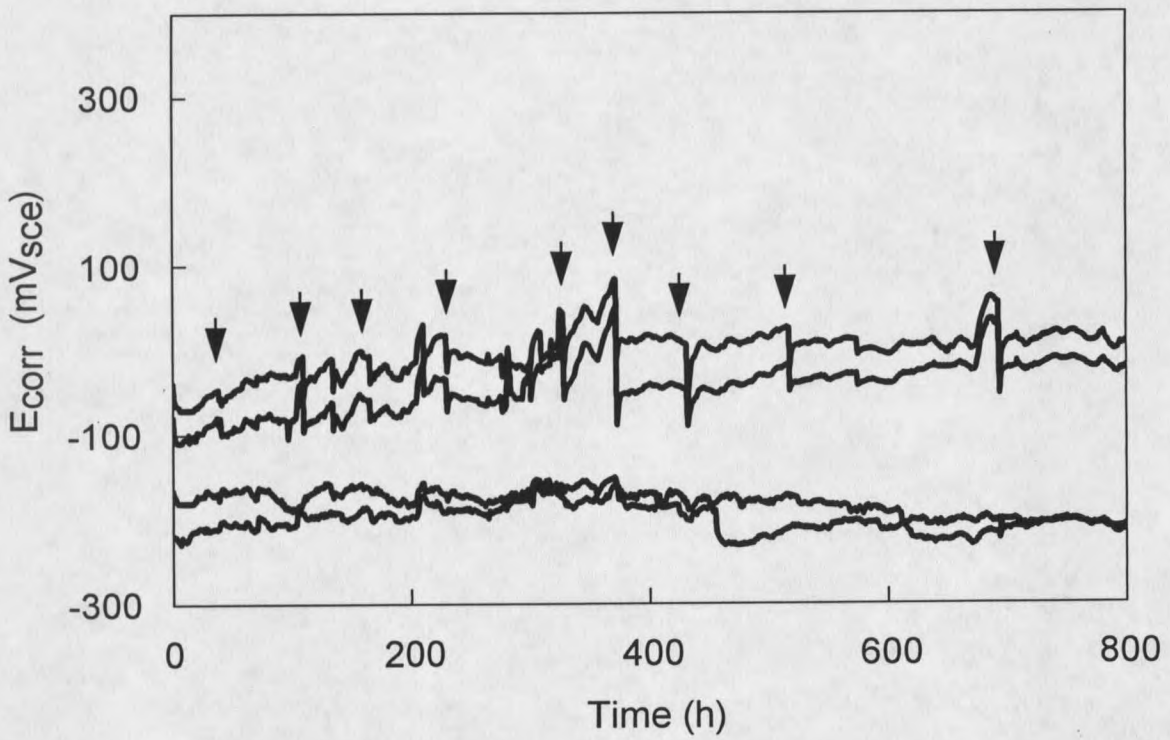

Figure 4.2. E_{corr} for four stainless steel control coupons during exposure to fresh river water. At times denoted by arrows, biofouling was removed from coupons by wiping surfaces with cotton.

Results from these experiments indicated that biofouling persistence in a freshwater environment caused an adherent material to accumulate at the metal surface, that was necessary for the development and retention of Ennoblement. The nature of the active component was not determined.

Data from figure 4.1 also revealed a link between Ennoblement and the value of E_{corr} near the beginning of exposure. Figure 4.3 shows final E_{corr} as a function of E_{corr} after 10 hours exposure, where 10 hours corresponded to an E_{corr} minimum for most samples studied. Only those coupons that exhibited E_{corr} more positive than -110 mV after 10 hours attained final potentials near +350 mV. In addition for Set #2, episodes of increasing potential occurred only for coupons with initial E_{corr} more positive than -110 mV. This relation was followed by all coupons from the second Set.

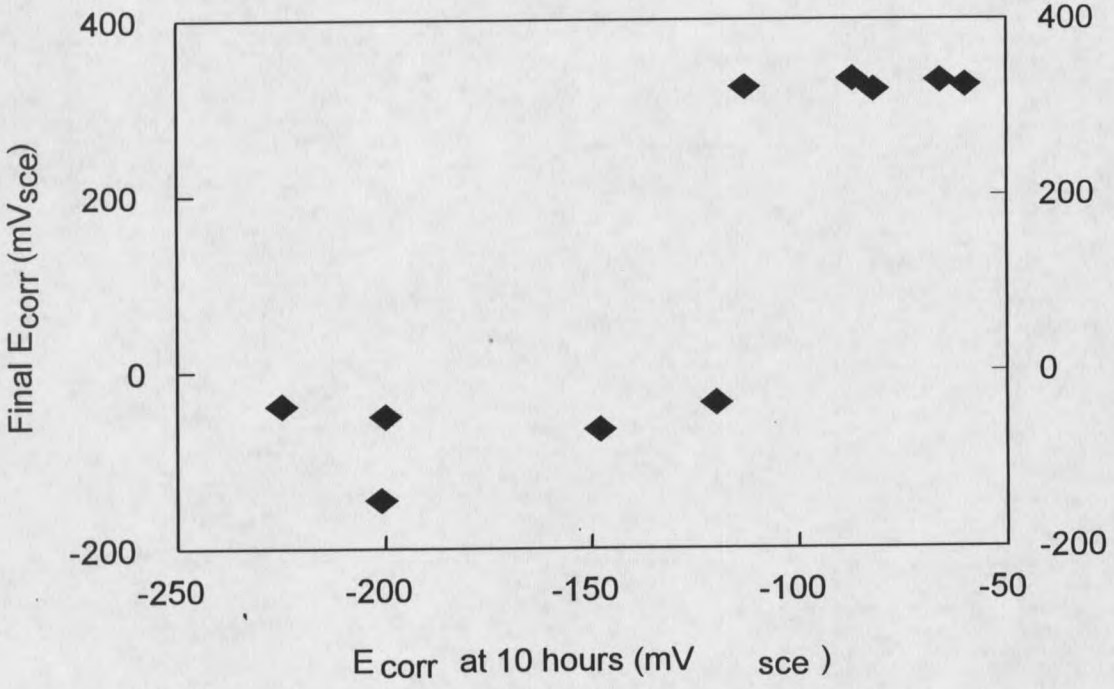

Figure 4.3. E_{corr} for 10 stainless steel coupons after 35 day exposure to fresh river water, vs. E_{corr} after 10 hours exposure. Data from figure 4.1.

For passive metal samples exposed to the same media, more negative values of E_{corr} may have reflected elevated passivation current, localized attack, and/or diminished cathodic

rate. The influence of these factors was examined using polarization measurements to determine corrosion current (i_{corr}) after a few hours exposure to river water. A positive correlation was observed between lower initial E_{corr} and elevated i_{corr}. Elevated i_{corr} may have indicated a more poorly formed passive film that was subject to breakdown, and that predisposed the coupons to localized attack. Active corrosion would have shifted E_{corr} to more negative values and offset the increased cathodic current thought to cause Ennoblement. If the foregoing is true, the net result would have been, as shown in figure 4.3, that coupons with initially lower values of E_{corr} did not Ennoble.

An alternate interpretation of the data in figure 4.3 involved the hypothetical formation of a new metal-oxide surface. As previously noted, SS Ennoblement is defined in part by a break in cathodic Tafel slope near -200 mV. This is shown by the upper curve in figure 4.4, which is representative of cathodic polarization observed by several authors[1,7,9]. For some SS samples in the present study, a less pronounced break was observed at the same potential after only a few minutes exposure to natural water or to simple electrolytes at neutral pH. This behavior is illustrated by the lower curve in figure 4.4. Polarization curves generated immediately following cathodic pre-treatment at -500 mV, or generated by scanning positively from cathodic potentials, did not show the break in slope; however the feature reappeared for curves generated a few hours after cathodic polarization. This behavior is characteristic of reversible oxide formation as reported for Fe[17,24]. If the break in Tafel slope was due to oxide reduction, then the more pronounced break after Ennoblement may have reflected an increase in oxide abundance or a change in the oxide mineralogy. Changes in oxide mineralogy can influence oxygen reduction rates[17], and so may have shifted E_{corr} in the noble direction by

enhancing oxygen reduction. Extending this scenario, figure 4.3 may be thought of as reflecting processes, such as deposition and discharge rates, that influenced oxide abundance.

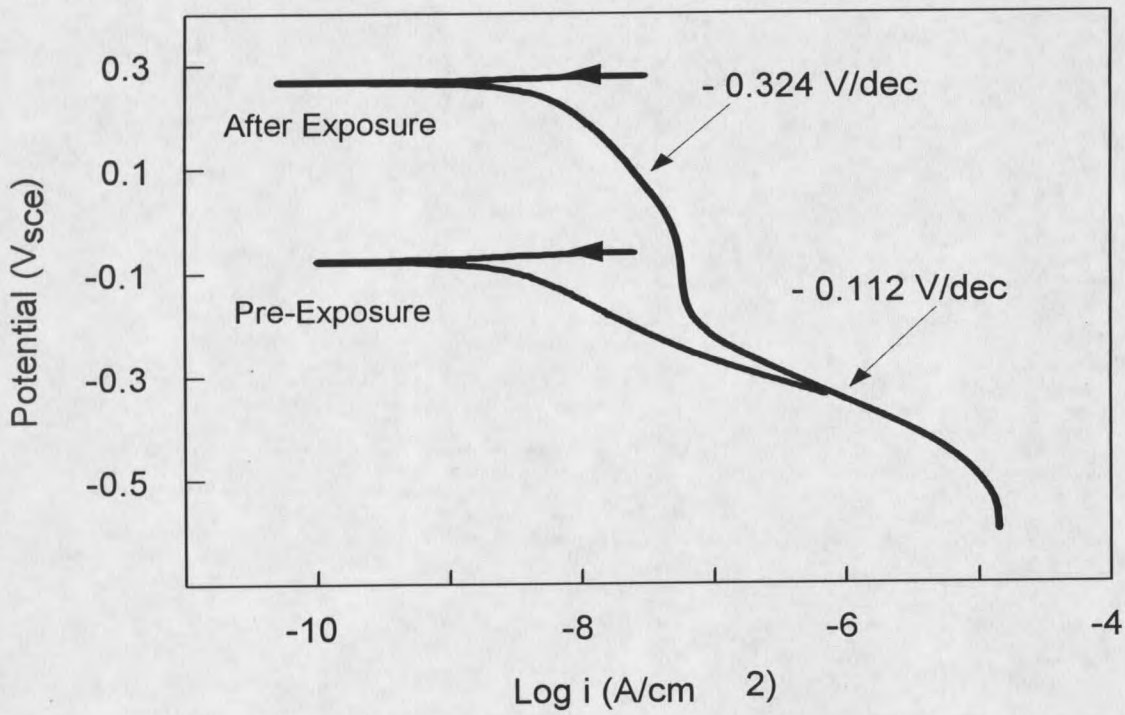

Figure 4.4. Potentiodynamic polarization curves for stainless steel before and after biofouling during 20 day exposure to fresh river water.

Accumulation of reducible oxide material would have reflected the difference between deposition rate and rate of discharge through the anodic current. On initial exposure to solution, anodic current would have been balanced primarily by cathodic oxygen reduction. Under this condition, new reducible material may have accumulated without being discharged. As E_{corr} increased however, more and more cathodic current would have been supplied by discharge of the new oxide material, until the point was reached where deposition and discharge rates balanced. At this point, E_{corr} would have stopped increasing. For higher

anodic current, as occurred for the lower curves in figure 4.1, the balance point would have occurred at a lower value of E_{corr}. This would have explained the relatively low limiting potential for the lower curves in figure 4.1 and would have explained why coupons with lower initial E_{corr} did not Ennoble (figure 4.3.)

Assuming that a new oxide with rate-enhancing properties towards oxygen reduction did develop, the polarization behavior for the upper curve in figure 4.4 could be explained as follows: 1) at noble potentials, oxygen reduction occurred on a modified oxide surface at an enhanced rate[2]. Greater Tafel slope in this region may have been related to changes in oxide thickness or conductivity that diminished activation overpotential at the oxide-solution interface as has been proposed to explain variations in Tafel slope on ruthenium-oxides[25], 2) in the region between 0 and -0.2 V, increasing activation overpotential was offset as the kinetically active surface was reduced, 3) at potentials below -200 mV the oxide phase was reduced and DO reduction shifted to the slower rate and lower Tafel slope characteristic of the unmodified surface.

On first examination, this hypothesis may appear to conflict with results from Johnsen and Bardal[11] who observed dramatically increased current density for SS polarized to -300 mV or below during exposure to seawater. Under these conditions, the new oxide phase would presumably have been reduced as it formed, and could not have influenced oxygen reduction rate. However, their findings must take into account the results of Mollica et al.[4], who observed a two decade growth in current density over approximately six days when

[2] Extrapolation of Tafel slopes to $E^{o'}_{O2}$ (0.478 V vs SCE at pH 8.5) indicates 3 to 4 decades enhancement for oxygen exchange current density (i_o) on the proposed modified surface.

samples previously Ennobled to more than +300 mV were polarized to -200 mV. From these and other findings the latter authors concluded that "once the potential has been fixed, the oxygen reduction current increases from i_1 (Tafel) to i_L (limiting current)..." and "There must be a more complicated relationship between bacterial settlement and the current to explain the dependence of this latter parameter on the duration of the polarization period." It appears then that cathodic polarization in the presence of bacteria may of itself have increased current density irrespective of the process(es) that caused Ennoblement. This assertion is supported by the work of Johnsen and Bardal[11], in which metal A, which had identical elemental composition to 316L SS, exhibited markedly increased current density during cathodic polarization, but showed E_{corr} values no greater than +30 mV when exposed at open-circuit, i.e. it could not be classified as Ennobled.

It must be emphasized that the above relationship between Ennoblement and oxide-formation is purely speculative; however it does provide a plausible explanation for the behavior shown in figures 4.3 and 4.4, and is consistent with the capacitance and galvanostatic reduction data presented later in this paper.

Microelectrode Studies

DO, H_2O_2, and SS probe potential within the biofouling on Ennobled coupons were measured to assess the contribution of elevated oxidant concentrations towards Ennobled potential. Measurements made at various heights above the substratum and at numerous sites over the coupon surface, showed H_2O_2 concentrations less than 2 μM and showed no

significant variation in E_{corr} for the SS microelectrode at any site. The number of profiles exceeded 40 for H_2O_2, and 100 for the SS probe and were made in areas of both thick (as great as 400 μm) and thin (as little as 20 μm) biofouling, as well as above biofouling-free regions. DO profiles made in the same regions showed saturation levels at all sites analyzed. Representative profiles are shown in figure 4.5.

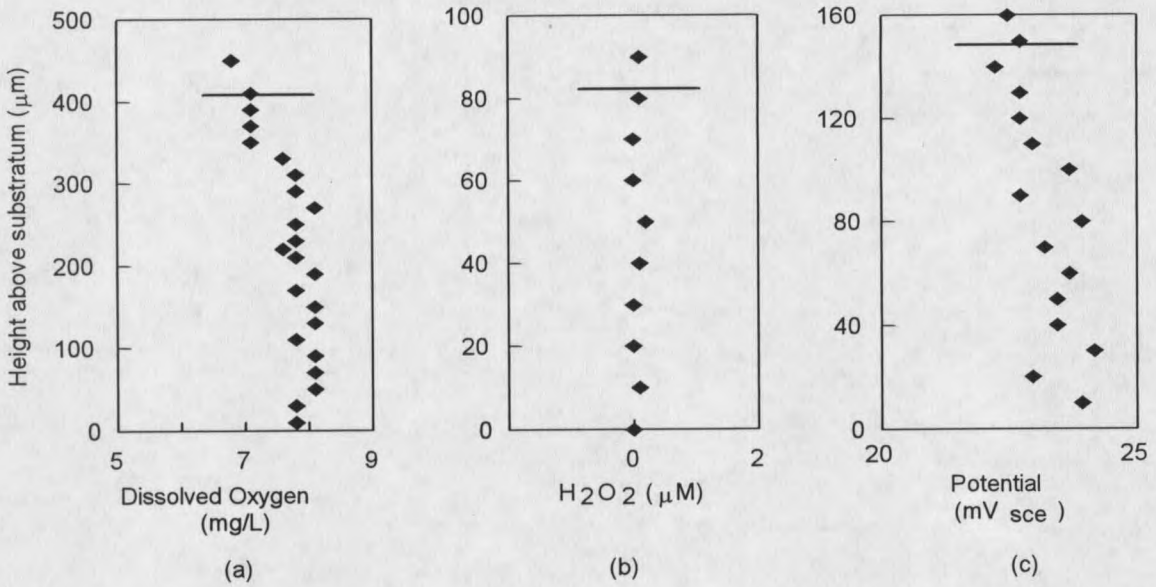

Figure 4.5. Microelectrode profiles in biofouling on Ennobled stainless steel coupons. Horizontal line indicates biofilm-solution interface. a) dissolved oxygen b) hydrogen peroxide c) E_{corr} for stainless steel probe.

The influence of H_2O_2 concentration on SS potential was determined by exposing a coupon to known concentrations of H_2O_2 in aerated river-water and measuring E_{corr} and pH. After correcting for -60 mV pH^{-1} unit change due to a slight acidification from the added H_2O_2, E_{corr} followed the relation:

$$E_{corr}\,(mV) = 283.2 + 91.8\ \mathrm{Log}\,[H_2O_2] \qquad (4.2)$$

over the H_2O_2 concentration range 0.1 to 100 mM. For H_2O_2 concentration less than 30 μM, E_{corr} was constant at -110 mV.

Equation 4.2 shows that H_2O_2 must reach nearly molar concentrations to account for Ennoblement. While microelectrodes cannot directly measure concentrations at the metal surface, simple mass transfer calculations based on linear diffusion put an upper limit on these concentrations. Specifically, H_2O_2 concentrations less than 2 μM at a distance just a few micrometers from the surface could not have coexisted with steady-state surface concentrations as great as 30 μM. It was concluded that H_2O_2 did not cause nor contribute to Ennoblement under the conditions of our study.

E_{corr} for the SS microelectrode reflects concentrations of dissolved oxidants. The purpose in using the SS microelectrode was to see how E_{corr} in the biofouling deposits compared with E_{corr} for the substratum. The fact that probe E_{corr} did not change was evidence that E_{corr} for the substratum was influenced by near surface conditions, and not by general accumulation of dissolved oxidants within the biofouling. These surface conditions did not appear to involve near surface accumulation of dissolved oxidants, since such accumulation would have been expected to cause a potential gradient near the surface, which was not observed.

Saturation DO levels throughout the biofouling indicated low net respiration rates possibly resulting from carbon limiting growth conditions. Oxygenated conditions are incompatible with growth of sulfate reducing bacteria[26], consequently it was unlikely that elevated cathodic depolarization caused by hydrogen sulfide reduction or formation of kinetically active iron sulfide were factors in Ennoblement. Evidence that aerobic conditions

were necessary for Ennoblement was obtained by adding excess glucose to reactor influent media, causing DO within the biofouling to decrease rapidly to less than 0.1 ppm. Within 48 hours after glucose addition, E_{corr} for Ennobled coupons decreased from +225 to -400 mV. Sixty hours after re-establishing aerated conditions, E_{corr} had regained values greater than +200 mV.

Results of microelectrode measurements indicated that Ennoblement was not caused by elevated levels of dissolved oxidants under the conditions of the present study, and was unlikely to have resulted from formation of reduced sulfur deposits. This focused attention on factors that could increase the reduction rate of DO, the dominant cathodic reactant.

Capacitance Studies

Capacitance and E_{corr} for a set of 11 coupons exposed by suspending into reactor solution from above, were measured during up to 50 days exposure to river water. E_{corr} alone was then monitored for up to 120 days exposure. E_{corr} for seven coupons from the set (Group #1) began to increase at 25-35 mV day^{-1} after four days exposure. E_{corr} for five samples from Group #1 stabilized at +400 to +410 mV after four weeks. After 120 days exposure, one of these five was removed for galvanostatic reduction measurements (coupon 1-A)[3]. The sixth sample from Group #1 reached +283 mV after 22 days and was then removed for galvanostatic reduction measurements (1-B). Potential for the last sample in Group #1 became unstable after reaching +143 mV, then decreased rapidly to -150 mV. Of

[3] Sample identification is indicated in parentheses following the sample description for each coupon used in galvanostatic reduction measurements

the remaining four coupons (Group #2), two showed a slower increase in E_{corr} and were removed after 22 days exposure for galvanostatic reduction measurements (2-A and 2-B), and two showed little change in potential during the exposure period. One of the last two was removed after 22 days (2-C), and one after 120 days (2-D) for galvanostatic reduction measurements.

Microscopic examination of several coupons from Group #1 and one coupon from Group #2 after 50 days exposure showed that approximately 20% of each coupon surface was covered with biofouling ranging from 2 to 60 μm in thickness. Over the remaining surface only the SS substratum was visible.

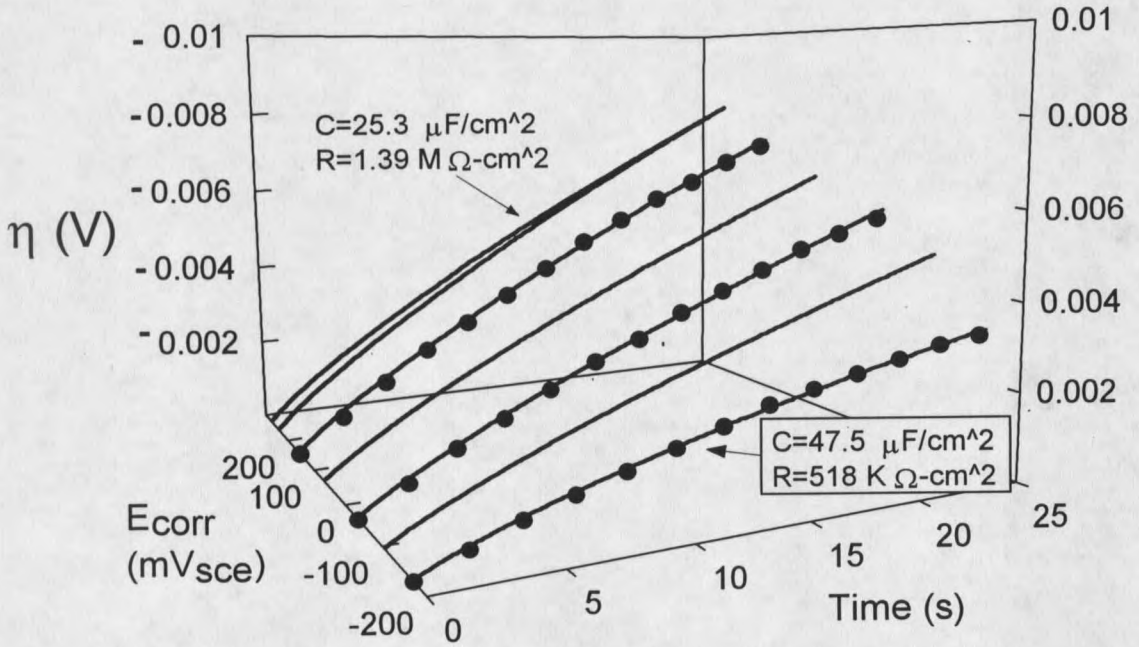

Figure 4.6. Evolution of cathodic response to 10 nA cm^{-2} galvanostatic pulse as E_{corr} increases during biofouling of stainless steel in fresh river water. Data shown by solid lines, solid circles indicate points generated from curve fit to equation 4.1.

Figure 4.6 shows the evolution of cathodic response to a 10 nA cm^{-2}, 25 second, galvanostatic pulse, for a representative sample from Group #1, as E_{corr} increased during the exposure period. The overvoltage-time response fit to equation 4.1 by non-linear regression was used to determine R_p and C. The 10 ms sampling interval during the measurements is reflected by the continuous data curves in the figure, while filled circles indicate individual points generated from the computed R_p and C values. It can be seen that data was fit well by the simple parallel RC model used to generate equation 4.1. Initial values of R_p and C for all samples in Groups #1 and #2 were in the ranges 0.5 to 1.5 megohms(MΩ)-cm^2 and 35-55 microfarads(μF)-cm^{-2} respectively, in good agreement with results obtained for SS by Mansfeld et al.[27] using electrochemical impedance spectroscopy techniques. The steady increase in final overvoltage with increasing E_{corr} shown in figure 4.6 likely reflected development of increasing cathodic Tafel slope during Ennoblement, and appeared as an increase in the value of R_p. A corresponding decrease in capacitance for data from figure 4.6 is shown clearly in figure 4.7a. In contrast, figure 4.7b shows constant capacitance vs. time behavior for one of the coupons from group #2 that exhibited little change in E_{corr} during exposure.

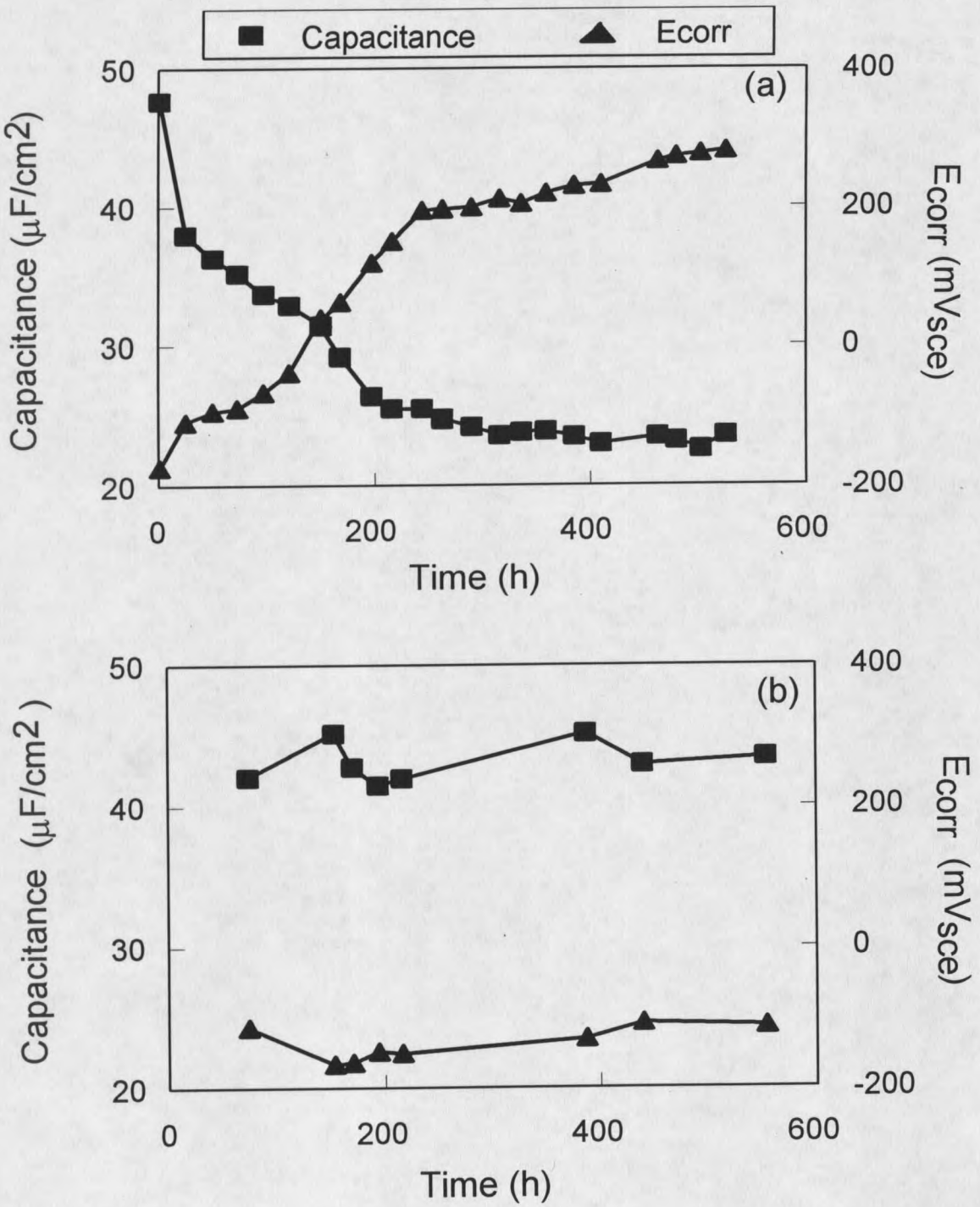

Figure 4.7. Capacitance and E_{corr} vs. time for two 316L stainless steel coupons during biofouling in fresh river water. (a) E_{corr} Ennobled during exposure (b) E_{corr} nearly constant during exposure.

To determine if the difference in capacitance behavior for coupons in figures 4.7a & 4.7b was due to a difference in biofouling accumulation, the extent of coverage and morphology of biofouling on the coupons was assessed by microscopic examination at the end of the exposure period. Biofouling on the two coupons was found to be indistinguishable. This finding indicated that neither duration of exposure nor the mere presence of biofouling could account for the decrease in capacitance shown in figure 4.7a, and suggested that the changes in capacitance correlated with the as yet undetermined factors that caused Ennoblement.

To determine if capacitance changes were due solely to increased potential, capacitance for a coupon that had been prepared in identical manner to the exposed coupons, was measured while the coupon was polarized by constant anodic current. For each potential, polarizing current was applied for approximately one hour until potential drift was less than 2 mV h^{-1} before making the capacitance measurements. Data given by open squares in figure 4.8 shows capacitance was independent of potential over the range -100 to +200 mV. This finding was in agreement with results obtained by Popat and Hackerman[28] for SS in 0.1 M Na_2SO_4 at neutral pH.

The strong correlation between capacitance and Ennobled E_{corr} is shown in figure 4.8 for six samples from Group #1. In the figure, capacitance is expressed as a fraction of initial capacitance (C_{init}) to account for variation in true surface area of the coupons. Data is satisfactorily expressed by the relation:

$$dC/dE_{corr} = -0.05 +/-0.009\ \mu F\ cm^{-2}\ mV^{-1} \qquad (4.3)$$

obtained by linear regression of the data between -100 and +200 mV for each of six coupons. The average and standard deviation of the slope for the six coupons is shown.

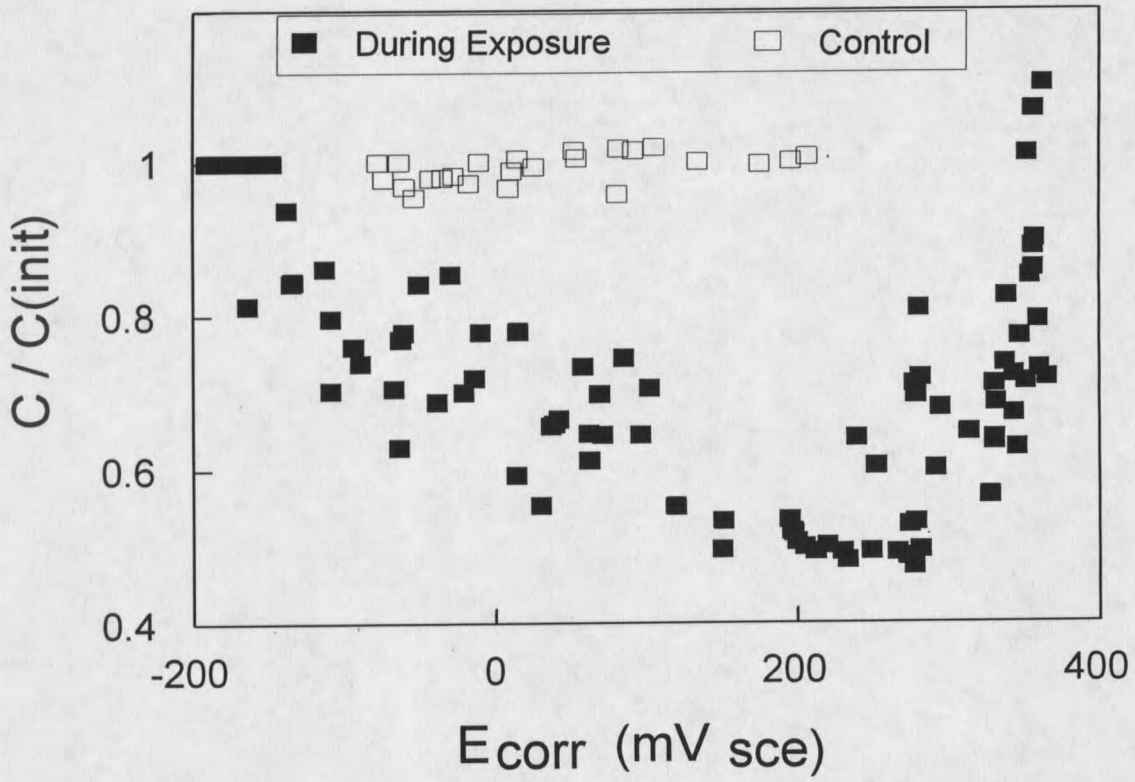

Figure 4.8. Capacitance ratio vs E_{corr} for 6 stainless steel coupons during biofouling in fresh river water and for control coupon. C(init) is capacitance prior to exposure.

Origin of the observed correlation was not established, and the relation was not interpreted as causal. It could be argued that sustained elevated potential due to as yet unknown microbial processes altered passive film characteristics, as is known to occur for metals anodized at dc potentials[29]. If these conditions thickened the oxide film or decreased the dielectric constant to the point where passive film capacitance was of the order of double layer capacitance, the series equivalent oxide-double layer capacitance would have begun to

reflect contribution from the oxide. In this scenario, decreased capacitance would have appeared as a consequence of sustained elevated potential.

In a reverse sense, microbial processes may have influenced capacitance by directly altering the oxide surface, which may at the same time have caused Ennoblement by the oxide scenario described under the *E_{corr} Measurements* section. Reported capacitance[17] for Fe_3O_4 in acidic and alkaline media ranges between 50 and 300 μF cm^{-2} while capacitance for γ-FeOOH at neutral pH is reported as 11 μF cm^{-2}. The decreased capacitance during Ennoblement was consistent with transformation of Fe_3O_4 to γ-FeOOH at the inner layer of a duplex passive film[30], and may have reflected formation of other +3 iron-oxides[31]. Vago et al.[17] showed DO reduction at -200 mV, pH 10, to be 5 times more rapid on γ-FeOOH than on Fe_3O_4. This difference in rate quite closely matched that shown at -200 mV in figure 4.4 for SS before and after Ennoblement. These considerations suggested that changes in capacitance and cathodic current density may have both arisen from changes in surface-oxide properties.

The nature of the increase in capacitance as potential approached +300 mV shown in figure 4.8 was not understood, however the shape of galvanostatic curves used to determine capacitance in this potential region showed increasing curvature for times less than 5 seconds. The curvature increased with increasing duration of exposure for the Ennobled coupons. It was necessary to incorporate an additional time constant in the model circuit by placing a second parallel RC pair in series with the first, to fit galvanostatic data for times less than 5 seconds at potentials above +300 mV. With this model, the analytical solution for constant applied current is:

$$\eta_{act} = I_{app}\left\{R_p\left(1 - e^{-\frac{t}{R_p C_{dl}}}\right) + R_f\left(1 - e^{-\frac{t}{R_f C_f}}\right)\right\} \qquad (4.4)$$

where R_f and C_f are the resistance and capacitance associated with the oxide layer, C_{dl} is the double layer capacitance, and other terms are as defined for equation 4.1. While the physical significance of the circuit model is equivocal, it is commonly invoked for defect free coatings[32,33], and provided a satisfactory fit to data in this study. Applying equation 4.4 to data obtained for a coupon at +330 mV, and 24 days later for the same coupon at +360 mV, showed a decrease in apparent oxide film capacitance from 50 to 28 μF cm^{-2} and an increase in double layer capacitance from 66 to 212 μF cm^{-2}. This corresponded to a slight increase in series equivalent capacitance and suggested that oxide film capacitance continued to decrease with time, at potentials above +300 mV. In light of the increasing curvature of galvanostatic measurements at these potentials however, data for the region above +300 mV in figure 4.8 should be taken as provisional. It is emphasized as shown in figure 4.6, that data for potentials below approximately +300 mV was fit well by equation 4.1.

R_p and E_{corr} vs. time for data in figure 4.6 is shown in figure 4.9. As noted, steeper cathodic polarization slopes characteristic of Ennoblement would have caused R_p to increase if i_{corr} and the slope (B_a) of the anodic polarization curve near E_{corr} remained constant. Figure 4.4 shows that i_{corr} increased only slightly if at all during Ennoblement, while B_a was expected to have changed little in the passive region. Consequently, it was likely that R_p reflected changes in cathodic polarization slope. These changes may have been related to electrical conductivity in the oxide, that would have limited cathodic rate if increasing oxygen reduction rate

approached the rate of electron conduction. The effect is analogous to a series reaction mechanism. The influence of oxide conductivity on net cathodic rate would have been even greater if the conductivity decreased during Ennoblement as would have occurred with transformation of conductive Fe_3O_4 to a semi-conducting, ferric-oxide phase. The latter consideration suggested that cathodic polarization behavior for Ennobled SS was consistent with an Fe_3O_4 / ferric-oxide transformation as was noted in interpreting the capacitance measurements.

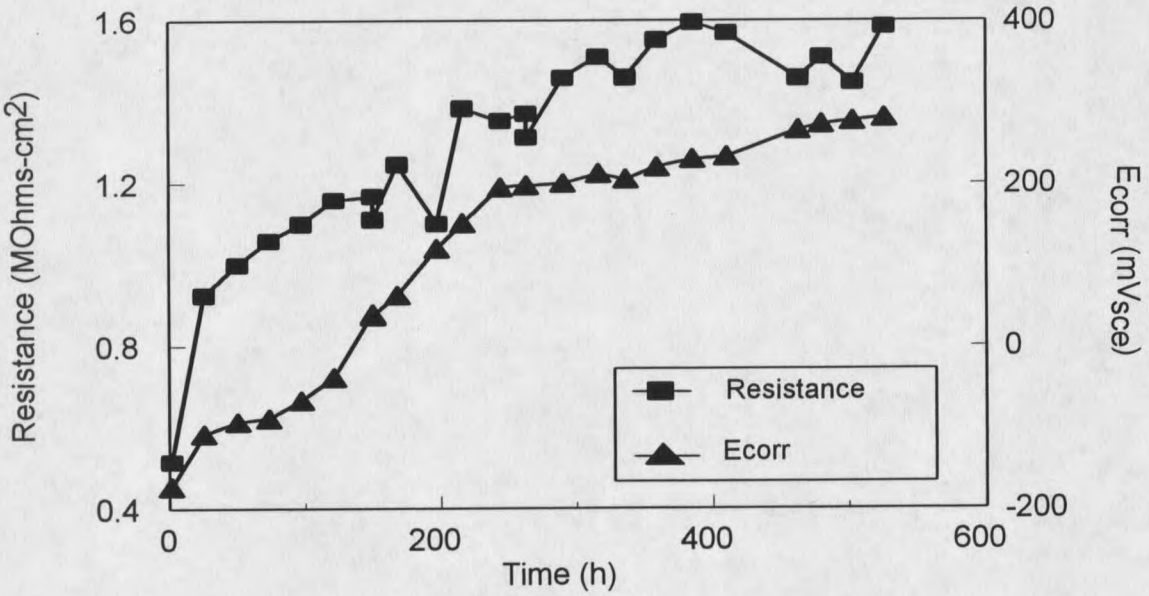

Figure 4.9. Polarization resistance and E_{corr} vs time for 316L stainless steel during biofouling in fresh river water.

Galvanostatic Reduction Measurements

Capacitance measurements suggested that in addition to biofouling accumulation, other surface changes occurred during Ennoblement. To investigate the nature of such

changes, constant cathodic current, applied to coupons in deaerated, depolarizer-free media, was used to analyze composition and quantity of reducible, surface-bound material on the metal. These galvanostatic reduction measurements were carried out prior to exposure for coupons 1-B, 2-A, 2-B, and 2-C identified in the previous Section. Replicate measurements were performed on coupons 2-A, 2-B, and 2-C prior to exposure by preparing the coupons as described under the Experimental Procedure section and carrying out galvanostatic reduction, then resurfacing the coupons and repeating the galvanostatic reduction measurements. Results of the replicate measurements shown as pre-exposure curves in figures 4.10a through 4.10c, indicated that the quantity of reducible, surface-bound material was highly reproducible over repeated surface preparations. The data also revealed dramatic sample to sample variation in the amount of reducible material present. The latter finding was surprising considering that all samples were from the same metallurgical heat. The coupon in figure 4.10a. showed a purely capacitive response until hydrogen evolution began at about -1.6 V, indicating a complete absence of reducible material. The capacitive response gave the value 68 $\mu F\ cm^{-2}$, which was obtained using the relation:

$$C = I_{app} / (dE/dt) \qquad (4.5)$$

The absence of a region of potential lag indicated that this coupon possessed little reducible surface-bound material. In contrast, coupons in figures 4.10b through 4.10d showed a clear potential lag between -0.5 and -0.8 V characteristic of Fe_2O_3[18] reduction, and a potential arrest at -0.85 V close to the potential, -0.92 V, reported for reduction of Fe_3O_4[30,31]. The inflection point at -0.77 V observed for the pre-exposure curves in figure 4.10b allowed

the charge (Q) associated with reduction of the surface-bound material to be estimated as 5.5 millicoulombs(mC) cm^{-2}. Using a roughness factor (γ) = 1.2 for Fe abraded on 600 grit paper[34]; a density (ρ) = 5.6 g cm^{-3} and formula weight (M) = 159.7 g for γ-Fe_2O_3[34]; and assuming the potential lag was due to the reaction:

$$3Fe_2O_3 + H_2O + 2e^- \Leftrightarrow 2Fe_3O_4 + 2OH^- \qquad ;E^{o'}_{(pH\,8.5)} = -0.529\ V_{SCE} \quad (4.6)$$

a thickness (x) of 6.8 nm for the Fe_2O_3 layer was calculated, where:

$$x = (Q\,M) / (n\,F\,\gamma\,\rho)\ ^{34} \qquad (4.7)$$

and F is Faraday's constant. This value was somewhat larger than reported values of 1-3 nm[35] and may have reflected the substantial region of potential lag for this coupon. Applying the same analysis to pre-exposure data from figures 4.10c and 4.10d, and assuming all Fe_2O_3 was reduced at potentials more positive than -0.82 V, gave Fe_2O_3 thickness of 2 and 1.5 nm for figure 4.10c and 4.10d respectively.

After obtaining pre-exposure reduction curves, the four coupons were again resurfaced and exposed to river water for 22 days. As indicated in figures 4.10a - 4.10d, potentials were -273, +81, +165, and +283 for coupons 2-C, 2-A, 2-B, and 1-B respectively after exposure. Microscopic examination after exposure showed the surfaces for all coupons were only 3 to 5% covered by biofouling ranging from 2 to 40 μm in thickness. No differences in biofouling or other surface properties were observed between coupons with the exception that a crevice, ranging from one to several μm in width and several hundred μm in length, was observed near the edge of the coupon in figure 4.10c. Figure 4.10a shows that

neither increased amounts of reducible surface-bound material nor elevated potential developed on a coupon initially possessing no reducible material. In contrast, both E_{corr} and the quantity of reducible material increased for the three coupons that did initially possess a reducible phase.

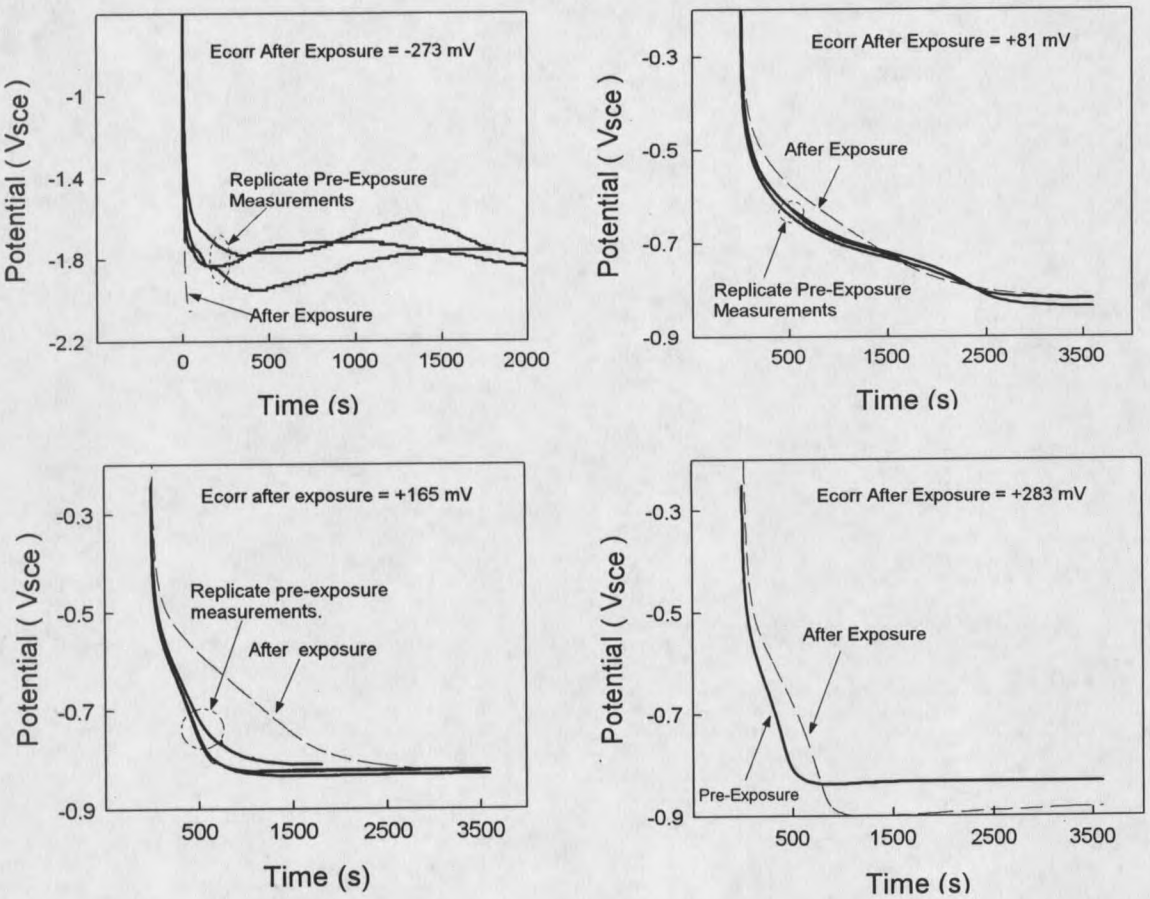

Figure 4.10. Galvanostatic reduction of 316L stainless steel in deareated 0.1 M Na_2SO_4, pH 8.5 for 4 coupons before and after 22 day exposure in fresh river water. 2.5 uA cm^{-2} applied current.

Figure 4.11 shows galvanostatic reduction behavior after 120 days exposure for an Ennobled coupon (1-A), and for a coupon showing no Ennoblement (2-D), identified in the previous section. Although E_{corr} for coupon 1-A decreased slightly during transfer to the

galvanostatic reactor, potentials for the two coupons were +314 and -75 mV respectively prior to galvanostatic reduction. The curves illustrate that in the absence of Ennoblement, galvanostatic reduction behavior was similar to that observed prior to exposure (cf. figure 4.10b), while for the Ennobled sample, a new region of potential lag appeared between 0 and -0.55 V, indicating the presence of a new reducible surface phase. Although the identity of this phase was not determined, its appearance was further indication that the surface state of the SS substratum was modified during Ennoblement.

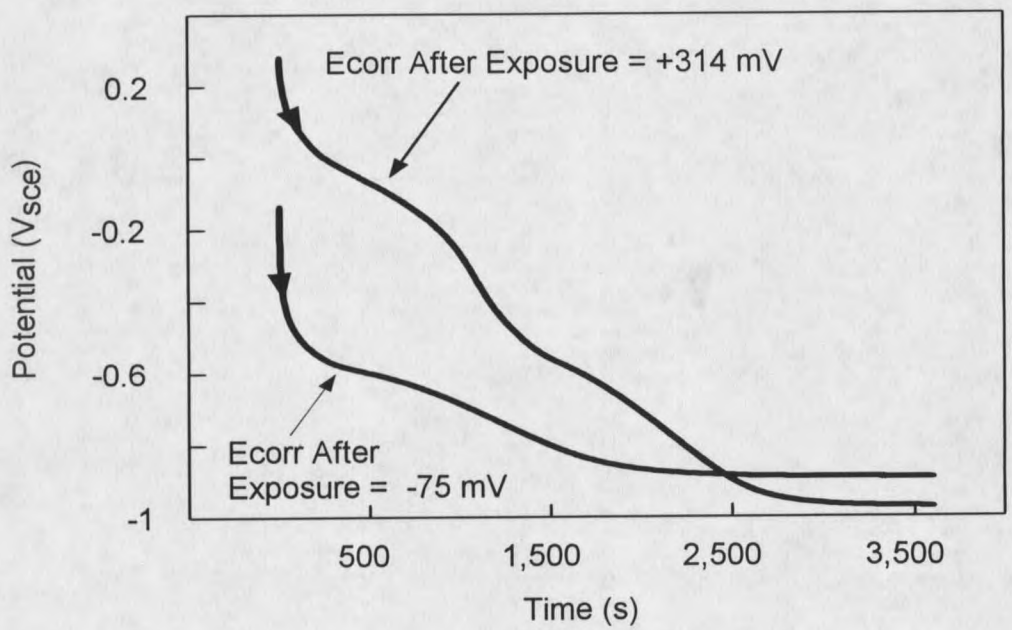

Figure 4.11. Galvanostatic reduction behavior for two 316L stainless steel coupons in deareated 0.1 M Na_2SO_4, pH 8.5 after biofouling during 4 months exposure to fresh river water. 2.5 uA cm^{-2} applied current.

Interpretation of results from the galvanostatic reduction experiments were complicated by the lack of a satisfactory control coupon, and by the substantial crevice that occurred for the coupon of figure 4.10c during the exposure period. Nevertheless, data from

figure 4.10a show that mere exposure and biofouling were not sufficient to increase the abundance of reducible surface-bound material. Rather, the increase seemed to be associated with increased E_{corr}. Similarly, figure 4.11 shows that a new reducible surface phase appeared in association with Ennoblement, not solely from exposure and biofouling. As for the results of the capacitance study, these relationships cannot be considered causal, but they do provide evidence that the amount of reducible surface-bound material on SS increased during the Ennoblement process.

Conclusions

- Stainless steel exposed to fresh river water developed elevated E_{corr} and increased cathodic current density characteristic of passive metal Ennoblement.
- Ennoblement was related to E_{corr} near the beginning of exposure. The apparent minimum E_{corr} at 10 hours exposure required for Ennoblement to develop was -110 mV.
- Ennoblement was not caused by elevated concentrations of dissolved oxidants under the conditions of this study.
- Capacitance and E_{corr} were correlated over the potential range -100 to +200 mV and followed the relation:

$$dC/dE_{corr} = -0.05 +/- 0.009\ \mu F\ cm^{-2}\ mV^{-1}$$

- A new reducible surface phase developed during Ennoblement, characterized by a potential lag at 0 mV_{SCE} for 2.5 $\mu A\ cm^{-2}$ applied cathodic current.

References Cited

1. Mollica, A., (1976). The Influence of the Microbiological Film on Stainless Steels in Natural Seawater, in: The 4th International Congress on Marine Corrosion and Fouling (Antibes, France, 1976), p. 351-365.

2. Scotto, V., R. DiCintio, and G. Marcenaro, (1985). The Influence of Marine Aerobic Microbial Film on Stainless Steel Corrosion Behaviour. Corr. Sci. **25:**185-194.

3. Dexter, S. C. and H-J Zhang, (1990). Effect of Biofilms on Corrosion Potential of Stainless Steel Alloys in Estuarine Waters, in: The 11th International Corrosion Congress (Associazone Italiana di Metallurgia, Florence, Italy) p. 333-340.

4. Mollica, A., *et al.*, (1989). Cathodic Performance of Stainless Steels in Natural Seawater as a Function of Microorganism Settlement and Temperature. Corrosion **45:**48-56.

5. Scotto, V., M. Beggiato, G. Marcenaro and R. Dellepiane, (1993). Microbial and Biochemical Factors Affecting the Corrosion Behaviour of Stainless Steels in Seawater. in: Marine Corrosion of Stainless Steels: Chlorination and Microbial Effects. Ijsseling, F.P., ed. (The Institute of Materials, London), pp. 21-33.

6. Chandrasekaran, P. and S. C. Dexter, (1993). Mechanism of Potential Ennoblement on Passive Metals by Seawater Biofilms, CORROSION/93 paper no. 493 (NACE, Houston, TX).

7. Holthe, R., P. O. Gartland, and E. Bardal, (1987). Influence of the Microbial Slime Layer on the Electrochemical Properties of Stainless Steel in Sea Water, SINTEF Report No. STF16 A87123 (Foundation for Scientific and Industrial Research at the Norwegian Institute of Technology, Trondheim, Norway).

8. Mollica, A. (1992). Biofilm and Corrosion on Active-Passive Alloys in Seawater. Internat. Biodeterior. Biodegrad. **29:**213-229.

9. Motoda, S., Y. Suzuki, T. Shinohara, and S. Tsujikawa, (1990). The Effect of Marine Fouling on the Ennoblement of Electrode Potential for Stainless Steels. Corr. Sci. **31:**515-520.

10. Dexter, S.C. and G.Y. Gao, (1988). Effect of Seawater Biofilms on Corrosion Potential and Oxygen Reduction of Stainless Steel. Corrosion **44:**717-723.

11. Johnsen, R. and E. Bardal, (1985). Cathodic Properties of Different Stainless Steels in Natural Seawater. Corrosion. **41:**296-305.

12. Uhlig, H. H., (1971). Corrosion and Corrosion Control. (John Wiley & Sons, New York, NY), 419 pp.

13. Hassan, H. M. and I. Fridovich, (1984). Oxygen Toxicity in Prokaryotes, in: The Biology and Chemistry of Active Oxygen, Bannister, J.V. and W. H. Bannister, eds., Developments in Biochemistry Vol. 26, (Elsevier, New York, NY) p. 134.

14. Glenn, J. K. and M. H. Gold, (1985). Purification and Characterization of an Extracellular Mn(II)-Dependent Peroxidase from the Lignin-Degrading Basidiomycete. Arch. Biochem. Biophys. **242:**329-341.

15. Jovancicevic, V. and J.O'M. Bockris, (1986). The Mechanism of Oxygen Reduction on Iron in Neutral Solutions. J. Electrochem. Soc. **133:**1797-1807.

16. Zecevic, S., D. M. Drazic, and S. Gojkovic, (1991). Oxygen Reduction on Iron-V. Processes in Boric Acid-Borate Buffer Solutions in the 7.4-9.8 pH Range. Corr. Sci. **32:**563-576.

17. Vago, E. R., E. J. Calvo, and M. Stratmann, (1994). Electrocatalysis of Oxygen Reduction at Well-Defined Iron Oxide Electrodes. Electrochim. Acta **39:**1655-1659.

18. Ramasubramanian, N., N. Preocanin, and R.D. Davidson, (1985). Analysis of Passive Films on Stainless Steel by Cyclic Voltammetry and Auger Spectroscopy. J. Electrochem. Soc. **132:**793-798.

19. Greenwood, N. N. and A. Earnshaw, (1990). Chemistry of the Elements (Pergamon Press, New York, NY) 1543 pp.

20. Mollica, A., G. Ventura, E. Traverso, and V. Scotto, (1988). Cathodic Behavior of Nickel and Titanium in Natural Seawater. Internat. Biodeterior. **24:**221-230.

21. Jones, D.A., (1992). Principles and Prevention of Corrosion, (Macmillan Publishing Company, New York, NY) 568 pp.

22. Lewandowski, Z., W.C. Lee, W.G. Characklis, and B. L. Little, (1988). Dissolved Oxygen and pH Microelectrode Measurements at Water Immersed Metal Surfaces, CORROSION/88 paper no. 93 (NACE, Houston, TX).

23. DeBeer, D., P. Stoodley, F. Roe, and Z. Lewandowski, (1994). Effects of Biofilm Structures on Oxygen Distribution and Mass Transport. Biotech. Bioeng. **43:**1131-1138.

24. Tomashov, N. D. and G. P. Chernova, (1967). Passivity and Protection of Metals

Against Corrosion, (Plenum Press, New York, NY) 208 pp.

25. Anastasijevic, N. A., Z. M. Dimitrijevic, and R.R. Adzic, (1986). Oxygen Reduction on Ruthenium. J. Electroanal. Chem. **199**:351-364.

26. Lee, W., *et al.*, (1993). Corrosion of Mild Steel Underneath Aerobic Biofilms Containing Sulfate-Reducing Bacteria. Part II: At High Dissolved Oxygen Concentration. Biofouling **7**:217-239.

27. Mansfeld, F., *et al.*, (1992). An Electrochemical and Surface Analytical Study of Stainless Steels and Titanium Exposed to Seawater. Corr. Sci. **33**:445-456.

28. Popat, P. V. and N. Hackerman, (1961). Electrical Double Layer Capacity of Passive Iron and Stainless Steel Electrodes. J. Phys. Chem. **65:**1201-1205.

29. Song, G. L., C. N. Cao, and H.C. Lin, (1993). Effects of AC-Modulated Passivation and Post-Treatment on Composition and Stability of Passive Films. Corrosion **49:**271-277.

30. Rozenfeld, I. L., (1981). Corrosion Inhibitors. (McGraw-Hill, San Francisco, CA), 327 pp.

31. Nagayama, M-I. and M. Cohen, (1961). The Anodic Oxidation of Iron in a Neutral Solution I. The Nature and Composition of the Passive Film. J. Electrochem. Soc. **109:**781-790.

32. Isaacs, H. S. and Y. Ishikawa, (1985). Current and Potential Transients During Localized Corrosion of Stainless Steel. J. Electrochem. Soc. **132:**1288-1293.

33. Grandle, J. A. and S. R. Taylor, (1994). Electrochemical Impedance Spectroscopy of Coated Aluminum Beverage Containers: Part 1 - Determination of an Optimal Parameter for Large Sample Evaluation. Corrosion **50:**792-803.

34. Ferreira, M. G. S. and J. L. Dawson, (1985). Electrochemical Studies of the Passive Film on 316 Stainless Steel in Chloride Media. J. Electrochem. Soc. **132:**760-765.

35. Babic, R. and M. Metikos-Hukovic, (1993). Oxygen Reduction on Stainless Steel. J. Appl. Electrochem. **23:**352-357.

CHAPTER 5

ENNOBLEMENT BY MANGANIC OXIDE BIOFOULING *

Overview

Twenty-three 316L stainless steel (SS) coupons were exposed *in situ* to fresh river-water for periods up to 35 days. All samples developed steady-state corrosion potentials (E_{corr}) near +350 mV(SCE) and polarization measurements showed enhanced cathodic current density characteristic of passive metal Ennoblement. Epifluorescence and scanning electron microscopy of the attached biofilm showed numerous 10-20 μm diameter Mn-rich annular deposits, associated clusters of bacterial cells, and abundant sheathed bacteria. Dissolution of the Mn deposits using Na_2SO_3 shifted E_{corr} to pre-exposure values. SS coated with MnO_2 paste displayed electrochemical behavior nearly identical to that of Ennobled samples. A mechanism of Ennoblement by MnO_2 biofouling is proposed which explains a variety of findings concerning the electrochemical behavior of microbially colonized SS.

---

* Published as: *The Ennoblement of Stainless Steel by Manganic Oxide Biofouling*, W. H. Dickinson, F. Caccavo Jr., and Z. Lewandowski (1996), Corrosion Science **38**:1407-1422.

Introduction

Microbial colonization of passive metals can shift corrosion potential (E_{corr}) in the noble direction[1-6] and produce accompanying increases in current density and polarization slope at mild cathodic potentials[7-11]. The phenomena, collectively known as Ennoblement, have been variously ascribed to depolarization of the oxygen reduction reaction[12,13], acidification of the electrode surface[14], the combined effect of elevated H_2O_2 and decreased pH[6], and production of passivating siderophores[15]. Under marine conditions, Ennobled potentials can exceed critical pitting potentials for low-molybdenum stainless steels[16], and several cases of rapid loss of Ennoblement have been attributed to localized corrosion[3,10] Once initiated, pitting may proceed at accelerated rates due to the rapid cathodic reaction. These concerns have led to the use of elevated E_{corr} as an *in situ* diagnostic for potentially destructive microbial colonization of stainless steels[17]. Despite the notable technical impact of Ennoblement, widespread efforts have made little progress in establishing the underlying mechanism.

In a previous report[18] we presented evidence that ferric oxide abundance increases during Ennoblement and noted the possibility that Ennoblement arises from changes in surface metal oxide properties. It is known that reduction of ferric oxides occurs simultaneously with oxygen reduction during mild cathodic polarization of iron[19], indicating that ferric oxides can serve as cathodic depolarizers. As early as 1967 it was also shown that manganese oxides could be used to cathodically depolarize stainless steel under strongly acidic conditions[20]. In these applications, galvanically coupled MnO_2 provided the high cathodic current density required for passivation in the acidic medium. Further, MnO_2 depolarization of stainless steel

under alkaline conditions is a key characteristic in alkaline-manganese battery design[21-23]. Clearly, iron and manganese oxides may be expected to contribute to cathodic current on stainless steel.

It is well known that iron and manganese oxides can be deposited by a variety of bacteria, including but not limited to the sheathed bacteria *Leptothrix*[24] and the capsule forming bacteria *Siderocapsa*[25]. Manganese-oxidizing bacteria are widely distributed in both marine and fresh waters, and have been investigated as a basis for biological removal of manganese from drinking water[26] and as a possible source of battery grade manganese dioxide[27]. In aqueous environments, sheathed bacteria are responsible for tubercle formation on mild steels and allegedly promote severe pitting of stainless steel by production of aggressive ferric and manganic chlorides[28-30]. A possible direct role of MnO_2 in microbially influenced corrosion has been noted[31,32], and massive structural failure due to microbial MnO_2 deposition has been reported[33]. Despite these considerations, the direct influence of microbially deposited MnO_2 on the electrochemical behavior of passive metals has received little attention.

The widespread natural abundance of manganese-oxidizing bacteria and the cathodic reactivity of MnO_2 suggest that the cathodic changes that occur during Ennoblement may be due to MnO_2 biofouling. The goal of this paper is to demonstrate that manganic oxide biofouling can account for the electrochemical phenomenon of Ennoblement.

Experimental Methods

A threefold approach was taken to assess the possible influence of MnO_2 biofouling on Ennoblement: 1) biofilms on Ennobled coupons were analyzed for the presence of Mn, 2) the electrochemical properties of SS coated with a chemically prepared MnO_2 paste were determined and compared with those for Ennobled coupons, and 3) E_{corr} was monitored as MnO_2 was dissolved from coupon surfaces by chemical reduction with Na_2SO_3.

In situ Exposure

A set of 23 epoxy-embedded 316L SS coupons (UNS S31603; 1.59 cm dia) were exposed to fresh, flowing stream-water at a field site near Bozeman, MT, by mounting the coupons in a 2 cm wide x 60 cm long open-channel polycarbonate reactor and submersing the reactor below the stream surface. Elemental composition of the coupons is given in Table 5.1. Mounting was such that a single face of each coupon was exposed in an inverted orientation that prevented suspended solids from settling onto the coupon surface. Based on chemical composition, the field site classifies as a clean stream (dissolved oxygen > 6 ppm; pH 8-8.5; alkalinity 3 meq L^{-1}; nitrate ion 1.2 ppm; Ca^{2+} 58 ppm; Mg^{2+} 15 ppm; Cl^- 3 ppm; dissolved Fe 200 ppb; conductivity 4 x 10^{-4} $ohm^{-1}cm^{-1}$; total organic carbon 110 ppm). Temperature during the exposure was between 11 and 15° C, and dissolved Mn concentration was 10-20 ppb. Prior to the exposure, coupons were abraded on wet 600 grit silicon carbide paper, rinsed and sonicated in distilled water, rinsed with 95% ethanol, and air dried. In addition to the

coupons, a set of glass microscope cover slips (18 mm x 18 mm x 1 mm) and several 1 cm x 1 cm x 0.5 cm pieces of reticulated vitreous carbon were exposed by submerging approximately 50 cm upstream from the coupons at the field site. These materials were used to determine if the metal substratum or dissolved metals from the stream water were the source of metal-rich microbial deposits, and to determine the influence of anodic passivation current on limiting values of Ennobled potentials.

Composition (Wt %)

C	Cr	Cu	Fe	Mn	Mo	Ni	P	S	Si
.020	17.01	--	bal	1.71	2.12	11.08	.035	.002	0.60

Table 5.1. Elemental composition of 316L SS coupons (as provided by vendor, Metal Samples Inc. Munford, AL)

E_{corr} was measured vs. the saturated calomel electrode (all potentials are reported vs. the SCE) at roughly 1 to 3 day intervals. At these times, any accumulated material on the reactor floor was removed by flushing in stream water. While some solids typically settled on the reactor floor between flushings, these were never in contact with the coupons. For polarization measurements, samples were transported in stream water to the laboratory then cathodically polarized at -0.167 mV sec^{-1} against the SCE in either filtered stream water or 0.01M Na_2SO_4- pH 8.4, using a Princeton Applied Research model 273A potentiostat. The counter electrode was Pt foil (12.5 cm^2). Polarization curves carried out in the two media were indistinguishable. To determine the influence of oxygen on cathodic behavior, one sample was placed in argon-deaerated media for 30 minutes then polarized in the same

deaerated media using the conditions given above. For these measurements, dissolved oxygen was measured using an Orion 97-08-00 dissolved-oxygen electrode.

Biofilm Characterization

Thickness of microbial deposits was evaluated using reflected-light microscopy by noting travel of the calibrated stage adjustment while focusing first at the substratum then at the top of the deposits. Surface coverage was determined by directly measuring the cross-sectional area (footprint) of several annular deposits using a calibrated graticule, then counting individual annular deposits within a fixed area and multiplying by the average area of the deposits. Bacteria within the biofilm were visualized by staining for 1-2 minutes with a 0.1% (w/v) solution of acridine-orange[34] followed by thorough rinsing with distilled water (DW), then viewing at either 400 or 1000x using an Olympus BH-2 epifluorescence microscope with 100W Hg-UV source. Qualitative tests for the presence of MnO_2 were based on development of the violet, oxidized form of leuco-crystal violet stain[35]. Briefly, 1 ml of 0.1% (w/v) leuco-crystal violet in 0.1N H_2SO_4 plus 2 ml 6M acetic acid / acetate buffer pH 4.0 were added to 7 ml DW and the resulting solution added dropwise to the material of interest. Acidified potassium ferrocyanide reagent[25] was used as a spot test for the presence of Fe(III) compounds. Morphology and elemental composition of the bacterial deposits were assessed by vapor coating specimens with 15 nm of graphite and analyzing using a Jeol JSM-6100 scanning electron microscope with energy-dispersive X-ray analysis (SEM/EDS). Total Mn abundance in the biofilm was determined by scraping material from the coupons using a

stainless steel razor blade, ashing 1 hour at 500° C, digesting to dryness in hot, concentrated HCl, redissolving in 3N HNO_3, and analyzing at 279.5 nm using a Perkin-Elmer 3100 flame atomic-absorption spectrophotometer.

Isolates of the naturally occurring Mn-oxidizing bacteria were obtained by streaking washed biofilm from the *in situ* exposed coupons onto a solid growth medium consisting of 1.0 g L^{-1} peptone, 0.1 g L^{-1} yeast extract, 0.5 g L^{-1} $MnSO_4 \cdot H_2O$ and 16 g L^{-1} Bacto Agar in DW[26]. Single colonies were then restreaked to obtain pure cultures. Mn-oxidizing capacity of these isolates was confirmed by formation of violet color on treatment with the leuco-crystal violet reagent.

MnO_2 Studies

The electrochemical behavior of MnO_2 coated SS was investigated by physically applying MnO_2 paste to a portion of the coupon surface using a wooden applicator, then making E_{corr} and polarization measurements as described above. These coupons were not part of the *in situ* exposure. For some of these measurements, the roughly 1 mm thick paste coating was allowed to stand in contact with the coupon overnight, and was then wiped off with a cotton swab. This left a thin, brown, surface film covering the area where the paste coating had been applied, that was easily visualized by light microscopy. Thickness and surface coverage of the film was assessed as described for the biofilm deposits.

The MnO_2 paste was prepared by reduction of permanganate with manganous ion under alkaline conditions[36] followed by repeated centrifugation and washing. pH of the final

MnO_2 suspension was 8.6. The paste was a finely divided material that produced a nearly continuous film when spread as a thin (<10 μm) coating on glass or SS.

MnO_2 was also deposited electrochemically by anodically polarizing coupons at 3 mA cm^{-2} for 20 seconds in a pH 6.4 solution containing 5 mM $MnSO_4$ and 0.1M Na_2SO_4. The quantity of electrodeposited MnO_2 was determined from the duration of the potential plateau corresponding to MnO_2 reduction as the deposited material was stripped from the surface by 10 uA cm^{-2} constant cathodic current.

Influence of MnO_2 on E_{corr} for SS was determined by reductively dissolving the MnO_2-rich deposits with sodium sulfite[37,38]. For these tests, Ennobled coupons or coupons partially covered with chemically prepared MnO_2 were mounted in a rotating disk electrode and rotated at 300 rpm in 75 ml argon-deaerated 1.0 M Na_2SO_4-pH 8.4 while E_{corr} was continuously monitored. At a specified time, 75 ml 1.0 M Na_2SO_3-pH 8.5 was added while E_{corr} monitoring was continued. At the end of these tests, the electrolyte was removed and analyzed for dissolved Mn by atomic-absorption spectrophotometry. The rotating disk electrode was used to ensure steady flux of reductant to the electrode and dispersion of soluble reaction products into solution.

Experimental Results

Electrochemical Behavior

E_{corr} for the set of 23 coupons exposed *in situ* began to increase within 24 hours of exposure and reached steady-state values near +350 mV within one to two weeks. Figure 5.1

shows data points for 3 samples from the set, depicting the varying rates of increase and illustrating that potentials for the coupons converge to a final value near +350 mV irrespective of the rate of increase. The shaded region in the figure envelopes the curves for all 23 coupons. For comparison, E_{corr} for a freshly prepared coupon, roughly one-third covered with a 100-200 μm thick layer of MnO_2 paste, is shown by the horizontal dashed line. Potential for this sample remained stable between +350 and +360 mV during a 24 hour monitoring period following coating.

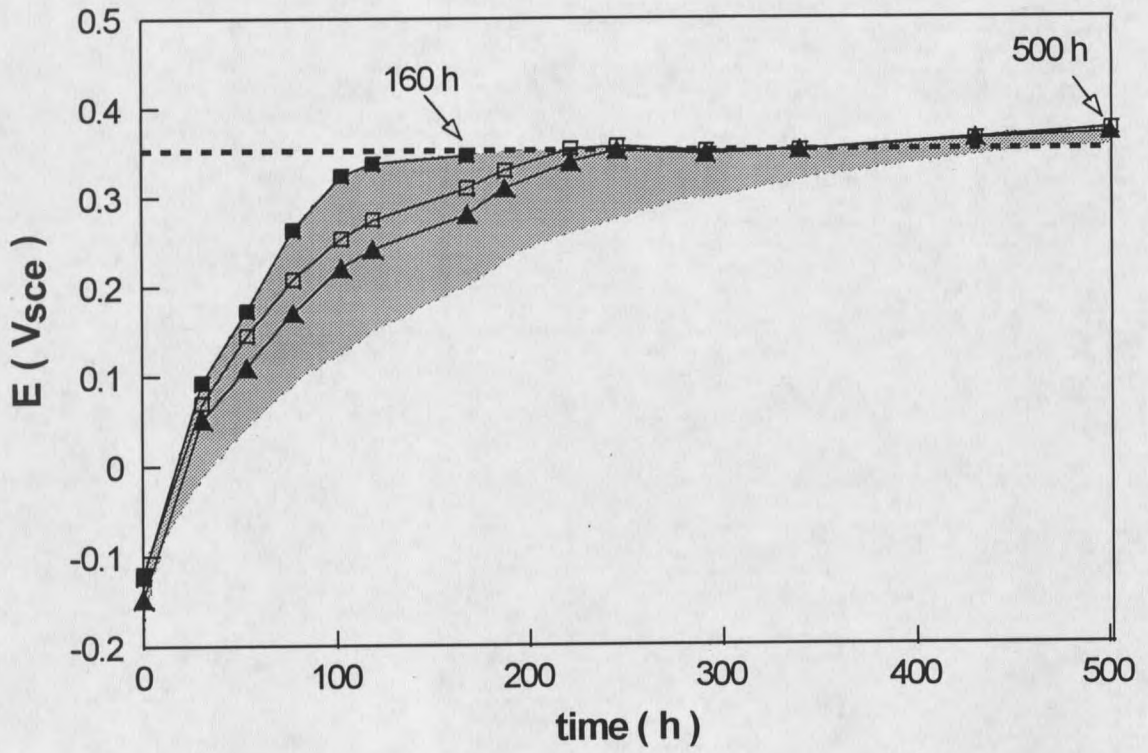

Figure 5.1. E_{corr} vs. time for 316L stainless steel coupons during *in situ* exposure to fresh river-water. Data points for 3 coupons used for polarization measurements are shown, while shaded area envelopes curves for full 23 coupon set. At times denoted by arrows, cathodic polarization curves were measured. Horizontal dashed line indicates potential for MnO_2 coated coupon.

Figure 5.2 shows cathodic polarization behavior before exposure and after 160 and 500 hours exposure for samples designated in figure 5.1. The marked increase in cathodic current density at potentials above -300 mV characteristic of Ennoblement is evident. It can also be seen that while E_{corr} remains nearly constant for the 160 and 500 hour curves, current density at -200 mV shows a threefold increase. This behavior is consistent with increasing surface coverage of the MnO_2 rich deposits as will be explained in the discussion section to follow. Figure 5.2 also shows polarization behavior for a coupon partially covered with an MnO_2 film. The film, roughly 10 μm thick and covering about 6% of the coupon surface, was deposited by wiping off a thicker MnO_2 paste coating that had been in contact with the coupon for 15 hours. The similarity in polarization behavior for the MnO_2 coated and *in situ* exposed samples is evident.

To determine if oxygen depolarization plays a role in Ennoblement, as has frequently been proposed[5,8,10,12], polarization curves in aerated and deaerated media were compared for the two coupons in figure 5.1 that displayed nearly identical E_{corr} behavior during 500 hours exposure. The results shown in figure 5.3 indicate that for potentials above -200 mV, where polarization changes associated with Ennoblement are most apparent, oxygen reduction does not contribute significantly to cathodic current. Only at more negative potentials approaching the limiting current density does oxygen become the dominant cathodic reactant, as illustrated by the diminished limiting current density of the deaerated curve. Dissolved oxygen concentration measured in the reaction vessel before and after the deaerated run was less than 0.1 ppm. These results rule out changes in oxygen reduction rate as the cause of Ennoblement under conditions of this study.

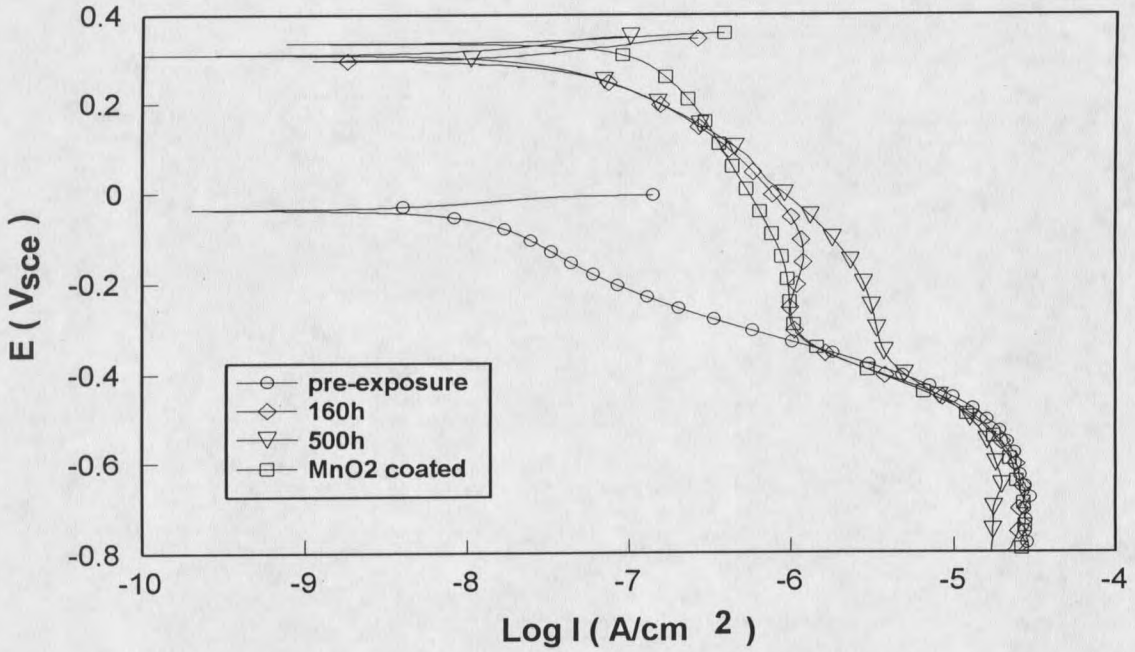

Figure 5.2. Cathodic polarization curves for 316L SS coupons after different exposure intervals in fresh river-water, and for MnO_2 coated coupon. Measurements were made in air saturated 0.01M Na_2SO_4 / pH 8.4.

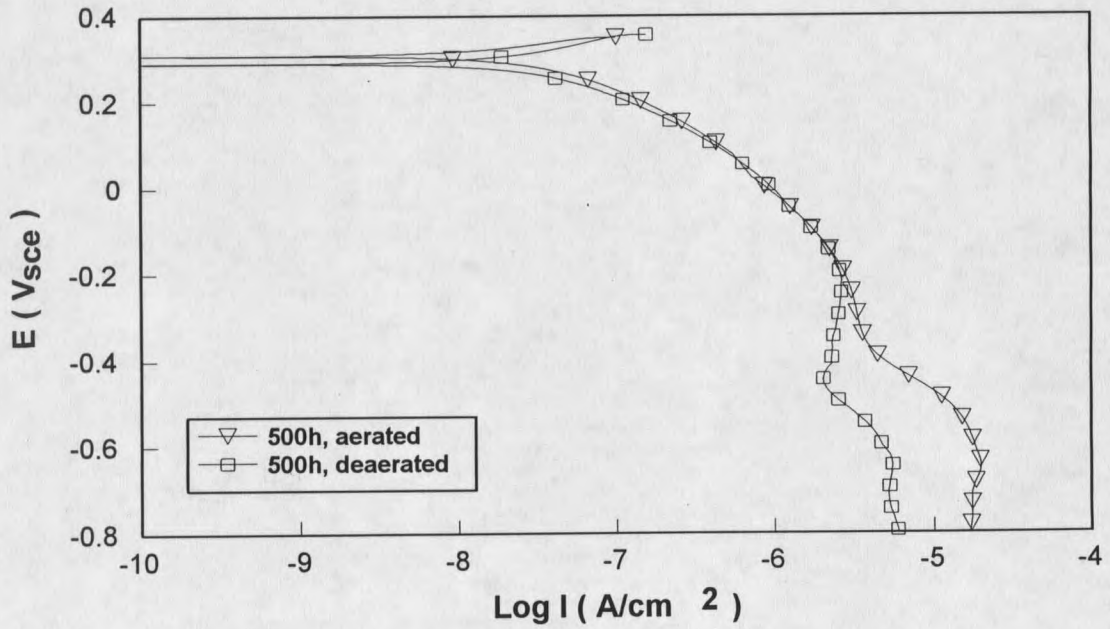

Figure 5.3. Cathodic polarization curves in aerated and dearated 0.01M Na_2SO_4/pH 8.4 for 316L SS coupons after 500 hours *in situ* exposure to fresh river-water.

Biofouling Deposits

After 4 days *in situ* exposure, one of the coupons having E_{corr} of +312 mV was removed for microscopic examination of the biofilm. Inspection at 400x under reflected light revealed an abundance of isolated, annular, orange-brown deposits approximately 10-20 μm in diameter and up to 3 μm thick that covered about 10% of the coupon surface. These deposits stained blue when treated with Prussian Blue reagent, and violet on treatment with leuco-crystal violet, indicating the presence of Fe(III) compounds and MnO_2. Identical deposits were observed on glass cover slips exposed to the same environment. Morphology and elemental composition of the annular deposits determined by SEM/EDS are shown in figure 5.4 and 5.5 respectively. The deposits are distinctly ring-shaped with diameters slightly more than 10 μm and central voids 3-4 μm in diameter. Within the voids, the SS substratum is visible. SEM examination of coupons after 5 and 13 days exposure showed no change in the physical appearance of the rings, however the abundance as determined by light microscopy increased from about 300 rings mm^{-2} after 5 days, to about 1100 rings mm^{-2} after 23 days; the later corresponds to 20% surface coverage.

Elemental mapping by EDS (fig. 5.5) clearly shows the presence of manganese in the annular deposits, as well as calcium, carbon and oxygen, suggesting a mixed oxide/carbonate mineralogy as previously noted[33] for bulky deposits associated with massive pitting of stainless steel turbine blades. Total Mn in the biofilm after 14 days exposure was 1.6 μg cm^{-2} or 0.2% by dry weight of the biofilm. Although iron was present within the annular deposits as determined by Prussian-Blue staining, detection by EDS was masked by background signal

from the metal substratum. Elemental maps for iron and chromium (not shown) indicated exposure of the substratum in the void area within the rings. Figure 5.6 shows the EDS spectrum of the ring for an interaction volume about 2 μm in extent denoted by the arrow in figure 5.4. By comparison with the spectrum for the bare substratum (not shown), the only element detectable other than those already noted was magnesium. The carbon map shown in figure 5.5 suggests that the filament visible on the lower annular deposit of figure 5.4 may have been a bacterial sheath.

Epifluorescence microscopy of the acridine-orange stained biofilm showed clusters of individual cells numbering from a few to several dozen within many of the annular deposits. A small cluster of 4 cells can be seen in the lower right portion of figure 5.7. Figure 5.7 also indicates the presence of distinct filamentous sheathed cells characteristic of iron and manganese-oxidizing bacteria. Leuco-crystal violet staining of biofilms grown *in situ* on glass cover slips and viewed under phase contrast show abundant manganic oxide deposits central to masses of radiating filamentous sheaths similar to the region visible in figure 5.7. These sheaths as well as isolated cells were abundant over the entire coupon surface. Both isolated subcultures of the filamentous bacteria and a separate isolate of sheath-free cells stained violet on treatment with leuco-crystal violet, indicating the presence of manganese-oxidizing bacteria within the biofilm. Morphology of the annular deposits seems suited to eventual capsule or microtubercle formation such as exhibited by the genus *Siderocapsaceae*[25] however, during the maximum exposure period of 5 weeks, neither encapsulation nor constriction of the area within the rings was observed.

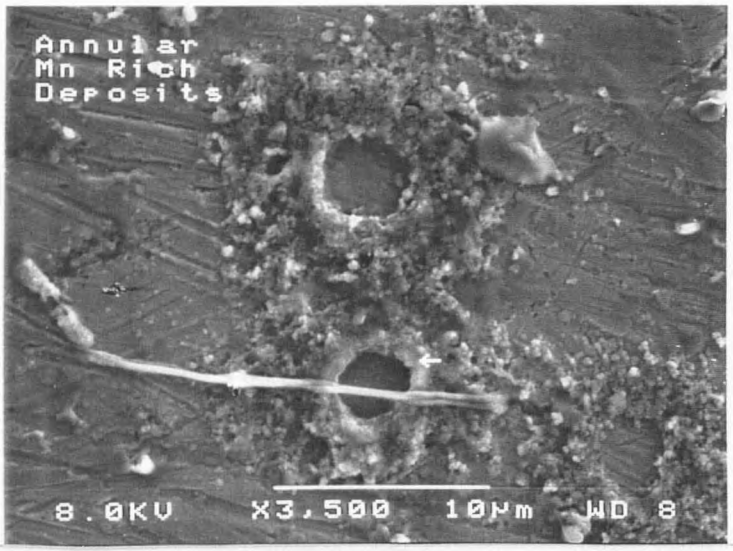

Figure 5.4. SEM micrograph of annular deposits on SS coupon after 13 day *in situ* exposure to fresh river-water. SS substratum is visible within the central void. Arrow indicates site for EDS spectrum shown in figure 5.6.

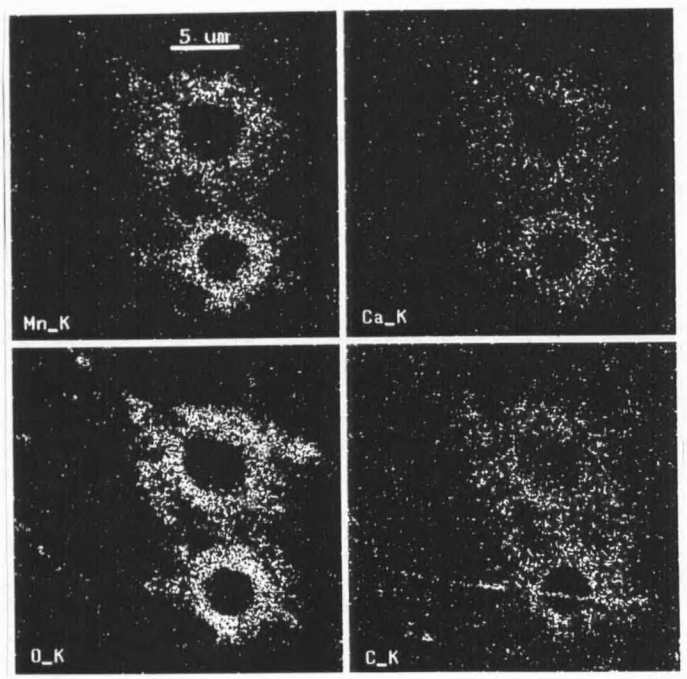

Figure 5.5. EDS maps of region shown in figure 5.4 confirming the presence of Mn, Ca, O, and C in the annular deposits.

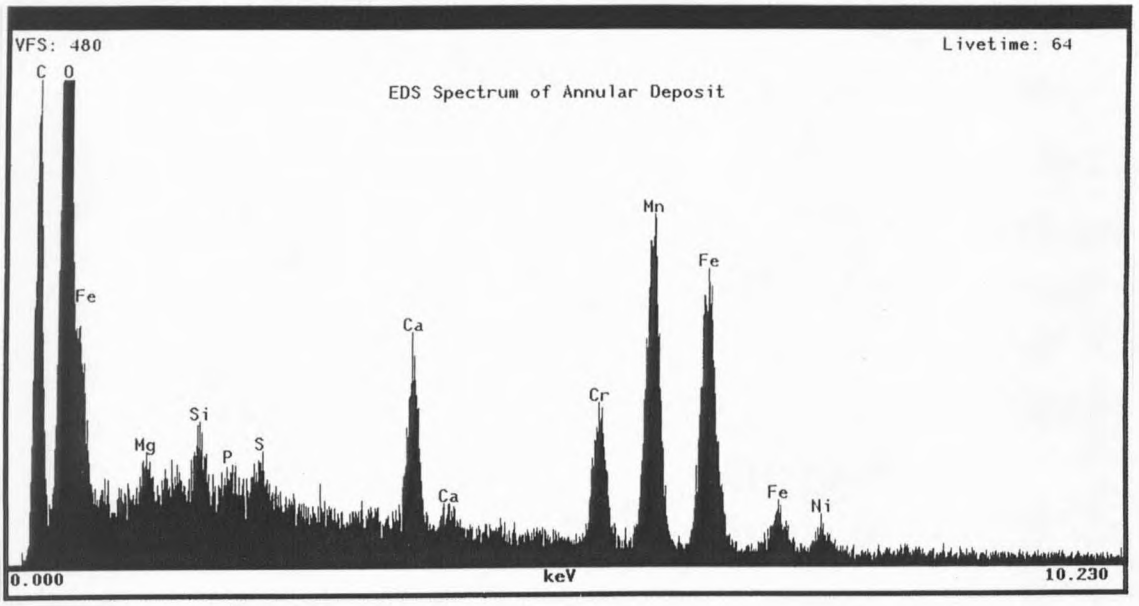

Figure 5.6. EDS spectrum for annular deposit on SS coupon at site designated by arrow in figure 5.4. Spectrum shows the presence of Mn and Ca which were undetectable at an adjacent site on the exposed substratum.

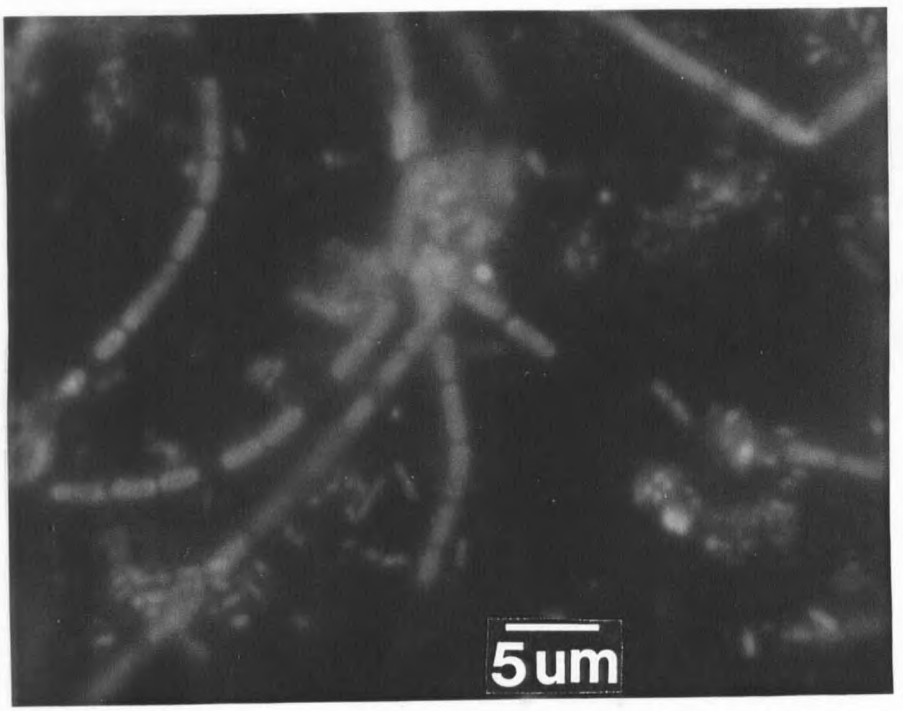

Figure 5.7. Epifluorescence micrograph of acridine-orange stained biofilm on 316L SS coupon after 4 day *in situ* exposure to fresh river-water. Individual bacterial cells centrally located within a Mn-rich annular deposit (lower right) as well as sheathed filamentous bacteria can be seen.

Sulfite Dissolution Experiment

The influence of MnO_2 deposits on E_{corr} was investigated by monitoring potential as the deposits were reductively dissolved by sulfite ion (figure 5.8). The experiments were carried out in argon-deaerated media to minimize changes in E_{corr} arising from rapid and quantitative removal of dissolved oxygen by SO_3^{2-}. Dissolved oxygen measured prior to SO_3^{2-} addition was less than 0.01ppm. In the first of three experiments, an *in situ* exposed coupon with E_{corr} of +335 mV and covered with numerous annular deposits was placed in deaerated medium and potential was monitored for 3 hours. E_{corr} decreased only slightly to +290 mV by the end of the period.

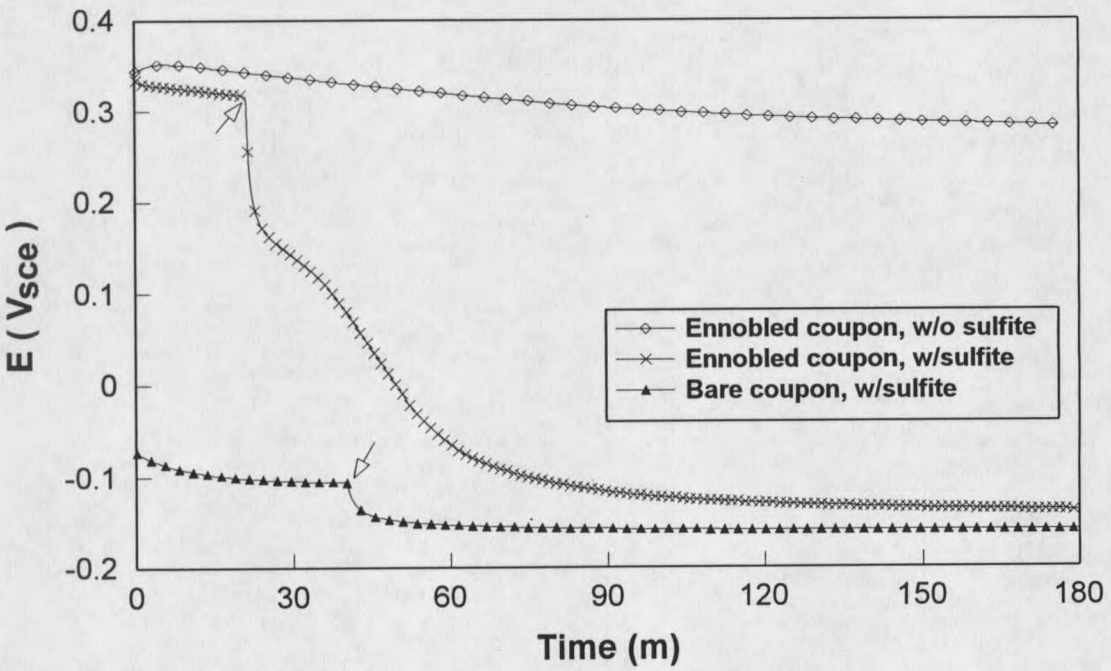

Figure 5.8. Influence of 0.5M SO_3^{2-} on E_{corr} for 316L SS after 20 day exposure to fresh river-water, and for unexposed coupon. Electrolyte was argon deaerated 0.5M Na_2SO_3 + 0.5M Na_2SO_4, pH 8.4. Arrows denote time of sulfite addition. E_{corr} for a separate Ennobled coupon in deaerated 1M Na_2SO_4, pH 8.4 is also shown.

An unexposed coupon was placed in fresh deaerated medium, and E_{corr} was monitored for 40 minutes prior to making the solution 0.5M in SO_3^{2-}. Addition of the SO_3^{2-} caused an abrupt potential decrease of approximately -50 mV, after which E_{corr} remained stable at -150 mV. Origin of the potential decrease is not clear, but may have arisen from removal of residual dissolved oxygen or from polarization accompanying direct oxidation of SO_3^{2-} at the electrode surface. The later explanation is consistent with a larger shift accompanying SO_3^{2-} addition to the Ennobled sample (see below), insofar as SO_3^{2-} oxidation would be more rapid at the more positive potential.

An *in situ* exposed coupon with E_{corr} of +330 mV and covered with numerous annular deposits was placed in fresh deaerated medium. After 20 minutes, during which E_{corr} decreased slightly to +310 mV, the solution was made 0.5M in SO_3^{2-}. SO_3^{2-} addition caused an abrupt drop in E_{corr} from +312 mV to +170 mV followed by a slower decrease to a near steady-state value of -140 mV over the ensuing 90 minutes. The final value agrees well with typical E_{corr} values for 316L SS in neutral abiotic solution. Following treatment, the coupon surface was examined at 400x by reflected-light microscopy. All annular deposits had dissolved, and no evidence of mineral encrustation could be seen. Analysis of the electrolyte used in the experiment showed a manganese concentration of 80 ppb corresponding to dissolution of 6 $\mu g\ cm^{-2}$ of Mn from the coupon surface. In contrast, Mn concentration in solution from the first experiment was indistinguishable from blank levels.

Results of these experiments imply that the slow decrease in E_{corr} following SO_3^{2-} addition to the Ennobled sample arose from gradual dissolution of the biomineralized MnO_2, with E_{corr} approaching values characteristic of unexposed coupons as dissolution became

complete. An identical experiment performed on an MnO_2 film coated coupon displayed similar results, with E_{corr} dropping abruptly from +250 to +150 on SO_3^{2-} addition followed by a gradual decrease to a near steady-state value of -160 mV over the ensuing 2 hours.

MnO_2 Studies

Results of experiments in which MnO_2 paste was applied to the SS coupons are shown in figures 5.1 and 5.2. The principal electrochemical effects of the MnO_2 coating were an increase in E_{corr} to a value virtually identical to the steady-state potential attained during *in situ* exposure, and an increase in cathodic current density at mild polarization again quite similar to the changes exhibited by *in situ* exposed coupons. Both electrochemical characteristics were influenced by the amount of MnO_2 applied, the extent of surface coverage, and the duration of exposure. In general, less than 100 μg of MnO_2 spread over approximately 20% of the coupon surface was sufficient to raise E_{corr} sharply to +350 mV. However for such treatment, potential began to decrease at rates of tens of mV min^{-1} after a few minutes exposure, presumably due to MnO_2 discharge through the anodic passivation current. Application of thicker deposits, up to several mg cm^{-2}, caused no greater shift in E_{corr} but sustained the potential for periods up to several days. It was also observed, that by allowing the thicker deposits to remain in contact with the surface for several hours, E_{corr} remained stable at potentials near +350 mV even after the bulk deposits were wiped off. Under these conditions, as little as a 10 μm thick residual coating covering 6% of the surface was sufficient to maintain E_{corr} in excess of +320 mV for several hours. These findings suggest

that time of contact enhances discharge kinetics between the substratum and the cathodic material. This may explain the small quantity of biofouling deposit (ca. 1-2 μg (Mn) cm^{-2}) required to effect Ennoblement, since for *in situ* exposure, continued bacterial renewal of the MnO_2 allows small quantities of material to remain in prolonged contact with the SS surface.

To obtain a better estimate of the amount of cathodically active MnO_2 required to induce Ennoblement, a thin, dark-brown film of MnO_2 was formed on several coupons by electrodeposition. It was assumed that electrodeposition would produce a coating of material in electrical contact with the substratum, whereas electrical continuity between the substratum and MnO_2 paste coatings was expected to be less uniform. After the electrodeposition, E_{corr} was measured, and the deposit was then stripped from the surface by applying a constant cathodic current. Coulombs of electroactive MnO_2 were calculated from the duration of the potential plateau. It was found that E_{corr} attained near steady-state values of +280 mV for deposition of 8.5 mcoul cm^{-2} of reducible MnO_2 (4.8 μg(Mn) cm^{-2} for a one-electron reduction). This is in fair agreement with the amount of Mn dissolved from the Ennobled coupon in the SO_3^{2-} experiments (6 ug cm^{-2}); however, interpretation of the electrodeposition experiment is complicated by the undetermined effect of the strongly anodic deposition potential on the electrochemical behavior of the substratum.

Thickness and areal coverage of the synthetic MnO_2 coatings also influenced shape and current density of the cathodic polarization curves. Thin deposits (<5 μm) covering more than about 20% of the surface frequently produced a current maximum of about 3 μA cm^{-2} near +50 mV. Similar peaks have been observed for Ennobled coupons[9]. Polarization curves for thicker but less broadly distributed deposits did not produce such peaks (e.g. the MnO_2

curve in figure 5.2) possibly due to incomplete reduction of the thicker deposits during the time-frame of the experiment.

Discussion

Mechanism of Ennoblement by MnO_2

The apparent limiting E_{corr} value of +350 mV attained during *in situ* exposure is in good agreement with the limiting potential range of +300 to +400 mV observed in the numerous studies on Ennoblement[3,4,5,7,8,9]. The potential for MnO_2 coated SS as shown in figure 5.1 is virtually identical to this limiting potential, and the experiments indicate that once the minimum quantity of MnO_2 paste required to attain +350 mV is deposited, application of additional material causes no further increase in potential. The apparent potential limit for both these treatments suggests a limiting potential set by the reduction potential for MnO_2 under the pH conditions of the experiments. At potentials below this value, MnO_2 is thermodynamically unstable with respect to reduction and cathodically depolarizes the electrode, shifting E_{corr} in the noble direction. Polarization continues as additional MnO_2 accumulation further enhances cathodic current, until the potential eventually stabilizes at the reversible MnO_2 reduction potential. While anodic current from oxidation of the substratum may be expected to influence this steady-state potential, it was found that reticulated vitreous carbon, when coated with MnO_2 paste or exposed at the field-site, attained the same steady-state potential (+350 mV) that was shown by 316L SS. This indicates that the limiting potential in Ennoblement reflects a reversible MnO_2 couple rather than a mixed potential.

Although E_{corr} remains constant, continued accumulation of MnO_2 causes cathodic current to increase at mild polarization as shown for the 160 and 500 hour curves in figure 5.2. As noted in the experimental section, a current maximum is observed during cathodic polarization for some Ennoblement studies and in the present study was observed at mild polarization for coupons more than about 20% covered with MnO_2 paste. These peaks may be essentially surface waves, as characteristically seen for voltammograms of adsorbed electroactive material[39], that arise due to reduction of the MnO_2 surface deposits. For such conditions, peak current is proportional not only to surface coverage, which would explain the increasingly prominent peaks as surface coverage is increased, but to polarization sweep rate as well. Variations in the latter may explain the diversity of polarization curve shapes observed in different reports on Ennoblement[5,9,10], and may also provide the means to investigate electroactive surface coverage of the MnO_2 deposits. It is evident from figure 5.2, that cathodic polarization behavior of SS partially covered with an MnO_2 film can mimic that of microbially Ennobled coupons very closely.

Although the electrochemistry of manganese oxides is complex, various arguments suggest that the well known battery reaction[40]:

$$MnO_2 + H_2O + e^- \Leftrightarrow MnOOH + OH^- \qquad (5.1)$$

may be the cathodic reaction in the above process. The reduction potential for this reaction at pH 8.0 and 25°C based on ΔG_f^o = -109.1 kcal mole^{-1} for γ-MnO_2[41] and -133.3 kcal mole^{-1} for γ-MnOOH[41] is +335 mV, which is in good agreement with the observed value of +350 mV

given the accuracy of ΔG_f^o for these oxides. Further, for such a solid phase reaction, the reduction potential is independent of dissolved Mn^{2+} concentration. The variation in exposure conditions for Ennoblement studies, including seawater, lake-water, and river-water, and the expected seasonal cycling of $[Mn^{2+}]$[24], would suggest greater variation in the limiting potential for Ennoblement if a cathodic reaction involving Mn^{+2}, such as

$$MnO_2 + 2H_2O + 2e^- \Leftrightarrow Mn^{2+} + 4OH^- \qquad (5.2)$$

were operative. In addition, based on the *in situ* $[Mn^{2+}]$ of 0.3 μM measured in the present study, the reduction potential at pH 8.0 for reaction (5.2) is +235 mV. A manganese(II) concentration almost 4 orders of magnitude lower would be required to account for the observed potential of +350 mV. Although it must be noted that microbially induced changes in near surface pH could shift reduction potentials for both reactions, previous microelectrode measurements on Ennobled coupons made in this laboratory (unpublished data) showed no near surface pH gradients. It is anticipated that measurements of dE_{corr} /dpH and dE_{corr} /$d[Mn^{2+}]$ will aid in establishing the stoichiometry of the cathodic reaction that develops during Ennoblement.

Relationship to Previous Studies

The proposed mechanism is consistent with a wide variety of published data on Ennoblement. The electrochemical characteristics of synthetic MnO_2 deposits on SS are strikingly similar to those observed both in the present study and in the literature[3,4,5,7,8,9] for

Ennobled SS. In the only published report containing elemental analysis of biofilms on Ennobled stainless steel, the presence of Mn (as well as oxygen and carbon) was noted[9], while in a separate report, EDS spectra show a complete absence of Mn[42] for microbially colonized stainless steel that failed to develop Ennobled potential. Interestingly, in a related study on cathodic polarization behavior of stainless steel colonized by aerobic microorganisms, Mn was observed on coupons that developed marked cathodic depolarization and pitting during colonization[43]. The occurrence of Ennoblement in some studies but not in others has led to considerable debate concerning the conditions necessary for Ennoblement[15,42,44]. In light of the proposed mechanism and the wide variability in abundance and redox state of Mn in natural waters, these different findings are not unexpected.

One of the most widely cited observations on Ennoblement is the shift in E_{corr} to pre-exposure values that occurs when sodium azide is added to the biofilm on Ennobled samples[2]. This finding has formed much of the basis for the proposed mechanisms of Ennoblement involving electrocatalysis of the oxygen reduction reaction[2,5,10], since it is assumed that sodium azide poisons extracellular enzymes or metallo-porphyrin compounds that might otherwise catalyze charge transfer to oxygen. Results shown in figure 5.3 indicate however that oxygen is not the dominant depolarizer at modest cathodic potentials for Ennobled SS. Further, it has been established that sodium azide and other respiratory inhibitors suppress oxidative removal of Mn^{2+} from solution by suppressing microbial growth[26]. Thus the observed drop in E_{corr} on azide addition may have arisen from suppression of MnO_2 deposition. Once microbial MnO_2 production ceases, slow self-discharge of the previously accumulated material would eventually cause E_{corr} to decay. It is interesting that the drop in E_{corr} observed in the above

study[2] was really quite slow, taking place over a period of 5 days; far longer than would be required for soluble electrocatalysts to diffuse away from the surface, but not an unreasonable time for passivation current densities of a few nA cm^{-2} to discharge a few mC cm^{-2} of MnO_2...

In other work on Ennoblement, an apparent exponential temporal increase in cathodic current density at fixed potential was reported[8]. While this was ascribed to autocatalysis of the oxygen reduction reaction, figure 5.3 indicates that oxygen reduction does not control cathodic current at mild polarization for Ennobled SS. In contrast, oxidation of Mn^{2+} to MnO_2 is autocatalytic, insofar as adsorption of Mn^{2+} onto MnO_2 dramatically increases the rate constant for oxidation[41]. Thus enhanced cathodic current due to biologically produced MnO_2 will be augmented by an increasing rate of chemical MnO_2 production as the deposit forms.

Ennoblement and Corrosion

As noted in the introduction, a principal concern regarding passive metal Ennoblement is the increased risk of localized corrosion that arises when E_{corr} exceeds the critical pitting potential of the metals. The morphology of the Mn-rich deposits that cause Ennoblement in the present study may aggravate this concern. The typically ring-shaped deposits fix the site of the dominant cathodic reaction and, coupled with cell colonization within the rings, may provide ideal conditions for localized oxygen depletion, with consequent diminished redox potential. This would increase activation overpotential for the anodic reaction at the exposed substratum within the rings, and raise the risk of exceeding the critical pitting potential even

beyond that anticipated by bulk solution chemistry. It is worth noting, that such a scheme for localized attack does not require formation of ferric or manganic chlorides, although chloride would presumably compound the risk of attack.

Mn-rich microbial deposits have been implicated in pitting of stainless steel turbine blades[33] indicating that this type of fouling can cause severe material degradation. Given the number of reports on Ennoblement, and the widespread distribution of manganese-oxidizing bacteria in natural waters, it is likely that conditions leading to MnO_2 deposition and possible material failure are common. These conditions can be found in heat exchangers and storage tanks where residual moisture following hydrostatic testing fosters bacterial growth[30]. Treatment for such fouling often includes mechanical disassembly and cleaning[45]. While previous work has shown that physical removal of biofilm prevents Ennoblement from occurring[18] and eliminates Ennoblement once it has developed[9], controlling Ennoblement by this method will often be impractical or expensive. The mechanism proposed in this paper, suggests that an alternative preventative measure may be to remove dissolved Mn(II) from influent water. This could be accomplished by chemical means, or using methods established for biological removal of Mn(II) from drinking water[26]; the latter possibly providing a lower cost approach for large-volume cooling water requirements. In such a design, Mn(II) removal by microbial sand filters placed upstream from the target facility would lower concentrations sufficiently to prevent MnO_2 biomineralization downstream.

Conclusions

Manganic oxide biofouling of 316L SS in fresh river-water shifts E_{corr} to steady-state values of +350 mV, and increases cathodic current density at mild polarization by more than two orders of magnitude compared to unexposed samples. These electrochemical changes are very closely mimicked by the behavior of SS coupons partially coated with MnO_2 paste. E_{corr} exhibited during Ennoblement agrees closely with the one-electron reduction potential for conversion of MnO_2 to MnOOH at the experimental pH. Origin of the Mn-rich deposits may be attributed to surface colonization by Mn-oxidizing bacteria.

Much of the data concerning Ennoblement can be understood in terms of MnO_2 biofouling, including the correlation between Ennoblement and the presence of Mn in biofilms, the influence of sodium azide on Ennobled potential, and the autocatalytic nature of increasing cathodic current density that develops during microbial colonization. Based on the proposed mechanism of Ennoblement, removal of dissolved Mn(II) from influent process waters may serve to prevent development of this potentially destructive microbial process.

References Cited

1. Mollica, A., (1985). The Influence of the Microbiological Film on Stainless Steels in Natural Seawater, in: The 4th International Congress on Marine Corrosion and Fouling (Antibes, France, 1976), p. 351.

2. Scotto, V., R. DiCintio, and G. Marcenaro, (1985). The Influence of Marine Aerobic Microbial Film on Stainless Steel Corrosion Behaviour. Corr. Sci. **25:**185-194.

3. Dexter, S.C. and H-J Zhang, (1990). Effect of Biofilms on Corrosion Potential of Stainless Steel Alloys in Estuarine Waters, in: The 11th International Corrosion Congress (Associazone Italiana di Metallurgia, Florence, Italy) p. 333-340.

4. Mollica, A., *et al.*, (1989). Cathodic Performance of Stainless Steels in Natural Seawater as a Function of Microorganism Settlement and Temperature. Corrosion **45:**48-57.

5. Scotto, V., M. Beggiato, G. Marcenaro and R. Dellepiane, (1993). Microbial and Biochemical Factors Affecting the Corrosion Behaviour of Stainless Steels in Seawater. in: Marine Corrosion of Stainless Steels: Chlorination and Microbial Effects. Ijsseling, F.P., ed. (The Institute of Materials, London), pp. 21-33.

6. Chandrasekaran, P. and S.C. Dexter, (1993). Mechanism of Potential Ennoblement on Passive Metals by Seawater Biofilms, CORROSION/93 paper no. 493 (NACE, Houston, TX).

7. Holthe, R., P. O. Gartland, and E. Bardal, (1987). Influence of the Microbial Slime Layer on the Electrochemical Properties of Stainless Steel in Sea Water, SINTEF Report No. STF16 A87123 (Foundation for Scientific and Industrial Research at the Norwegian Institute of Technology, Trondheim, Norway).

8. Mollica, A., (1992). Biofilm and Corrosion on Active-Passive Alloys in Seawater. Internat. Biodeterio. Biodegrad. **29**:213-229.

9. Motoda, S., Y. Suzuki, T. Shinohara, and S. Tsujikawa, (1990). The Effect of Marine Fouling on the Ennoblement of Electrode Potential for Stainless Steels. Corr. Sci. **31:**515-520.

10. Dexter, S.C. and G.Y. Gao, (1988). Effect of Seawater Biofilms on Corrosion Potential and Oxygen Reduction of Stainless Steel. Corrosion **44:**717-723.

11. Johnsen, R. and E. Bardal, (1985). Cathodic Properties of Different Stainless Steels in Natural Seawater. Corrosion. **41:**296-305.

12. Mollica, A., E. Traverso and G. Ventura, (1993). Biofilm Monitoring in Seawater. in: Marine Corrosion of Stainless Steels: Chlorination and Microbial Effects. Ijsseling, F.P., ed., (The Institute of Materials, London) pp. 149-160.

13. Mollica, A. and G. Ventura, (1993). Use of Biofilm Electrochemical Monitoring Device for an Automatic Application of Antifouling Procedures in Seawater. in: Proceedings 12th International Corrosion Congress, (NACE, Houston, TX), p. 3807.

14. Dexter, S. and S-H. Lin, (1988). Mechanism of Corrosion Potential Ennoblement by Marine Biofilms, Proc. 7th International Congress on Marine Corrosion and Fouling, Valencia, Spain (International Committee for Research on the Prevention of Marine Corrosion, Bussels).

15. Eashwar, M. and S. Maruthamuthu, (1995). Mechanism of Biologically Produced Ennoblement: Ecological Perspectives and a Hypothetical Model. Biofouling **8**:203-213.

16. Uhlig, H. H., (1971). Corrosion and Corrosion Control. (John Wiley & Sons, New York, NY) 419 pp.

17. Licina, G., G. Nekoksa and G. Ward, (1990). An Electrochemical Method for Monitoring the Development of Biofilms in Cooling Water. in: Microbially Influenced Corrosion and Biodeterioration. Dowling, N. J, M. W. Nittleman, and J. C. Denko eds., (University of Tennessee, Knoxville, TN), p. 5/41-5/46.

18. Dickinson. W., and Z. Lewandowski, (1995). Electrochemical and Microelectrode Studies of Stainless Steel Ennoblement. CORROSION/95, paper no. 223, (NACE, Houston, TX).

19. Vago, E.R., E.J. Calvo, and M. Stratmann, (1994). Electrocatalysis of Oxygen Reduction at Well-Defined Iron Oxide Electrodes. Electrochim. Acta **39:**1655-1659.

20. Tomashov, N. D. and G. P. Chernova, (1967). Passivity and Protection of Metals Against Corrosion, (Plenum Press, New York, NY) 208 pp.

21. Okazaki, R., K. Morigaki, T. Ohhira, H. Fukuda, S. Kondo and Y. Matsuda, (1994). Influence of Current Collector Materials of the Positive Electrode on Storage Characteristics of Li/MnO2 Batteries. Denki Kagaku oyobi Kogyo Butsuri Kagaku **62:**975-981.

22. Hayasaka, T., T. Harada, T. Sakai and J. Ohshida, (1993). Stainless Steel Cathode Case for Compact High-Capacity Nonaqueous Electrolyte Battery. Europ. Patent Application CODEN:EPXXDW, Seiko Electronic Co. Ltd. 12 pp.

23. Ohira, T., T. Fujii, H. Fukuda and K. Ando, (1986). Cathode Collectors for Cylindrical Lithium Batteries. Japan. Kokai Tokkyo Koho CODEN: JKXXAF, Matsushita Electric Industrial Co. Ltd. 3 pp.

24. Gounot, A-M., (1994). Microbial Oxidation and Reduction of Manganese: Consequences in Groundwater and Applications. FEMS Microbio.Rev. **14:**339-350.

25. Hanert, H., (1981). The Genus Siderocapsa (and Other Iron- or Manganese-Oxidizing Eubacteria, in: The Prokaryotes, A Handbook on Habitats, Isolation, and Identification of Bacteria. Starr, M., H. Truper, A. Balows, and H Schlegel eds., (Springer-Verlag, New York, NY) pp. 1049-1059.

26. Vandenabeele, J., D. DeBeer, R. Germonpre and W. Verstraete, (1992). Manganese Oxidation by Microbial Consortia from Sand Filters. Microb. Ecol. **24:**91-108

27. Greene, A. and J. Madgwick, (1991). Microbial Formation of Manganese Oxides. Appl. Environ. Microbiol. **57:**1114-1120.

28. Kobrin, G., (1976). Corrosion by Microbiological Organisms in Natural Waters. Mat. Perform. **15**:38-43.

29. Pope, D., D. Duquette, A. Johannes and P. Wayner, (1984). Microbiologically Influenced Corrosion of Industrial Alloys. Mat. Perform. **23:**14-18.

30. Tatnall, R.E., (1981). Case histories: Bacteria induced corrosion. Mat. Perform. **20:**41-48.

31. Kobrin, G., (1986). Reflections on Microbiologically Induced Corrosion of Stainless Steels in: Biologically Induced Corrosion, Dexter, S. C. ed., (NACE, Houston, TX) pp. 33-46.

32. Duquette, D. and R. Ricker, (1986). Electrochemical Aspects of Microbially Induced Corrosion, in: Biologically Induced Corrosion, Dexter, S. C. ed., (NACE, Houston, TX), pp 121-130.

33. Linhardt, P.,(1994). Manganese Oxidizing Bacteria and Pitting of Turbine Components Made of CrNi Steel in a Hydroelectric Power Plant. Werks. Korr. **45:**79-83.

34. Hobbie, J., R. Daley and S. Jasper, (1977). Use of Nucleopore Filters for Counting Bacteria by Fluorescence Microscopy. Appl. Environ. Microbiol. **33:**1225-1228.

35. Kessick, M., J. Vuceta and J. Morgan, (1972). Spectrometric Determination of Oxidized Manganese with Leuco Crystal Violet. Environm. Sci. Technol. **6**:642-644.

36. Lovley, D. and E. Phillips, (1988). Novel Mode of Microbial Energy Metabolism: Organic Carbon Oxidation Coupled to Dissimilatory Reduction of Iron or Manganese. Appl. Environ. Microbiol. **54:**1472-1480.

37. Herring, A. and S. Ravitz., (1965). Rate of Dissolution of Manganese Dioxide in Sulfurous Acid. Soc. Mining Engineers. **September:**191-196.

38. Asai, S., H. Negi and Y. Konishi, (1986). Reductive Dissolution of Manganese Dioxide in Aqueous Sulfur Dioxide Solutions. Can. J. Chem. Eng. **64:**237-241.

39. Bard, A. and L. Faulkner, (1980). Electrochemical Methods: Fundamentals and Applications, (John Wiley & Sons, New York, NY) 718 pp.

40. Scarr, R. and J. Hunter, (1995). Alkaline-Manganese Dioxide Cells in: Handbook of Batteries, Linden, D. ed., (McGraw-Hill, New York, NY), p. 10.1.

41. Stumm, W. and J. J. Morgan, (1970). Aquatic Chemistry, (Wiley-Interscience, New York, NY) 526 pp.

42. Little, B.J., *et al.*, (1991). Impact of Biofouling on the Electrochemical Behaviour of 304 Stainless Steel in Natural Seawater. Biofouling **3**:45-49.

43. Little, B., P. Wagner and D. Duquette, (1988). Microbiologically Induced Increase in Corrosion Current Density of Stainless Steel Under Cathodic Protection. Corrosion **44**:270-274.

44. Mansfeld, F. and B. Little, (1989). Discussion: Effect of Seawater Biofilms on Corrosion Potential and Oxygen Reduction of Stainless Steel. Corrosion **45:**786-789.

45. Tatnall, R., (1981). Fundamentals of Bacteria Induced Corrosion. Mat. Perform. **20:**32-38.

CHAPTER 6

MANGANESE DEPOSITION RATES *

Overview

Corrosion potential (E_{corr}) for 316L stainless steel coupons was monitored during 9 days *in situ* exposure to fresh river water. E_{corr} increased at 300 mV day^{-1} reaching potentials of +350 mV (SCE) within 48 hours, then remained fixed at this potential. The coulometric reduction technique was used to determine rate and total abundance of cathodically active manganese biofouling during the exposure. A deposition rate of 0.57 mcoul cm^{-2} d^{-1} was measured during the initial 7 days, increasing to 3.1 mcoul cm^{-2} d^{-1} between day 7 and 9. Based on a one-electron reduction of MnO_2 to MnOOH, 8.8 μg cm^{-2} electroactive MnO_2 was deposited during the 9 day exposure. Comparison with published data for manganese deposition in drinking water distribution systems suggests rapid biological MnO_2 deposition consistent with the rapid rate of Ennoblement. Deposition rate is used to estimate the potential impact of manganese biofouling on stainless steel pitting.

---

* Published as: *Manganese Biofouling of Stainless Steel: Deposition Rates and Influence on Corrosion Processes.* W.H. Dickinson and Z. Lewandowski (1996). **Corrosion/96** paper no. 291, National Association of Corrosion Engineers, Houston, TX.

Introduction

The noble shift in corrosion potential (E_{corr}) and accompanying increase in cathodic current density that develop during microbial colonization of passive metals have been the subject of considerable controversy over the past decade[1-10]. The phenomena, collectively known as Ennoblement, have been variously ascribed to depolarization of the oxygen reduction reaction[7,8] , acidification of the electrode surface[9], the combined effect of elevated H_2O_2 and decreased pH[3], and production of passivating siderophores[10]. One of the principal concerns in Ennoblement is the enhanced risk of pit formation that arises as E_{corr} exceeds the critical pitting potential (E_{pit}). Recent findings in this laboratory[11] have demonstrated that Ennoblement is accounted for by manganic oxide biofouling attributable to surface colonization by manganese-oxidizing bacteria. Results from this work showed that annular manganese-rich deposits 10-20 μm in diameter and approximately 3 μm thick formed on a variety of materials including stainless steel, carbon, and glass, during exposure to fresh river water. Commonly the substratum surface within the rings was colonized by bacterial cell clusters. Cell colonies present within annular manganese-rich deposits is a prime diagnostic characteristic for *Siderocapsa* bacteria[12]. These taxonomic characteristics, shown in figures 6.1a and 6.1b, may further enhance the risk of pit formation caused by Ennoblement. Oxygen consumption by the bacterial clusters coupled with impeded oxygen transport into the rings may diminish redox potential and so cause E_{corr} to exceed E_{pit} at these local sites even before E_{pit} for metal exposed to the bulk solution is reached. Depolarization by the fixed MnO_2 cathode surrounding such sites would prevent pit broadening but could sustain rapid

attack within the rings, leading to commonly observed tunneling corrosion, in which large subsurface cavities are connected to solution at microporous surface sites[13].

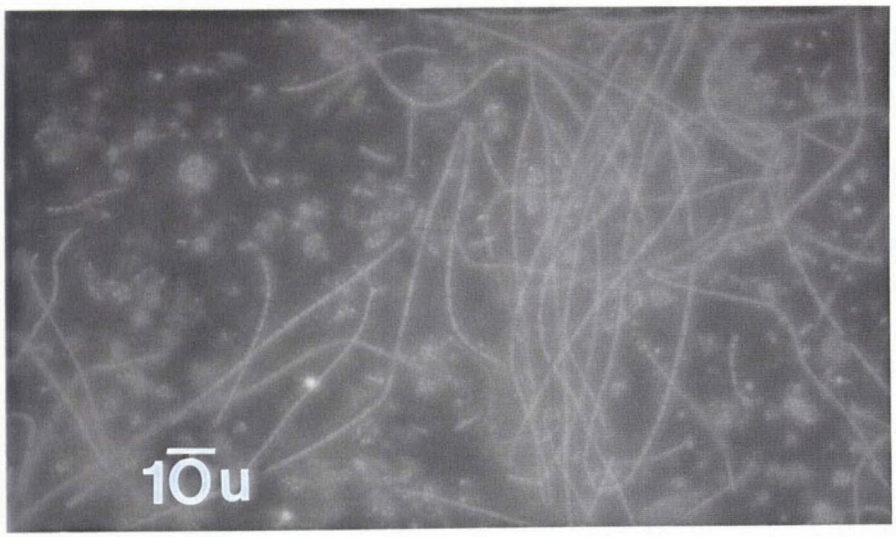

(a)

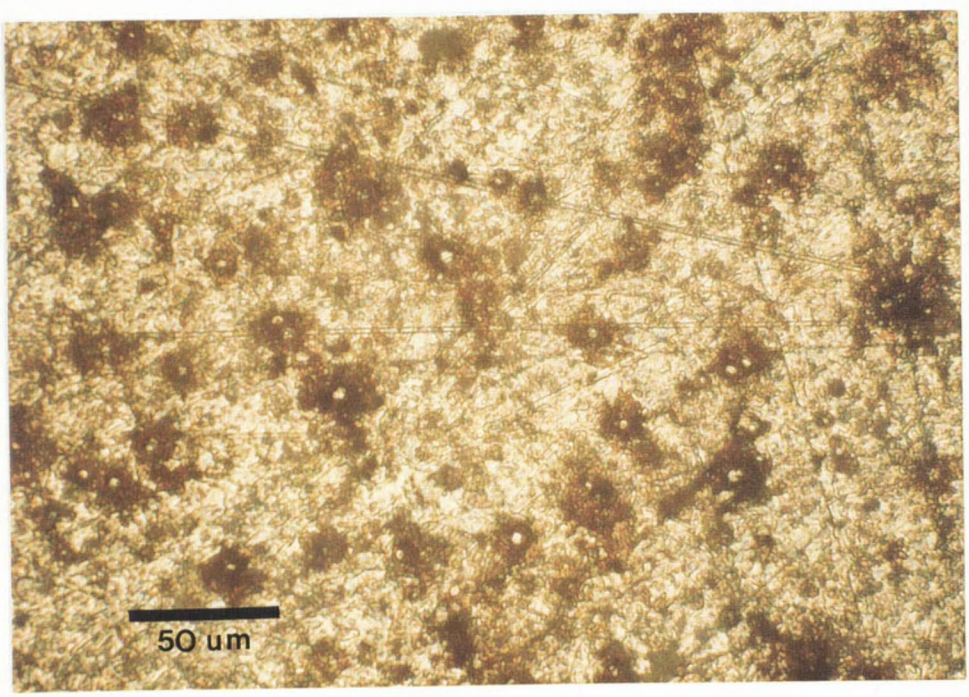

(b)

Figure 6.1. Micrographs of microbially colonized 316L stainless steel after 23 day exposure to fresh river water. (a) Epifluorescence image of acridine-orange stained biofilm showing distribution of cell clusters and presence of sheathed bacteria. (b) Reflected light image showing morphology and distribution of manganese-rich deposits.

In light of widespread biofouling by iron- and manganese-oxidizing bacteria in natural waters[14,15], cathodic depolarization by microbial MnO_2 may be anticipated on a variety of metals including mild steel. If this is true, then the influence of manganese-oxidizing bacteria has significance not only to understanding Ennoblement and the enhanced risk of aggressive pitting, but to the broader issue of microbially influenced corrosion of mild steels, where elevated cathodic current density will activate the anodic reaction and support higher corrosion currents. While microbially related formation of aggressive manganic chlorides has been cited repeatedly in the corrosion literature[16-21], little effort has been made to characterize and evaluate the corrosive impact of manganese oxide biofouling. The present work attempts to quantify the rate of electroactive MnO_2 deposition by microorganisms as a step towards establishing the influence of MnO_2 biofouling on corrosion rates.

Experimental Methods

Epoxy embedded type 316L stainless steel coupons (1.59 cm. dia) were prepared as previously described[22]. A set of 5 coupons were exposed to fresh flowing stream water at a field site near Bozeman, MT, by mounting the coupons in a 2 cm x 60 cm open-channel poly-carbonate reactor and submersing the reactor below the stream surface. Based on chemical composition, the field site classifies as a clean stream (dissolved oxygen (DO) > 6 ppm; pH 8-8.5; alkalinity 3 meq/L; nitrate ion 1.2 ppm; Ca^{2+} 58 ppm; Mg^{2+} 15 ppm; Cl^- 3 ppm; dissolved Fe 200 ppb; conductivity 4×10^{-4} $ohm^{-1}cm^{-1}$; total organic carbon 110 ppm). E_{corr} was measured daily vs. the saturated calomel electrode (all potentials are reported vs. the SCE). At

specified intervals, coupons were transported in stream water to the laboratory for microscopic evaluation and coulometric titration of the surface deposits.

The coupons were examined at 400x by reflected light microscopy prior to titration. Abundance of the annular manganese-rich deposits was determined by counting individual rings within an area bounded by a calibrated graticule. Thickness of the deposits was evaluated by noting travel of the calibrated microscope stage adjustment while focusing first at the substratum then at the top of the deposits.

Titrations were carried out in aerated 0.01M sodium sulfate (Na_2SO_4) / pH 8.2 using a commercial computer-controlled potentiostat/galvanostat operating in galvanostatic mode. Aerated electrolyte was used to ensure chemical stability of the manganic oxide phase during the experiments. The counter electrode was a graphite rod (3 cm^2 exposed area) and potentials were recorded vs. the SCE. Based on previously established polarization characteristics (cf. figure 6.2)[11], for coupons exposed at the above field site, a current density of 250 nA cm^{-2} was chosen for the coulometric titration. The current density was sufficient to polarize the coupon significantly from the Ennobled E_{corr} but small enough to allow a distinct shift in potential to occur upon depletion of the electroactive surface phase. Titration curves shown in figure 6.3, exhibit a clear potential plateau corresponding to reduction of surface bound phases, as typically observed for measurements of passive film thickness[23], followed by a shift to the polarization potential corresponding to oxygen reduction. Plateau potentials agree very closely with values anticipated from the cathodic polarization data in figure 6.2.

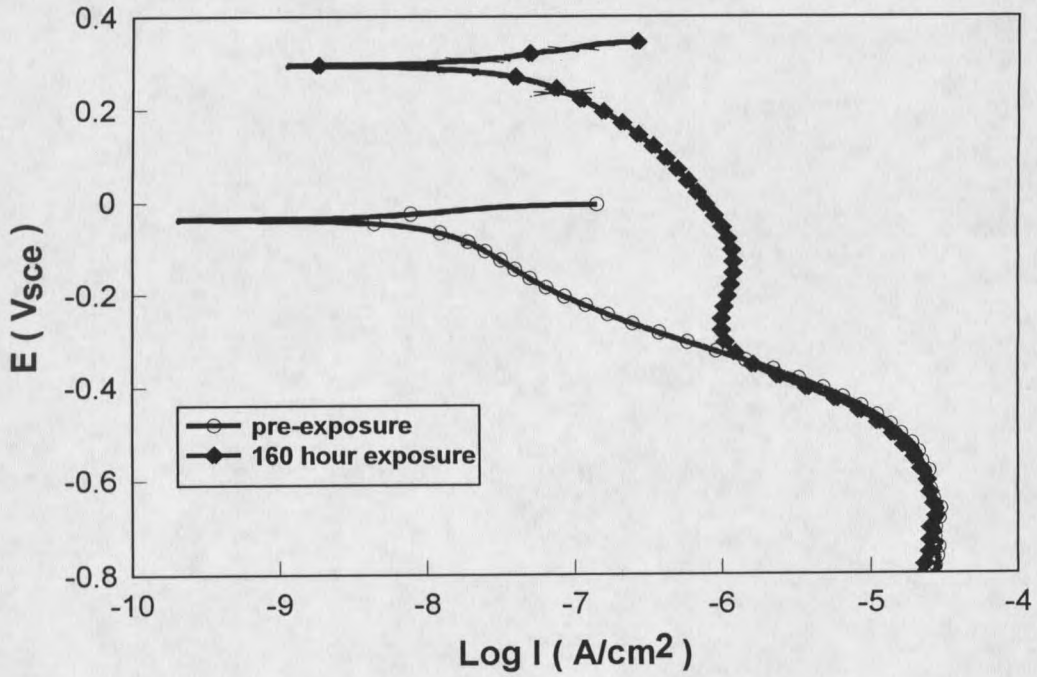

Figure 6.2. Cathodic polarization curves for 316L stainless steel before and after formation of manganese-rich biofouling deposits.

Coulometric behavior of MnO_2 paste coated stainless steel was also determined. The MnO_2 paste was prepared by reduction of permanganate with manganous ion under alkaline conditions[24] followed by centrifugation. pH of the MnO_2 suspension was 8.6. A coating of MnO_2 paste several hundred μm thick was applied to the coupon surface, and the coupon allowed to stand overnight in 0.01 M Na_2SO_4 / pH 8.2. The bulk of the paste was then wiped off, leaving an MnO_2 film about 5 μm thick covering 20% of the coupon surface. The sample was placed in fresh aerated 0.01 M Na_2SO_4 / pH 8.2 and coulometrically titrated at 250 nA cm^{-2} as described above. E_{corr} for the coupon at the beginning of titration was stable at +335 mV.

Results

E_{corr} for the 5 *in situ* exposed coupons increased rapidly at a rate of nearly 300 mV day^{-1}. While one coupon removed for titration after 24 hours had reached only +286 mV, all others attained steady-state values of +350 mV within 48 hours of exposure. Microscopic inspection showed an abundance of annular deposits on all the coupons, with a surface abundance of 300 - 400 rings mm^{-2} after 24 hours increasing to 1000-1300 rings mm^{-2} after 121 hours. Beyond 164 hours, the abundance had stabilized at 1400-1600 rings mm^{-2} but an increasing amount of translucent brown film about one micrometer in thickness was evident surrounding the deposits.

Curves for the coulometric titrations are shown in figure 6.3. The clear evolution in extent of the plateau region with duration of exposure indicates an increasing surface density of electroactive material. Similarity between curves for Ennobled coupons and the curve for MnO_2 paste coated coupon is evident. Figure 6.4 shows the relationship between exposure time and coulombs cm^{-2} of electroactive material. Accumulation rate during the initial 164 hours of exposure is 0.57 mcoul cm^{-2} d^{-1} and increases to 3.1 mcoul cm^{-2} d^{-1} after 164 hours. Based on a one-electron reduction of MnO_2 to MnOOH [11] these rates correspond to 0.5 and 2.8 μg (MnO_2) cm^{-2} d^{-1} respectively. Total accumulation after 210 hours exposure was 9.8 mcoul cm^{-2} or 8.8 μg (MnO_2) cm^{-2} .

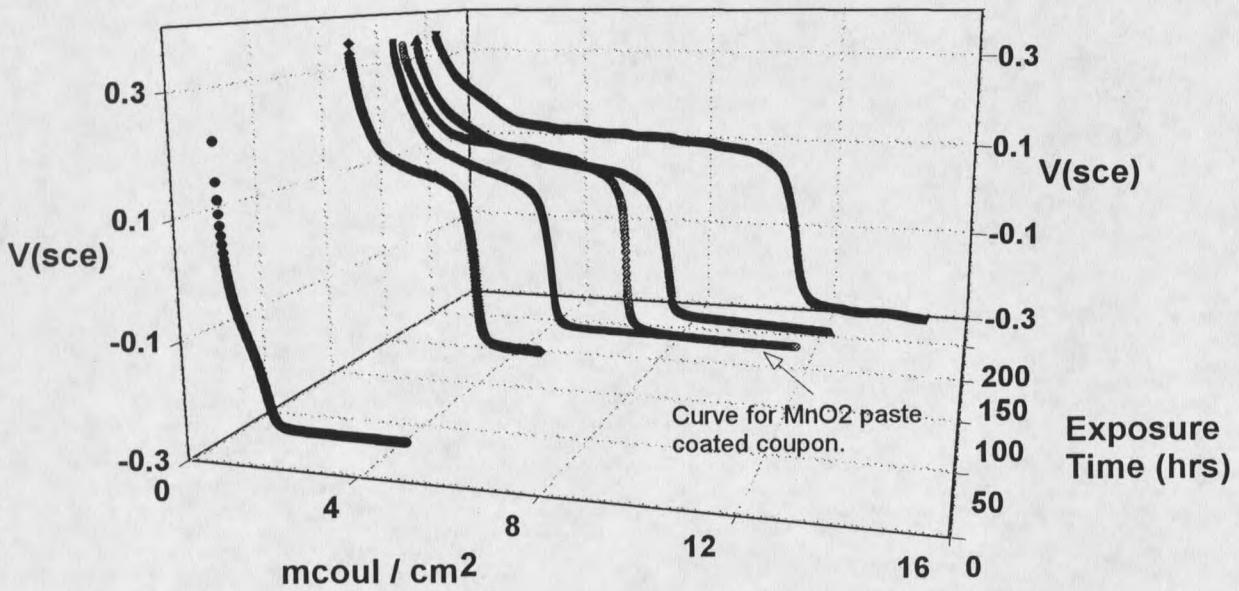

Figure 6.3. Evolution of coulometric titration curves for 316L stainless steel with increasing duration of exposure to fresh river water. The curve for an MnO_2 paste coated coupon is also shown. 250 nA cm^{-2} applied current in aerated 0.01 M Na_2SO_4 / pH 8.4.

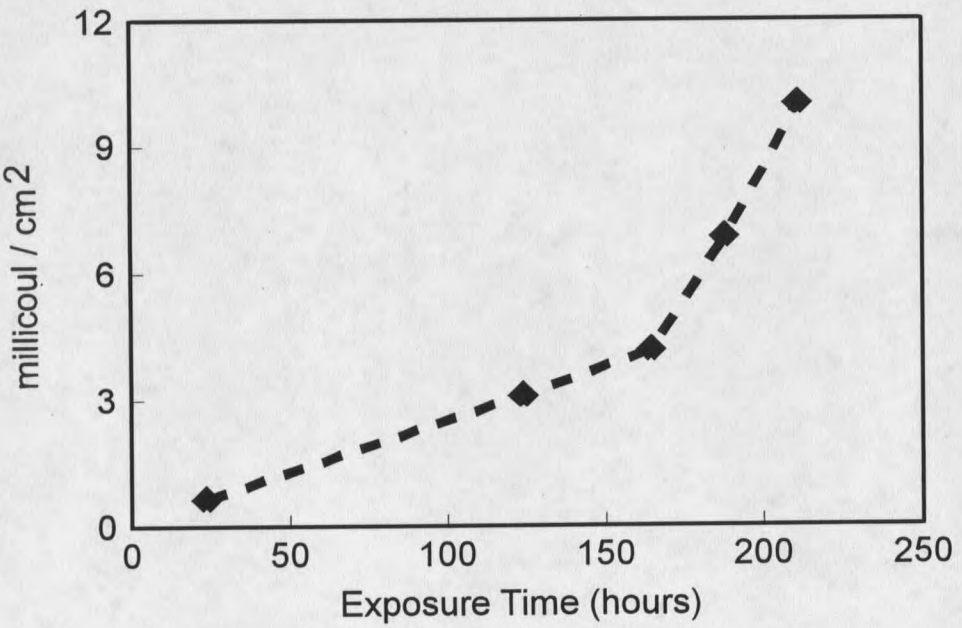

Figure 6.4. Accumulation of cathodically active MnO_2 based on coulometric titration curves. Initial rate is 0.5 μg cm^{-2} day^{-1} for a one-electron reduction.

Discussion

Deposition Rates

The coulometric technique is well suited to evaluating the corrosive impact of MnO_2 biofouling in that only the electroactive portion of the deposits is measured. MnO_2 has modest electrical conductivity, consequently electroactivity is expected to extend beyond the first few atomic layers within the mineral deposit. Nevertheless, only a small fraction of the total deposit is likely to be accessible for cathodic reaction, and this complicates comparison of results obtained in the present experiments with deposition rates determined by dissolution or physical removal of MnO_2. Comparison can still be carried out however, if the present results are acknowledged as a lower limit of MnO_2 deposition. Total particulate manganese previously determined in this laboratory[11] for biofouling deposits from the same exposure site, was 9.6 μg (MnO_2) cm^{-2} after 20 days exposure or a net deposition rate of about 0.5 μg (MnO_2) cm^{-2} d^{-1}. During those exposures, E_{corr} increased more slowly (110-200 mV day^{-1}) than in the present study. The rate of electroactive MnO_2 deposition in the present study is roughly twice the total MnO_2 deposition rate observed previously, consistent with the more rapid rate of Ennoblement in the present work. The former study was conducted during early summer and the latter in early fall, so that differences in rate may arise from seasonal variations in microbial activity. In a separate study of MnO_2 precipitation in a drinking water distribution system containing 10 ppb Mn(II)[25], biological deposition rates of 0.8 μg (MnO_2) cm^{-2} d^{-1} were observed during the initial two weeks of exposure

Model for Pit Formation

Under environmental conditions for which Ennobled $E_{corr} < E_{pit}$, manganic oxide biofouling of passive metals is not detrimental and may indeed serve to enhance passivity. Cathodic depolarization by MnO_2 shifts E_{corr} in the noble direction until the stability potential for the reaction:

$$MnO_2 + H_2O + e^- \Leftrightarrow MnOOH + OH^- \qquad :E^{o'}_{pH\,8} = +335\ mV_{SCE} \quad (6.1)$$

is reached. Above this potential, MnO_2 is stable with respect to reduction and increased cathodic current from continued MnO_2 deposition is offset by decreased current density at the individual deposits. This situation is depicted in figure 6.5

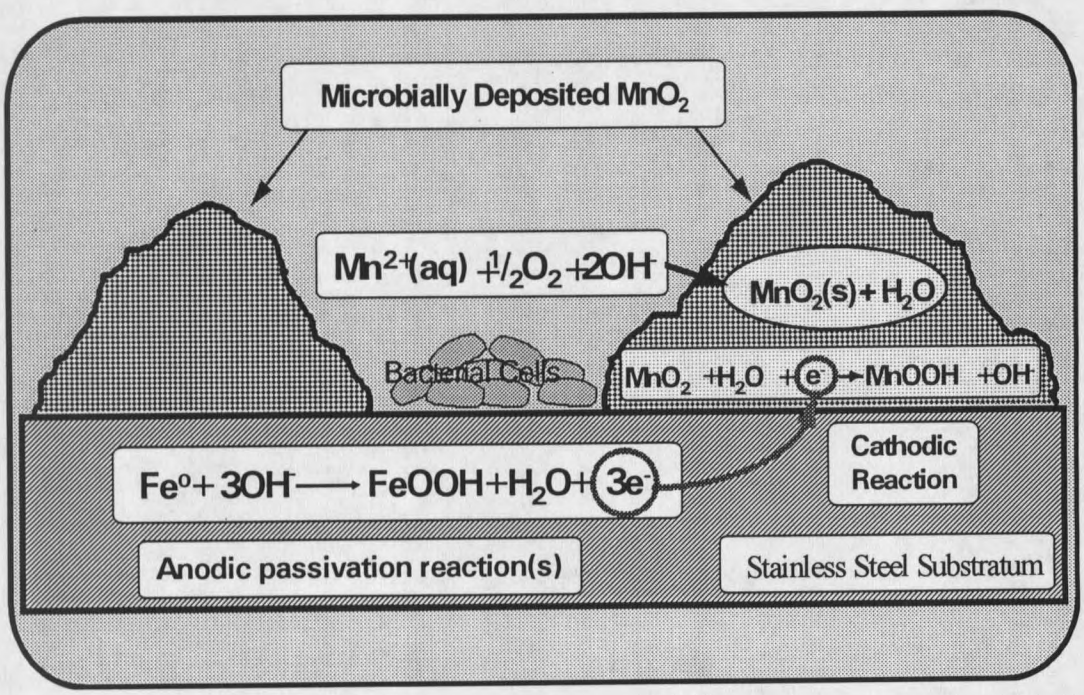

Figure 6.5. Model of stainless steel Ennoblement by microbially deposited MnO_2. E_{corr} shifts to the stability potential for MnO_2 reduction at experimental pH. For $E_{corr} < E_{pit}$, passivity is enhanced.

As noted in the introduction, the specific biofouling morphology observed in the present study may, however, aggravate the risk of pit formation and suggests a new pitting mechanism which for clarity is restated here. Oxygen consumption by bacterial clusters within the annular MnO_2 deposits coupled with impeded oxygen transport into the rings may diminish redox potential and so cause E_{corr} to exceed E_{pit} at these local sites even before E_{pit} for metal exposed to the bulk solution is reached. This would lead to preferential pit formation within the annular deposits. Depolarization by the fixed MnO_2 cathode surrounding such sites would prevent pit broadening but could sustain attack within the rings, leading to the common form of MIC for stainless steel in which large subsurface cavities are connected to solution by microporous surface openings. Figure 6.6 illustrates this model.

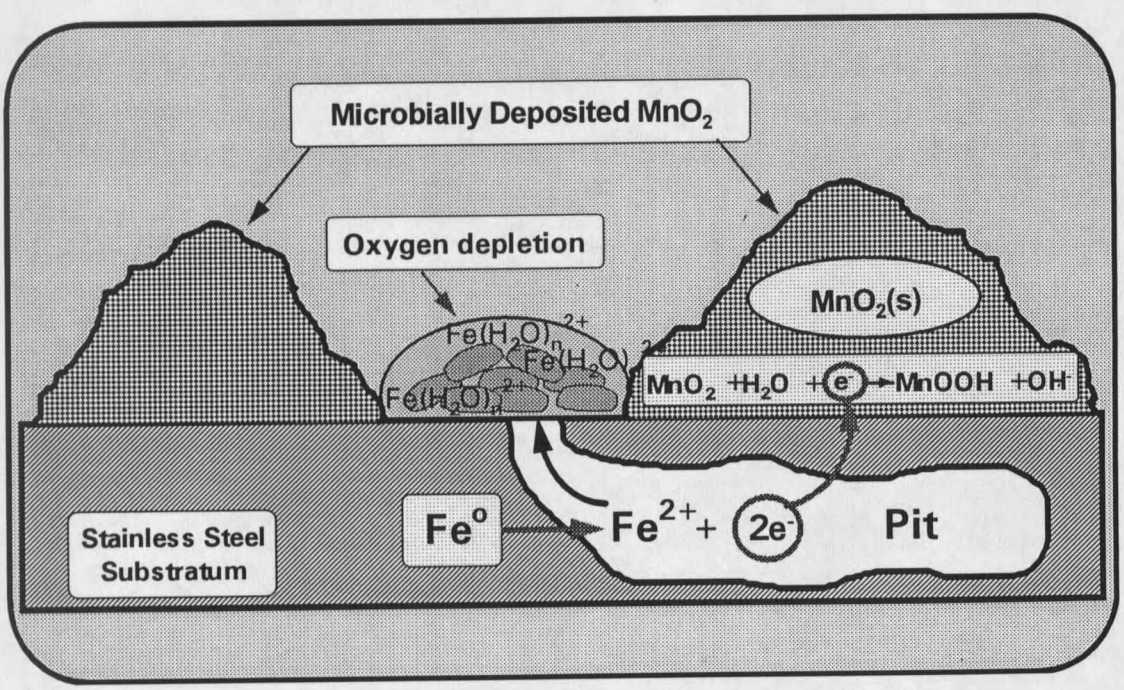

Figure 6.6. Conceptualized subsurface pit formation arising from microbial oxygen depletion within annular MnO_2 deposit. MnO_2 depolarization shifts E_{corr} to values exceeding E_{pit} at local sites of diminished redox potential.

Corrosion Rates

The curves shown in figure 6.3 indicate that once formed, MnO_2 biodeposits can support current densities of 250 nA cm^{-2} at potentials near +100 mV. This is approximately 350 mV above the potential required to support the same current using oxygen as the sole depolarizer. Despite fairly rapid kinetics for oxidation of elemental iron[26], the higher potential may still activate the anodic reaction, so that once a pit is initiated, penetration may proceed at an accelerated rate. The high rate would persist until the MnO_2 cathode material was consumed, after which time the potential would drop to the value sustained by oxygen reduction. Based on a continuous deposition rate of 3.1 mcoul cm^{-2} d^{-1} measured during the later part of the experiment, however, a sustained corrosion current of 36 nA cm^{-2} can be supported indefinitely at a potential near +300 mV (cf. figure 6.2). The penetration rate supported by this current will depend on the number and area of pitting sites, however for microporous sites, such as those constrained to the 3-4 μm diameter void within the annular MnO_2 cathodes, and assuming an arbitrary pit density of 100 pits cm^{-2}, the initial pitting area would be 10^{-5} cm^2, and an initial penetration rate greater than 100 μm day^{-1} for 2-electron iron oxidation would result.

Conclusions

Coulometric titrations of electroactive manganic oxide deposits formed during freshwater biofouling of stainless steel indicate a net deposition rate of 1.1 mcoul cm^{-2} d^{-1} over

a 9 day exposure period. The rate is approximately twice the previously reported values for total manganic oxide biofouling under similar environmental conditions, suggesting higher manganese-oxidizing bacterial activity in the present study. The conclusion is consistent with the very rapid rates of Ennoblement noted in the present work. Taxonomy of the biofouling deposits suggests a new mechanism of pit initiation for stainless steels colonized by manganic oxide ring forming bacteria such as the genus *Siderocapsa*. The model can be used to explain subsurface pitting corrosion frequently observed in microbially influenced corrosion of stainless steels.

References Cited

1. Scotto, V., R. DiCintio, and G. Marcenaro, (1985). The Influence of Marine Aerobic Microbial Film on Stainless Steel Corrosion Behavior. Corr. Sci. **25:**185-194.

2. Mollica, A., *et al.*, (1989). Cathodic Performance of Stainless Steels in Natural Seawater as a Function of Microorganism Settlement and Temperature. Corrosion **45**:48-56.

3. Chandrasekaran, P. and S.C. Dexter, (1993). Mechanism of Potential Ennoblement on Passive Metals by Seawater Biofilms, CORROSION/93 paper no. 493 (NACE, Houston, TX).

4. Motoda, S., Y. Suzuki, T. Shinohara, and S. Tsujikawa, (1990). The Effect of Marine Fouling on the Ennoblement of Electrode Potential for Stainless Steels. Corr. Sci. **31:**515-520.

5. Dexter, S.C. and G.Y. Gao, (1988). Effect of Seawater Biofilms on Corrosion Potential and Oxygen Reduction of Stainless Steel. Corrosion **44:**717-723.

6. Johnsen, R. and E. Bardal, (1985). Cathodic Properties of Different Stainless Steels in Natural Seawater. Corrosion. **41:**296-305.

7. Mollica, A., E. Traverso and G. Ventura, (1993). Biofilm Monitoring in Seawater. in: Marine Corrosion of Stainless Steels: Chlorination and Microbial Effects. Ijsseling, F.P., ed., (The Institute of Materials, London) pp. 149-160.

8. Mollica, A. and G. Ventura, (1993). Use of Biofilm Electrochemical Monitoring Device for an Automatic Application of Antifouling Procedures in Seawater. in: Proceedings 12th International Corrosion Congress, (NACE, Houston, TX), p. 3807.

9. Dexter, S. and S-H. Lin, (1988). Mechanism of Corrosion Potential Ennoblement by Marine Biofilms, Proc. 7th International Congress on Marine Corrosion and Fouling, Valencia, Spain (International Committee for Research on the Prevention of Marine Corrosion, Bussels).

10. Eashwar, M., S. Maruthamuthu, S. Palanichamy and K. Balakrishnan, (1995). Sunlight Irradiation of Seawater Eliminates Ennoblement-Causation by Biofilms. Biofouling **8**:215-221.

11. Dickinson, W., F. Caccavo Jr. and Z. Lewandowski, (1996). The Ennoblement of

Stainless Steel by Manganic Oxide Biofouling. Corr. Sci. **38**:1407-1422.

12 Tuovinen, O., P. Hirsch, and G. Zavarzin, (1989). Family "Siderocapsaceae" Pribram, 1929, in: Bergey's Manual of Systematic Bacteriology, Vol. 3, Staley, J. ed., (Williams and Wilkins, Baltimore), pp. 1874-1878.

13. Tatnall, R., (1990). Case Histories: Biocorrosion, in: Biofouling and Biocorrosion in Industrial Water Systems. Flemming, H-C, and G. Geesey eds., (Springer-Verlag, New York, NY) pp. 165-168.

14. Ghiorse, W. C., (1984). Biology of Iron- and Manganese-Depositing Bacteria. Ann. Rev. Microbiol. **38**:515-550.

15. Mulder, E., (1989). Genus Leptothrix Kutzing, 1843, in: Bergey's Manual of Systematic Bacteriology, Vol. 3, Staley, J. ed., (Williams and Wilkins, Baltimore), pp. 1998-2003.

16. Tatnall, R.E., (1981). Case histories: Bacteria induced corrosion. Mat. Perform. **20:**41-48.

17. Tatnall, R., (1981). Fundamentals of Bacteria Induced Corrosion. Mat. Perform. **20:**32-38.

18. Pope, D., D. Duquette, A. Johannes and P. Wayner, (1984). Microbiologically Influenced Corrosion of Industrial Alloys. Mat. Perform. **23:**14-18.

19. Kobrin, G., (1976). Corrosion by Microbiological Organisms in Natural Waters. Mat. Perform. **15**:38-43.

20. Geesey, G., (1990). What is Biocorrosion?, in: Biofouling and Biocorrosion in Industrial Water Systems. Flemming, H-C, and G. Geesey eds., (Springer-Verlag, New York, NY), pp. 154-164.

21. Duquette, D. and R. Ricker, (1986). Electrochemical Aspects of Microbially Induced Corrosion, in: Biologically Induced Corrosion, Dexter, S. C. ed., (NACE, Houston, TX), pp 121-130.

22. Dickinson. W., and Z. Lewandowski, (1995). Electrochemical and Microelectrode Studies of Stainless Steel Ennoblement. CORROSION/95, paper no. 223, (NACE, Houston, TX).

23. Ramasubramanian, N., N. Preocanin, and R. D. Davidson, (1985). Analysis of Passive Films on Stainless Steel by Cyclic Voltammetry and Auger Spectroscopy. J. Electrochem. Soc. **132**:793-798.

24. Lovley, D. and E. Phillips, (1988). Novel Mode of Microbial Energy Metabolism: Organic Carbon Oxidation Coupled to Dissimilatory Reduction of Iron or Manganese. Appl. Environ. Microbiol. **54:**1472-1480.

25. Sly, L., M. Hodgkinson, and V. Arunpairojana, (1990). Deposition of Manganese in a Drinking Water Distribution System. Appl. Environ. Microbiol. **56**:628-639.

26. Uhlig, H. H., (1971). Corrosion and Corrosion Control. (John Wiley & Sons, New York, NY) 419 pp.

CHAPTER 7

ENNOBLEMENT BY *LEPTOTHRIX DISCOPHORA*

Overview

The relationship between surface colonization, manganese deposition, and corrosion potential (E_{corr}) for stainless steel coupons exposed to batch cultures of the manganese-depositing bacterium *Leptothrix discophora* was investigated to establish whether biological manganic oxide deposition could induce Ennoblement. E_{corr} shifted from -100 to +330 mV_{SCE} as a biofilm containing 75 nmoles cm^{-2} MnO_x formed on the coupon surface but changed little further with continued MnO_x deposition up to 260 nmoles cm^{-2}. Mn(II) uptake, MnO_x deposition, and attached cell density covaried with increasing E_{corr}. Mn(II) enhanced the areal density of attached cells. The experimental results validate a mechanism of Ennoblement in which E_{corr} is fixed near +350 mV_{SCE} by the cathodic activity of biomineralized MnO_x.

Introduction

Stainless steel and other passive metals can be corroded by exposure to biologically active natural waters[1,2]. Complex deposits of microbial cells, extracellular polymers, and organic and inorganic debris that accumulate on the metal surface accelerate corrosion by changing the electrochemical behavior of the metal[3-5]. The principal electrochemical changes, which are collectively termed Ennoblement, are an increase in corrosion potential (E_{corr}) to noble values approaching +350 mV vs. the saturated calomel electrode (SCE) and a two to three orders of magnitude increase in the cathodic reaction rate at potentials above -300 mV_{SCE} [6]. Elevated E_{corr} promotes corrosion initiation on type 304 and other low molybdenum stainless steels in seawater[2], and the concurrent increase in cathodic rate stabilizes and propagates the corrosion[7,8]. The concerted effect of these two corrosive events can cause perforation failure of piping and containment vessels that are exposed to natural waters. In order to prevent increased service costs (eg. biofouling removal, cathodic protection), decreased life-expectancy, and catastrophic failure of structural materials[9-11], the petrochemical, pulp and paper, and electric-power industries must employ increasingly expensive alloys that are able to withstand the corrosive effects of the biofilms.

A number of studies have attempted to establish a direct link between biofilm formation and Ennoblement since the effect was first observed in the mid-1960's [12]. Ennobled potential has been correlated with bacterial cell density[3] and with biological activity in the biofilms by measuring ATP accumulation[5] and electron transport activity and lipopolysaccharide content[4]. These studies, coupled with studies using filter sterilized, heat

pasteurized, and artificial seawater[2,3] as experimental controls support the hypothesis that biofilm formation is a prerequisite for Ennoblement. However, a biological mechanism explaining Ennoblement has not been established.

We have recently demonstrated that Ennoblement of stainless steel coupons placed within a freshwater stream in Bozeman, MT was caused by the deposition of manganese-rich material on the coupon surface[13]. Ennoblement could also be induced by coating the metal surface with pure manganese dioxide paste. This study established a chemical mechanism for Ennoblement in which manganese dioxide acts as a galvanic cathode to elevate cathodic current and shift E_{corr} in the noble direction. The MnO_2-MnOOH redox couple ($E^{o'}$= +335 mV_{SCE} at pH 8) was proposed as the reaction that fixes E_{corr} near +350 mV_{SCE}. Since manganese-rich deposits and manganese-oxidizing bacteria frequently occur at sites of stainless steel corrosion[14-16], this study also unified the previously separate issues of Ennoblement and manganese-related corrosion.

While the origin of the manganese-rich material deposited on stainless steel coupons exposed to Bozeman streamwater was not rigorously established, mineral-encrusted bacterial sheaths characteristic of *Leptothrix sp.*[17] and mineralized torroidal capsules characteristic of *Siderocapsa treubii*[18] were abundant on the surface of the Ennobled stainless steel coupons[19], and manganese-oxidizing bacteria were isolated from the manganese-rich deposits. While both of the genera mentioned are known to deposit manganese, principally in the sheaths and capsules, this ability is often lost during laboratory culturing and efforts to obtain manganese-depositing axenic cultures of *Siderocapsa treubii* have been unsuccessful[18]. A strain of *Leptothrix discophora* that maintains its ability to form sheaths in laboratory culture has

recently been described[17]. This strain was chosen as a model bacterium to test the hypothesis that Ennoblement of stainless steel can be induced by manganese biomineralization. We report that concomitant biofilm formation and manganese dioxide deposition by *Leptothrix discophora* induce stainless steel Ennoblement. These results establish the biological basis for Ennoblement and advance our ability to control this phenomenon by quantifying the surface abundance of manganese that is required to shift E_{corr} to +350 mV_{SCE}.

Experimental

Inoculum and Growth Medium

Stock cultures of *Leptothrix discophora* SP-6 [17] obtained from the American Type Culture Collection, (ATCC 51168, Rockville, MD), were maintained at 4°C on ATCC 1917 mineral salts-vitamin-pyruvate (MSVP) medium solidified by addition of 1.5% agar noble (Difco, Rockville, MD). The experimental medium consisted of MSVP medium amended with 35 mg l^{-1} pyruvate and ca. 200 uM Mn(II). Mn(II) was supplied from a filter-sterilized 0.1 M $MnSO_4$ stock solution. Colonies from the plated stock culture were incubated for 72 hours at room temperature (20-22°C) in 100 ml MSVP. An aliquot of this culture (1.0 ml) was used to inoculate 20.0 ml MSVP medium, which served as the inoculum for the experimental reactors. The cell density of the experimental inoculum after 20 hours of static incubation at room temperature was 1 x 10^8 cells ml^{-1}.

Materials and Apparatus

Type 316L stainless steel coupons (1.6 cm diam, Metal Samples Inc, Munford, AL) that were epoxy-embedded in polycarbonate tubes (1.9 cm diam x 10 cm) were exposed to 600 ml of the test medium in polycarbonate reaction vessels (12 cm diam x 10 cm). Each reactor contained 18 coupons. The coupons were mounted in the reactors such that only one face was exposed to the test medium and electrical connection was made to the coupons by fixing conductive copper tape to the unexposed side. The coupons were abraded and washed as previously described[13] and mounted through the reactor lids with the exposed coupon face oriented downward to prevent suspended solids from settling onto the surface. In this orientation, each coupon face was equidistant (2.5 cm) from the reactor bottom and the solution surface.

E_{corr} for each coupon was measured hourly by computer against the SCE using a high impedance ($>10^{11}$ ohm), 64 channel, analog to digital converter (Keithley, Taunton, MA). A single SCE reference electrode was connected to each of three reactors through salt bridges filled with 1 mM Na_2SO_4 solution. The salt-bridges made contact with medium in the reactors through Vycor glass tips (EG&G, Princeton, NJ) which served as a bacterial barrier to prevent reference electrode filling solution from contaminating the reactors. The salt bridges introduced a second electrical junction in the circuit used to measure E_{corr}, producing an offset of roughly -30 mV. This offset was determined before and after each experiment and was subtracted from measured E_{corr} values to give E_{corr} verses the SCE.

The reactors were filled with 600 ml of mineral salts medium and autoclaved at 121°C and 16 psi for 20 minutes. Appropriate amounts of filter sterilized vitamin, pyruvate, and Mn(II) solutions were then added to the cooled medium in the reactors. Autoclaved salt bridges and coupons which had been soaked for 1 minute in 70% ethanol and UV irradiated for 12 hours were mounted in the reactors and connected to the analog to digital converter. The absence of bacteria, as determined by direct cell counts, in the uninoculated control experiment confirmed that this treatment maintained solution sterility. Coupons were exposed to the MSVP medium for ca. 24 hours to attain stable values of E_{corr} before initiating the Ennoblement experiments.

Experimental Procedure

The Ennoblement hypothesis was tested by exposing the coupons to three treatments (Table 7.1) with each treatment performed in triplicate. Where error bars are shown or reported, they refer to one standard deviation about the mean of the triplicate measurements. Coupons were exposed to inoculated MSVP in the presence and absence of Mn, and to uninoculated MSVP containing Mn. For the inoculated treatments, 20 ml of inoculum were repeatedly aspirated through a 22 gauge needle attached to a 10 cc syringe to break up cell aggregates and produce a uniform cell suspension[17]. Each reactor was inoculated with 6 ml of the aspirated cell suspension and stirred for one minute to distribute the cells. Thereafter, the reactors were stirred for one minute prior to each sampling but were otherwise left unstirred. After inoculation or after Mn addition for the cell free control experiment, E_{corr}, Mn(II),

attached cell density, and surface-bound manganese abundance were measured at intervals over a 36 hour period. The pH for all treatments was between 7.1 and 7.2, the temperature was 25 +/- 2°C, and the initial cell densities in the reactors for treatments 1 and 2 were 1.0 +/- 0.3 and 1.0 +/- 0.1 x 10^6 cells ml^{-1}, respectively.

Table 7.1. Experimental approach to test the manganese biomineralization hypothesis[a]

Treatment	Bacterial Cells	Mn(II)
1	+	+
2	+	-
3	-	+

[a] +, present; - absent.

Analytical Methods

The dissolved Mn(II) concentration was measured by the formaldoxime method[20]. At each sampling interval, 1.5 ml of solution was removed from each reactor and filtered through a 0.2 μm cellulose acetate filter to remove suspended solids. Mixed ammonia-formaldoxime reagent (1.5 ml) was added to 0.5 ml of each sample, incubated for 30 minutes, and the absorbance at 450 nm was measured using a Shimadzu 2101PC Spectrophotometer. The spectrophotometer was calibrated using Mn(II) solutions that were previously standardized against atomic absorption standard Mn(II) (Fisher Scientific). The manganese concentration on the coupon surfaces, hereafter referred to as MnO_x ($x \sim 1.7$) [21], was monitored by removing a coupon from each reactor at each sampling interval and reductively dissolving the

MnO_x using sodium sulfite[13]. The coupon was soaked for 30 minutes in 5.0 ml of stirred 0.5 M Na_2SO_3 (pH 7.3), the solution filtered (0.2 μm cellulose acetate), and Mn(II) concentration determined as described above. For these measurements, analytical standards were prepared in 0.5 M Na_2SO_3 to correct for a 10-20% increase in sensitivity caused by the presence of sulfite. Although the reductive dissolution of manganese does not distinguish solid manganic oxides from Mn(II) adsorbed onto the oxide phase, previous work[22,23] indicates that more than 90% of the total dissolved Mn comes from the oxide fraction. This is important in relating surface manganese abundance to the amount of MnO_x required to produce Ennoblement since only manganese in oxidation states above two behaves as a galvanic cathode.

Cells were removed from the coupon surface by scraping with a sterile razor blade, suspending the scrapings and washing the coupon surface in three 100 μl aliquots of sterile ammonium oxalate-glutaraldehyde reagent (28 g ammonium oxalate, 15 g oxalic acid, and 0.1 ml glutaraldehyde per liter), and transferring the washings to a vial containing 4.8 ml of the ammonium oxalate-glutaraldehyde reagent. After extracting for at least one hour, the solution was aspirated five times through a 22 gauge needle attached to a 10 cc syringe to suspend and break up cell aggregates. The cells were then stained and counted using a modification of the epifluorescence microscopy technique[24] as described previously[25].

Results and Discussion

Bacterial Colonization

The number of cells attached to the surface in Mn(II) containing media increased exponentially at a rate of 0.31 doublings h^{-1} (Fig. 7.1) and reached an apparent maximum density of 8×10^7 cells cm^{-2} after 31 hours. This growth rate is in accordance with that reported by Adams and Ghiorse[26] (0.08 - 0.15 doublings h^{-1}) for *Leptothrix discophora* grown on glass slides. In medium without Mn(II), the growth rate was similar (0.26 doublings h^{-1}) however, the maximum cell density was lower by 63%, and the cell density decreased after reaching a maximum at 27 hours. For both treatments, a mucaliginous biofilm was readily apparent on the coupon surfaces after 20 hours of cell growth. Formation of such a biofilm, in which cathodically active MnO_x can be deposited close to the metal substratum, is considered a prerequisite for Ennoblement, since electron transfer can take place only when MnO_x is in electrical contact with the metal.

Sub-millimolar Mn(II) concentrations have been previously shown to either stimulate[27] or repress[22] the maximum cell yields of *Sphaerotilus* and *Leptothrix* sp. during batch culture. The present results, in which an Mn(II) concentration of 200 μM stimulates attached cell yield, may be explained by the activity of the manganese-oxidizing factor excreted by different *Leptothrix discophora* strains under sessile vs. planktonic growth conditions. The sheath-forming strain SP-6, used in our work produces higher manganese-oxidizing activity and retains the activity closer to the cell than does the sheathless strain SS-1 used previously[17]. In addition, the polymeric biofilm matrix produced during sessile growth may impede advective-

diffusive loss of the excreted activity, further concentrating the activity near the cells. It has been suggested that Mn(II) levels > 55 μM may be toxic to cells, but that MnO_x may enhance cell survival by removing toxic active oxygen species (eg. O_2^- or H_2O_2) [22] produced during cell growth. The elevated manganese-oxidizing activity posed for sessile growth of SP-6 could mediate these factors by more completely precipitating toxic Mn(II) as MnO_x and by more effectively destroying active oxygen species on the MnO_x surface. The result of such mediation would explain the stimulated cell yield that we observed.

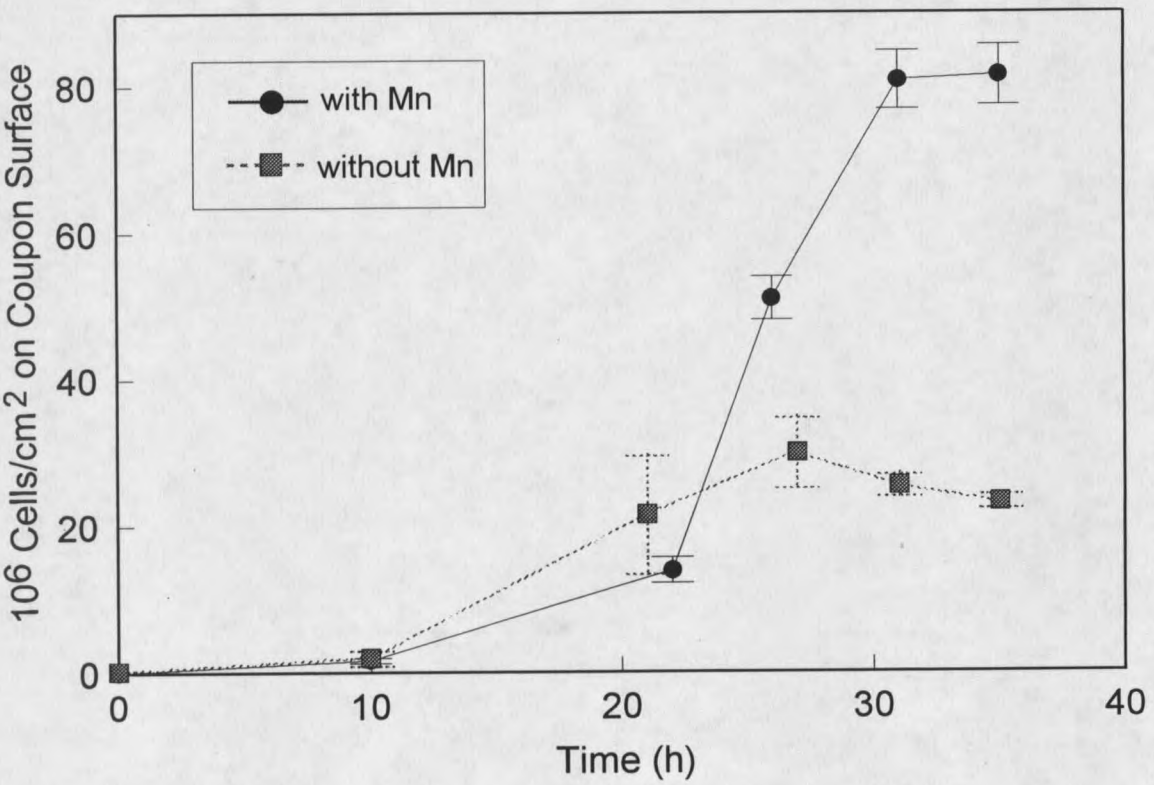

Figure 7.1. Influence of Mn(II) on attached cell density for stainless steel coupons exposed to *Leptothrix discophora*. Initial Mn(II) = 200 μM.

Manganese Uptake and Deposition.

After 21 hours of exposure to the SP-6 culture in Mn(II)-containing medium, coupon surfaces were dark brown and were coated with a biofilm ca. 100 μm in thickness. Manganese uptake from solution and deposition on the coupons began during the exponential phase of cell growth, continued through the stationary phase, and correlated with attached cell density (Fig. 7.1 and 7.2). The Mn(II) concentration in the uninoculated control remained unchanged and no MnO_x accumulated on the coupon surfaces. These results confirm that chemical oxidation of Mn(II) did not contribute to MnO_x deposition and that Mn mineralization was caused by the bacteria.

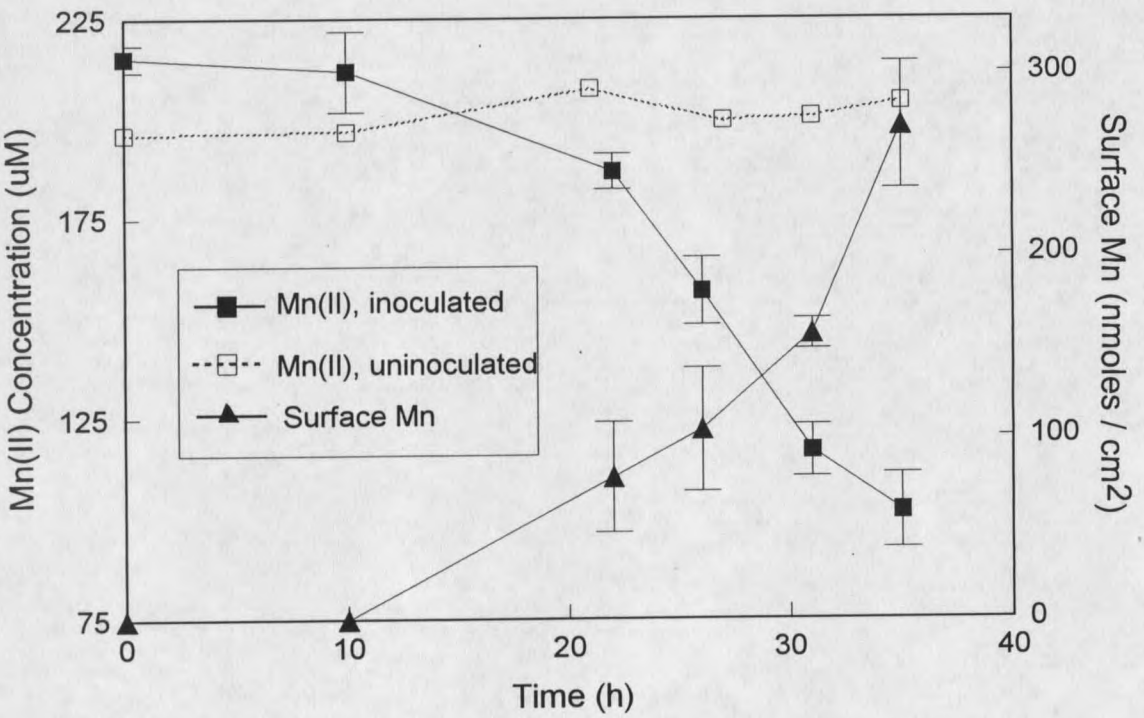

Figure 7.2. Time dependence of soluble Mn(II) concentration and surface manganese abundance on stainless steel coupons. Surface manganese for an uninoculated control experiment was undetectable and is not shown.

The Mn(II) uptake rate at the end of the experiment was 3.7 +/- 0.8 μM h^{-1} (3.5 +/- 1.1 % h^{-1} based on the final Mn(II) concentration) and MnO_x deposition rate was 28 +/-13 nmole cm^{-2} h^{-1}. After 36 hours, 270 +/-42 nmoles (MnO_x) cm^{-2} had accumulated on the coupons and 68 +/-7 μmoles Mn(II) had been removed from solution. The dark brown biofilm that covered the coupon surfaces and the reactor walls at the end of the experiment indicated that much of the MnO_x had accumulated as an attached surface deposit.

Effect of Bacteria and MnO_x on Ennoblement

Figure 7.3 shows E_{corr} over time for the three experimental treatments. In inoculated media containing Mn(II), E_{corr} began to increase after 10 hours, exceeded +300 mV_{SCE} after 25 hours, and approached +350 mV_{SCE} at the end of the experiment. The maximum rate of increase was 48 mV h^{-1} between hours 16 and 21, after which the rate diminished rapidly to 4 mV h^{-1} for times greater than 25 hours. The increase in E_{corr} began with the onset of MnO_x deposition and cell growth, and E_{corr} was correlated with both cell density and surface MnO_x up to potentials of ca. +300 mV_{SCE} (Fig. 7.4). In contrast, little change in E_{corr} was observed for coupons exposed to uninoculated media containing Mn(II) or to inoculated media without Mn(II). The small changes that were observed in controls are of the magnitude commonly observed in abiotic medium, and are usually attributed to changes in passivation current that occur as the passive film ages[1]. The lower cell density in reactors without Mn(II) cannot explain the absence of Ennoblement since E_{corr} increased no more than 50 mV at a maximum

cell density of 3 x 10^7 cells cm^{-2} under these conditions while less than half this cell density corresponded to an increase of more than 350 mV for cells grown with Mn(II).

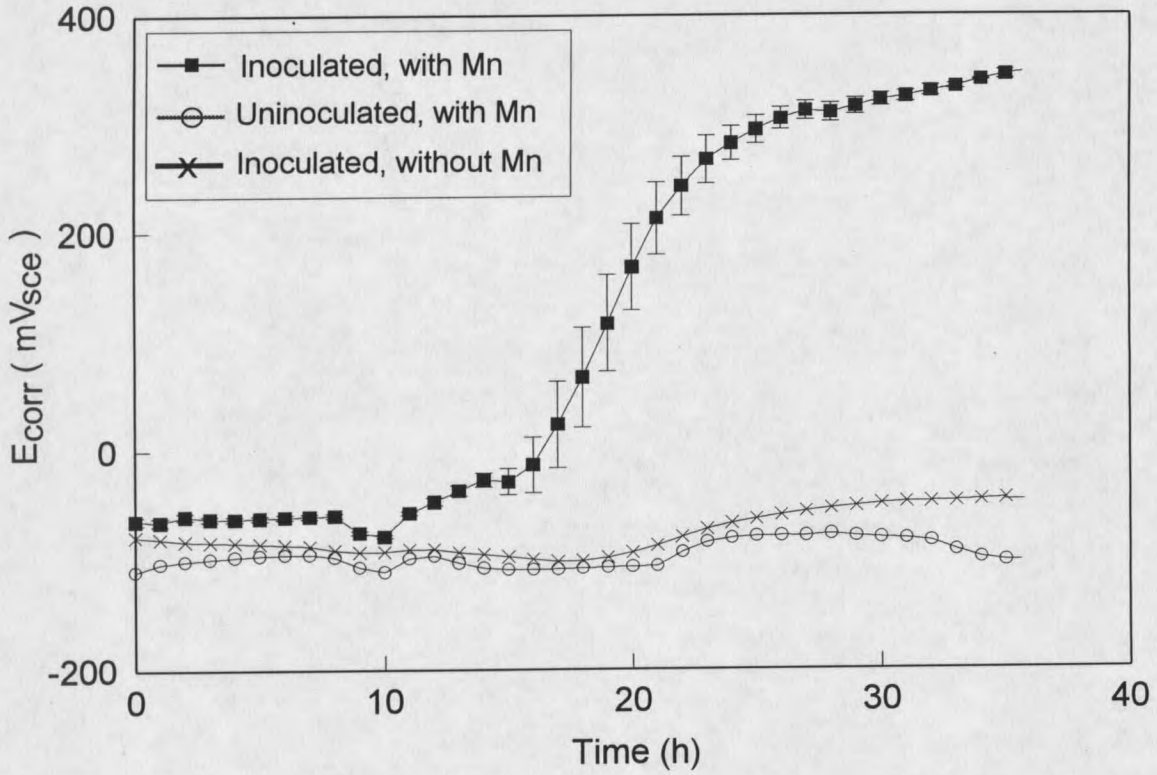

Figure 7.3. Effect of *Leptothrix discophora* grown in media containing Mn(II) on E_{corr} for stainless steel.

Figure 7.4 illustrates the relationship between Ennoblement, biofilm formation, and MnO_x deposition. E_{corr} increased ca. 5 mV per nmole cm^{-2} MnO_x up to +300 mV_{SCE} and was shifted to an Ennobled value of +330 mV_{SCE} by 75 nmole cm^{-2} MnO_x. Deposition of additional MnO_x caused little further change in E_{corr}. These results are similar to findings for stainless steel exposed to Bozeman stream water in which 15 nmole cm^{-2} MnO_x Ennobled E_{corr} to +350 mV_{SCE} and additional MnO_x deposition caused no further potential increase[28].

Variation in the amount of MnO_x required for Ennoblement in the two studies may be attributable to the different characteristics of the MnO_x deposits. In Bozeman stream water, MnO_x occurred as 3-4 μm thick deposits that adhered tightly to the coupon surface. In the present work, the sheaths of SP-6 resulted in easily dislodged sessile mats in which MnO_x deposition occurred as far as 100 μm from the substratum. We speculate that a greater fraction of the MnO_x in the present study was not in electrical contact with the coupon and therefore did not influence E_{corr}.

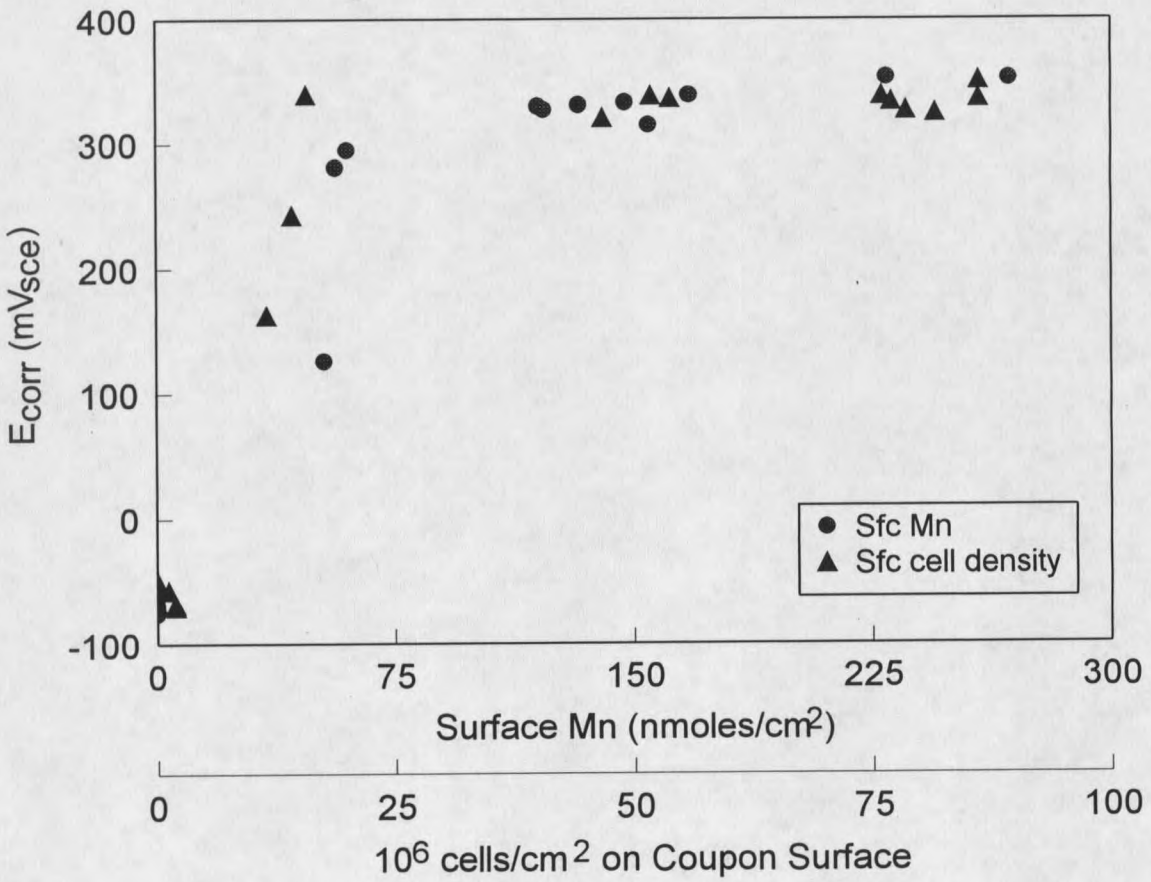

Figure 7.4. Relationship between E_{corr}, surface manganese, and attached cell density for stainless steel coupons exposed to inoculated media containing Mn(II).

The relationship shown in Figure 7.4 supports our previous finding that MnO_x shifts E_{corr} to the reduction potential for the MnO_x phase[13]. Data from figures 7.2 and 7.3 demonstrate that bacterial MnO_x deposition induces this process and confirm that manganese biomineralization by *Leptothrix discophora* results in Ennoblement.

The proposed half-reaction that fixes E_{corr} is:

$$MnO_2 + H_2O + e^- \Leftrightarrow MnOOH + OH^- \qquad (7.1)$$

which has a reduction potential of +335 mV_{SCE} at pH 8.0 [13]. At the pH used in this study (7.2), the reduction potential would be +382 mV_{SCE}, ca. 30 mV higher than observed. This difference is expected to decrease with time. It has been reported that the Mn oxidation state for MnO_x formed by *Leptothrix discophora* increases as the oxide ages, from a value of 3.32 after 11 hours to 3.62 after 30 days[21]. Such a change would increase the oxidizing power of the oxide and thus shift the reduction potential to more positive values. Figure 7.3 shows clearly that E_{corr} continued to increase at the end of the experiment suggesting that the final potential would have been higher than +350 mV_{SCE}. Many reports on Ennoblement in natural waters show an increase in E_{corr} to values greater than +300 mV_{SCE} over a period of a few days followed by a gradual increase during the ensuing few weeks[8,29]. Such findings are consistent with an increase in Mn oxidation state that would occur as microbially deposited MnO_x ages.

Relationship to Ennoblement in Natural Waters

Partitioning of MnO_x between suspended cells and sessile cells is a key issue in determining the effectiveness of natural populations of manganese-oxidizing microorganisms

in promoting Ennoblement. Mn(II) uptake has been measured widely in natural waters and microbially mediated Mn(II) oxidation has been found to be the dominant Mn(II) removal mechanism[30-33]. These experiments are usually carried out in acid leached containers and Mn(II) is recovered primarily as MnO_x on suspended particulate material. The degree to which the manganese-oxidizing activity would be concentrated at untreated metal surfaces by sessile cell growth in these same waters has not been investigated. However, the tendency for biofilms to form under these conditions is undisputed and it has been reported that sessile growth greatly enhances manganese-oxidation rate[34]. In light of this, at least part of the manganese-oxidizing activity is expected to reside near the metal surface. Moffet[35] reported Mn(II) uptake rates of 0.6 to 3.2 nM h^{-1} (0.2% to 4% h^{-1}) for Mn(II) concentrations between 20 and 1000 nM in the surface waters of Vineyard Sound, MA and similar rates were observed in the shallow waters of the Newport River estuary, NC [31]. The rates indicate daily MnO_x deposition of 14 to 75 nmoles L^{-1}. In the shallow waters of the northern Chesapeake Bay, MD, daily rates as high as 4000 nmoles L^{-1} have been estimated[30]. If even a few percent of this MnO_x deposition occurs at the surface of metal coupons, MnO_x levels of ca. 15 to 75 nmoles cm^{-2} required to induce Ennoblement would be reached within a few hours to a few months. This time scale agrees with the period of a few days to ca. one month[29] required for Ennoblement to develop on metals exposed to oxic natural waters.

Conclusions

Manganese-oxidizing bacteria are widely distributed in nature and cause a variety of industrial problems ranging from 'dirty' drinking water[36] to fouled heat exchangers[37]. Numerous reports during the past two decades have also associated these bacteria with stainless steel corrosion[15, 16, 38, 39] but the biological origin of the corrosion process has never been established. Over roughly the same period, an increasing awareness of the corrosive effects of biofilm formation on stainless steel has evolved and the Ennoblement phenomenon has been considered a principal factor in the corrosion process[1,29]. The results presented here link these separate observations to a common cause, biomineralization of MnO_x, and validate the biological mechanism of Ennoblement. Based on these findings, Ennoblement and the associated risk of corrosion must be added to an already extensive list of industrial problems caused by manganese-oxidizing bacteria.

References Cited

1. Gartland, P.O., (1993). Aspects of Testing Stainless Steels for Seawater Applications. in: Marine Corrosion of Stainless Steels: Chlorination and Microbial Effects. Ijsseling, F.P., ed. (The Institute of Materials, London), pp. 134-148.

2. Dexter, S., (1995). Effect of Biofilms on Marine Corrosion of Passive Alloys. in: Bioextraction and Biodeterioration of Metals. Gaylarde, C. and H. Videla eds., (Cambridge University Press, Cambridge, UK), pp. 129-168.

3. Dexter, S. C. and H.-J. Zhang, (1990). Effect of Biofilms on Corrosion Potential of Stainless Steel Alloys in Estuarine Waters, in: The 11th International Corrosion Congress (Associazione Italiana di Metallurgia, Florence, Italy) pp. 333-340.

4. Scotto, V., M. Beggiato, G. Marcenaro and R. Dellepiane, (1993). Microbial and Biochemical Factors Affecting the Corrosion Behaviour of Stainless Steels in Seawater. in: Marine Corrosion of Stainless Steels: Chlorination and Microbial Effects. Ijsseling, F.P., ed. (The Institute of Materials, London), pp. 21-33.

5. Mollica, A., *et al.*, (1989). Cathodic Performance of Stainless Steels in Natural Seawater as a Function of Microorganism Settlement and Temperature. Corrosion **45**:48-56 .

6. Motoda, S., Y. Suzuki, T. Shinohara and S. Tsujikawa, (1990). The Effect of Marine Fouling on the Ennoblement of Electrode Potential for Stainless Steels. Corr. Sci. **31**:515-520.

7. Mollica, A., (1992). Biofilm and Corrosion on Active-Passive Alloys in Seawater. Internat. Biodeterio. Biodegrad. **29**:213-229.

8. Holthe, R., P. O. Gartland, and E. Bardal, (1987). Influence of the Microbial Slime Layer on the Electrochemical Properties of Stainless Steel in Sea Water, SINTEF Report No. STF16 A87123 (Foundation for Scientific and Industrial Research at the Norwegian Institute of Technology, Trondheim, Norway).

9. Brennenstuhl, A. and P. Doherty, (1990). The Economic Impact of Microbiologically Influenced Corrosion at Ontario Hydro's Nuclear Power Plants. in: International Congress on Microbially Influenced Corrosion. Dowling, N.J., M. Mittelman, and J. Danko eds., (Institute for Applied Microbiology, Knoxville, TN), pp. 7/5 - 7/10.

10. Edyvean, R.G.J. and H.A. Videla, (1991). Biofouling and MIC Interactions in the Marine Environment: An Overview. in: Microbial Corrosion: Proceedings of the 2nd EFC Workshop. Sequeira, C.A.C. and A. Tiller eds., (The Institute of Materials,

London), pp. 18-32.

11. Marmo, S.A., E.-L. Nurmiaho-Lassila, O. Varjonen and M.S. Salkinoja-Salonen, (1990). Biofouling and Microbially Induced Corrosion on Paper Machines in: International Congress on Microbially Influenced Corrosion. Dowling, N.J., M. Mittelman, and J. Danko eds., (Institute for Applied Microbiology, Knoxville, TN), pp. 4/33 - 4/38.

12. Crolet, J.-L. (1991). From Biology and Corrosion to Biocorrosion, in: Microbial Corrosion: Proceedings of the 2nd EFC Workshop. Sequeira, C.A.C., and A. K. Tiller eds., (Sesimbra, Portugal, 3-6 March 1991, The Institute of Materials, London), pp. 50-60.

13. Dickinson, W., F. Caccavo Jr. and Z. Lewandowski, (1996). The Ennoblement of Stainless Steel by Manganic Oxide Biofouling. Corr. Sci. **38**:1407-1422 .

14. Kobrin, G., (1986). Reflections on Microbiologically Induced Corrosion of Stainless Steels in: Biologically Induced Corrosion, Dexter, S. C. ed., (NACE, Houston, TX) pp. 33-46.

15. Linhardt, P.,(1994). Manganese Oxidizing Bacteria and Pitting of Turbine Components Made of CrNi Steel in a Hydroelectric Power Plant. Werks. Korros. **45**:79-83.

16. Tatnall, R., (1990). Case Histories: Biocorrosion. in: Biofouling and Biocorrosion in Industrial Water Systems. Flemming, H-C. and G. Geesey, eds., (Springer-Verlag, New York) pp. 165-185.

17. Emerson, D. and W. Ghiorse, (1992). Isolation, Cultural Maintenance, and Taxonomy of a Sheath-Forming Strain of *Leptothrix discophora* and Characterization of Manganese-Oxidizing Activity Associated with the Sheath. Appl. Environ. Microbiol. **58**:4001-4010.

18. Hanert, H., (1981). The Genus Siderocapsa (and Other Iron- or Manganese-Oxidizing Eubacteria, in: The Prokaryotes, A Handbook on Habitats, Isolation, and Identification of Bacteria. Starr, M., H. Truper, A. Balows, and H Schlegel eds., (Springer-Verlag, New York, NY) pp. 1049-1059.

19. Dickinson, W. and Z. Lewandowski, (1996). Manganese Biofouling and the Corrosion Behavior of Stainless Steel. Biofouling **10**:79-93.

20. Brewer, P. and D. Spencer, (1971). Colorimetric Determination of Manganese in Anoxic Waters. Limnol. Oceangr. **16**:107-110.

21. Adams, L. and W. Ghiorse, (1988). Oxidation State of Mn in the Mn oxide Produced by

Leptothrix discophora SS-1. Geochim. Cosmochim. **52**:2073-2076.

22. Adams, L. and W. Ghiorse, (1985). Influence of Manganese on Growth of a Sheathless Strain of *Leptothrix discophora*. Appl. Environ. Microbiol. **49**:556-562.

23. Kepkay, P., (1985). Kinetics of Microbial Manganese Oxidation and Trace Metal Binding in Sediments: Results from an in situ Dialysis Technique. Limnol. Oceanogr. **30**:713-726.

24. Hobbie, J., R. Daley and S. Jasper, (1977). Use of Nucleopore Filters for Counting Bacteria by Fluorescence Microscopy. Appl. Environ. Microbiol. **33**:1225-1228.

25. Lovley, D. and E. Phillips, (1988). Novel Mode of Microbial Energy Metabolism: Organic Carbon Oxidation Coupled to Dissimilatory Reduction of Iron or Manganese. Appl. Environ. Microbiol. **54**:1472-1480.

26. Adams, L. and W. Ghiorse, (1986). Physiology and Ultrastructure of *Leptothrix discophora* SS-1. Archiv. Microbiol. **145**:126-135.

27. Habib Ali, S. and J. Stokes, (1971). Stimulation of Heterotrophic and Autotrophic Growth of Sphaerotilus discophorus by Manganous Ions. Antonie van Leeuwenhoek **37**:519-528.

28. Dickinson, W. and Z. Lewandowski, (1996). Manganese Biofouling of Stainless Steel: Deposition Rates and Influence on Corrosion Processes. CORROSION/96 paper no. 291 (NACE, Houston, TX).

29. Audouard, J., *et al.*,(1994). Effect of Marine Biofilm on High Performance Stainless Steels Exposed in European Coastal Waters. in: The Third European Federation of Corrosion Workshop on Microbial Corrosion. Tiller, A.K. and C.A.C Sequeira, eds., (Estoril, Portugal, 13-16 March 1994, The Institute of Materials, London). pp. 198-210.

30. Moffett, J., (1994). A Radiotracer Study of Cerium and Manganese Uptake onto Suspended Particles in Chesapeake Bay. Geochim. Cosmochim. **58**:695-703.

31. Sunda, W. and S. Huntsman, (1987). Microbial Oxidation of Manganese in a North Carolina Estuary. Limnol. Oceanogr. **32**:552-564.

32. Tebo, B. and S. Emerson, (1986). Microbial Manganese(II) Oxidation in the Marine Environment: a Quantitave Study. Biogeochemistry **2**:149-161.

33. Johnston, C. and G. Kipphut, (1988). Microbially Mediated Mn(II) Oxidation in an Oligotrophic Arctic Lake. Appl. Environ. Microbiol. **54**:1440-1445.

34. Nealson, K. and J. Ford, (1980). Surface Enhancement of Bacterial Manganese

Oxidation: Implications for Aquatic Environments. Geomicrobiol. J. **2**:21-37.

35. Moffett, J., (1994). The Relationship Between Cerium and Manganese Oxidation in the Marine Environment. Limnol. Oceanogr. **39**:1309-1318.

36. Sly, L., M. Hodgkinson and V. Arunpairojana, (1990). Deposition of Manganese in a Drinking Water Distribution System. Appl. Environ. Microbiol. **56**:628-639.

37. Herro, H., (1989). Deposit-related Corrosion in Industrial Cooling Water Systems. CORROSION/89 paper no. 197. (NACE, Houston, TX).

38. Kobrin, G., (1976). Corrosion by Microbiological Organisms in Natural Waters. Mat. Perform. **15**:38-43.

39. Tatnall, R., (1981). Fundamentals of Bacteria Induced Corrosion. Mat. Perform. **20:**32-38.

CHAPTER 8

SUMMARY AND CONCLUSIONS

Overview

Manganese- and iron-oxidizing bacteria (MFOB) are widely implicated in microbially influenced corrosion, often in association with sulfate-reducing bacteria (SRB). Traditionally MFOB have been assigned a passive role in the corrosion process, promoting differential aeration cells, and providing oxygen depleted conditions conducive to the growth and corrosive attack of SRB. Recent work, summarized in this article, demonstrates that manganese biofouling alters the electrochemical behavior of stainless steel (SS), and suggests that MFOB are more active in localized corrosion than traditionally held. The paper discusses the chemistry and potentially corrosive impact of manganese and iron oxides on SS, explores the possible relationship between MFOB and SRB, and proposes a model to describe the synergistic influence these organisms may exert in the corrosion process.

Introduction

A survey of the literature on microbially influenced corrosion raises several notable points: 1) sulfate-reducing bacteria (SRB) have an unparalleled reputation as agents of localized microbial attack of ferrous metals, 2) manganese- and iron -oxidizing bacteria (MFOB) are often present within the tubercles surrounding the corrosion sites, and 3) MFOB are considered to promote corrosion primarily by forming mineral deposits that occlude the metal surface. Consequent corrosion is attributed to differential aeration, colonization succession by SRB, and the SRB related processes thought to occur within the corrosion tubercle (e.g. diminished redox potential, cathodic iron sulfide formation, hydrogen depolarization, chloride counter-ion accumulation, acidifying metal-ion hydrolysis).

During the past decade, a few reports have suggested that MFOB play a more active electrochemical role in localized corrosion of SS. Duquette and Ricker[1] proposed a chemical basis for MFOB attack entailing formation of aggressive ferric and manganic chlorides and Linhardt[2] demonstrated that MFOB can induce massive pitting failure of SS. In addition, it is known that manganese oxides exhibit strong cathodic activity when coupled to passive metals[3]. Despite these considerations, the electrochemical basis for MFOB induced corrosion has as yet received little attention. Recent work in our laboratory[4] has demonstrated that manganic oxide biofouling can account for the phenomenon known as Ennoblement, in which corrosion potential (E_{corr}) and cathodic current density increase dramatically during microbial colonization of passive metals. The findings support the electrochemical role of MFOB in corrosion processes and invite closer consideration of the corrosive influence of MnO_2. The

present work summarizes our findings concerning the nature and electrochemical consequences of manganese biofouling and outlines the possible scope of MFOB related corrosion. The paper also proposes a mechanism for MFOB induced pitting of SS, and suggests a basis for synergistic corrosive attack by MFOB and SRB.

MFOB and Localized Corrosion

Reports linking MFOB to localized corrosion consist largely in detection of MFOB and elevated iron and manganese levels at the corrosion site. A quote from Tatnall[5] is illustrative;

> "scattered throughout the (corrosion) mound will often be found filamentous or stalked iron-oxidizing bacteria ... high numbers of *Gallionella* iron-oxidizing bacteria and *Siderocapsa* iron- and manganese-concentrating bacteria...and high levels of iron, manganese, and chloride. Under each of these mounds was found a subsurface pit... Failures of this sort have been reported at numerous sites world-wide."

While reports of corrosion attributed solely to MFOB activity are becoming more numerous[2,5,6] by far the majority of case histories still note an association between MFOB and SRB at the corrosion sites. Thus Videla and Characklis[7] state that

> "metal-oxidizing microorganisms create environments for the accumulation of chloride ions and form acidic ferric chloride and manganic chloride, which are corrosive to SS. However the main mechanism used by this kind of tubercle-forming bacteria is the production of differential aeration cells. ... In all cases, corrosion enhancement is largely due to the presence of SRB in the inner area of the tubercle."

Although there is an increasing awareness that 'in cases of anaerobic corrosion, SRB are seldom if ever the sole organisms present, and other mechanisms of microbial corrosion are at least potentially active'[8] the prevailing opinion remains that MFOB promote corrosion primarily by establishing differential aeration cells and oxygen-depleted conditions conducive to SRB growth. Our recent work on Ennoblement suggests that another mechanism is indeed 'potentially active'.

Stainless Steel Ennoblement

Ennoblement refers to the several hundred millivolt noble shift in E_{corr} and the accompanying 2 to 3 decade increase in cathodic current density that develop when SS or other passive metals are colonized by microorganisms in natural waters. Figures 8.1 and 8.2 illustrate this behavior for Type 316L SS (UNS 31603) during *in situ* exposure to fresh river-water. The apparent limiting potential between +300 and +400 mV (all potentials vs. the saturated calomel electrode, SCE) is characteristic of nearly all reported cases of Ennoblement. In a series of recent experiments[4,9], we demonstrated the following points concerning these phenomena: 1) MFOB and Mn-rich mineral deposits accumulate during Ennoblement; 2) chemical dissolution of the manganese deposits shifts E_{corr} to pre-exposure values; and 3) SS coated with MnO_2 paste exhibits electrochemical behavior nearly identical to that displayed by Ennobled coupons (Figures 8.1 and 8.2 include the electrochemical behavior of MnO_2 paste coated coupons). Based on these results and the thermodynamic potential for one-electron reduction of MnO_2 we concluded that biomineralized manganese,

reacting according to equation 8.1, is responsible for the increase in potential and cathodic current density observed during Ennoblement.

$$\gamma MnO_2 + H_2O + e^- \Leftrightarrow \gamma MnOOH + OH^- \quad : E^{o'}_{pH=8} = +335\ mV_{SCE} \quad (8.1)$$

MnO_2 deposited on the metal surface acts as an attached cathode to depolarize the metal. The increasing cathodic current density shifts E_{corr} in the noble direction until the reduction potential for MnO_2 at the experimental pH is reached; at this point E_{corr} remains fixed by the solid-phase redox equilibrium. Our experiments confirmed that once sufficient MnO_2 was applied to shift E_{corr} to +350 mV, application of additional material caused no further increase in potential.

The electrochemical influence of metal-oxide biofouling very likely extends to iron-oxides as well. The thermodynamic potential for reduction of ferric oxide to magnetite[10] is given as:

$$3Fe_2O_3 + H_2O + 2e^- \Rightarrow 2Fe_3O_4 + 2OH^- \quad : E^{o'}_{pH=8.5} = -529\ mV_{SCE} \quad (8.2)$$

Typical values of E_{corr} for mild steel at neutral pH lie near -700 mV, significantly more negative than the reduction potential shown in equation 8.2. Thus, ferric oxides are thermodynamically unstable on mild steel in aerated media and may accelerate corrosion by cathodically depolarizing the metal. The possibility has been investigated for wet/dry rust cycles[11,12] but the influence of ferric oxide biomineralization on the corrosion of mild steel has yet to be investigated. In contrast, the potential in equation 8.2 is lower than E_{corr} for SS in aerated media, indicating that under aerobic conditions, ferric oxides will not cathodically depolarize SS.

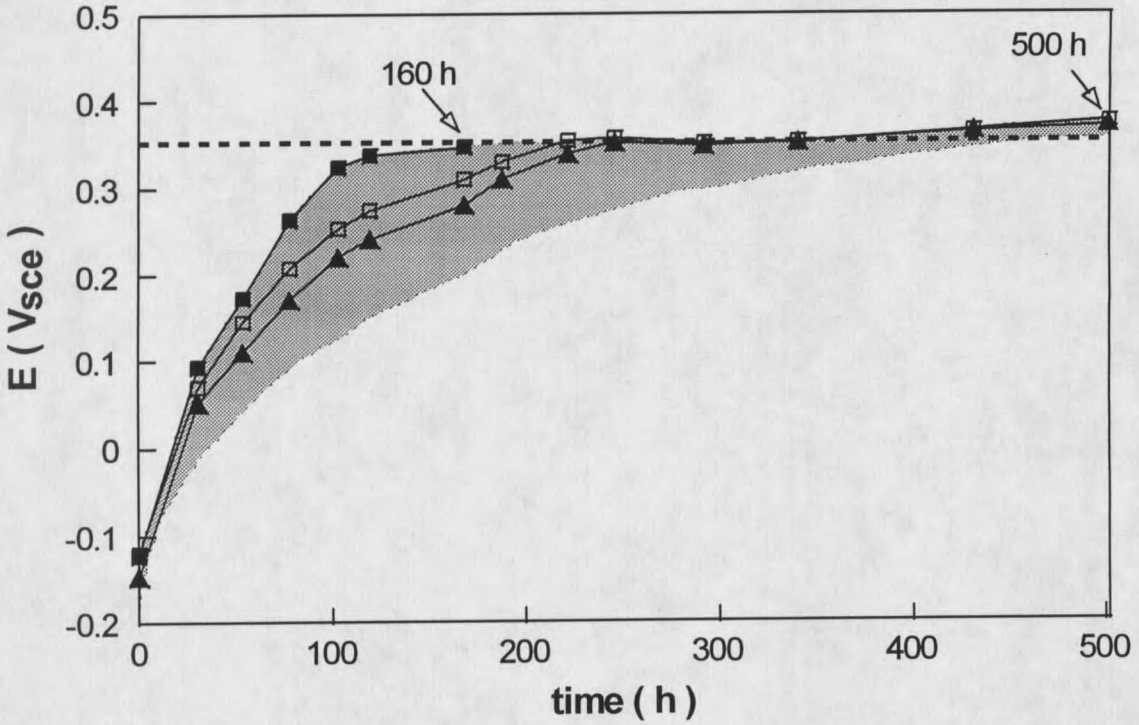

Figure 8.1. E_{corr} vs. time for 316L stainless steel coupons during *in situ* exposure to fresh river-water. Data points for 3 coupons used for polarization measurements are shown, while shaded area envelopes curves for 23 coupon set. At times denoted by arrows, cathodic polarization curves were measured. Horizontal dashed line indicates potential for MnO_2-paste coated coupon.

Galvanostatic reduction behavior shown in figure 8.3, for 316L SS in the presence and absence of Ennoblement illustrates the cathodic character of surface oxides. Galvanostatic reduction is commonly applied to investigations of passive films[13] and in battery research[14] and is carried out by applying constant cathodic current to samples in deaerated (depolarizer-free) electrolyte. In the absence of dissolved faradaic reactants, the electrode is rapidly polarized to the stability potential of adsorbed surface phases, followed by a potential lag as the surface phase is reduced. The potential lag near -550 mV visible in figure 8.3 is attributed to ferric

oxide reduction[13] and shows the close agreement between thermodynamic stability potential (cf. equation 8.2) and onset of oxide reduction. The lag at more positive potential exhibited by the Ennobled coupon is assigned to MnO_2 reduction. While, in this latter case, lag potential and stability potential (cf. equation 8.1) do not match, the difference can be attributed to polarization effects, and indeed, the potentials converge as the applied current density is diminished[9].

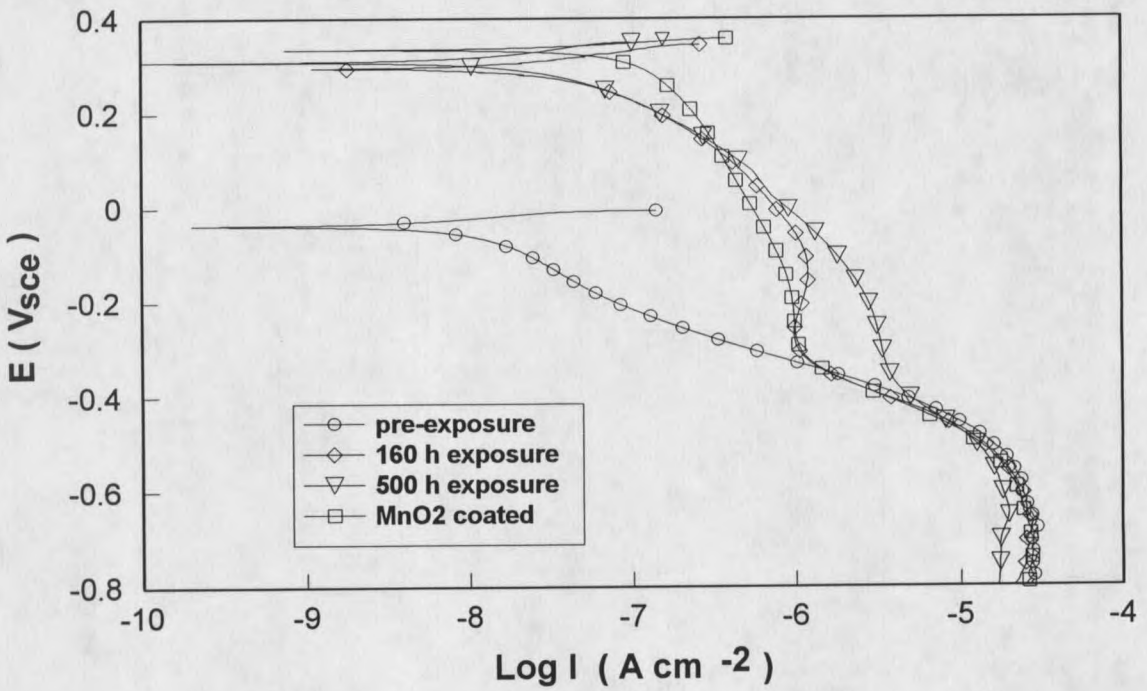

Figure 8.2. Cathodic polarization curves for 316L stainless steel coupons after different exposure intervals in fresh river-water, and for an unexposed coupon coated with MnO_2 paste. Measurements were made in air saturated 0.01M Na_2SO_4 / pH 8.4.

MIC of SS is characterized by reddish-brown mound-shaped or volcano-like deposits connected by pin-hole perforations to large subsurface cavities[5,15]. In some cases, the surface

perforations can be microscopic[16,17]. Based on our Ennoblement studies, we propose that this form of MIC may result from the electroactivity and specific morphology of the manganese deposits produced by MFOB.

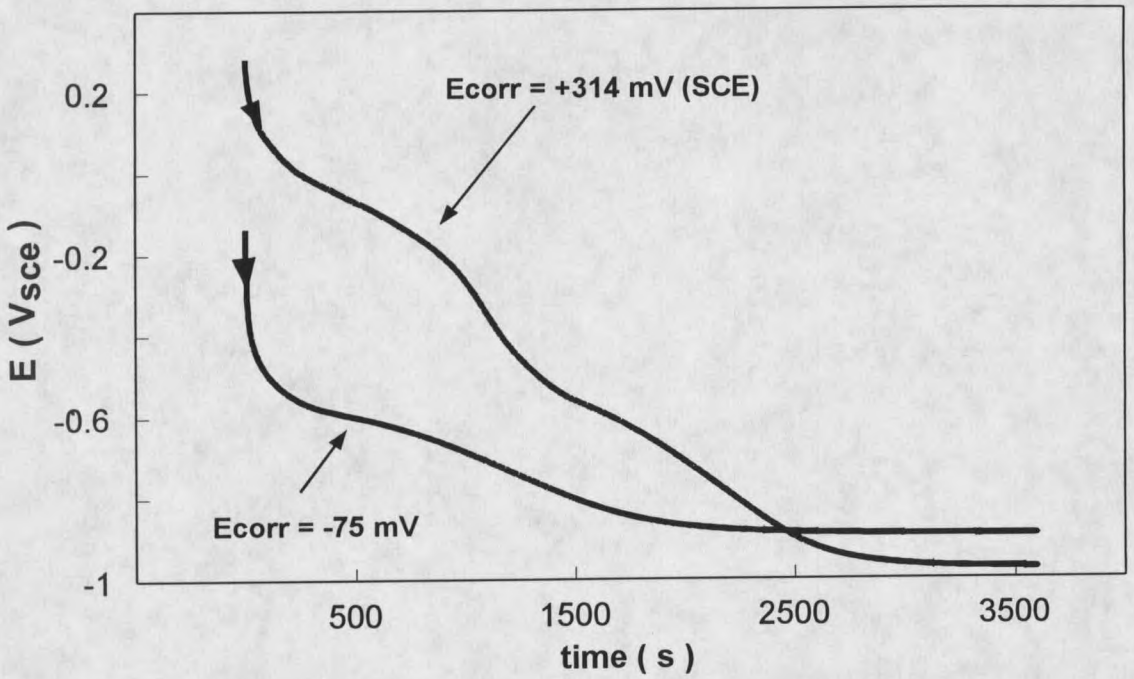

Figure 8.3. Galvanostatic reduction behavior for two 316L stainless steel coupons in deareated 0.1 M Na_2SO_4 / pH 8.5 after 4 months exposure to fresh river-water. 2.5 μA cm^{-2} applied current. E_{corr} values are at the end of the exposure period.

Proposed Mechanism of Pit Formation by MFOB

It was shown[4,9] that stainless steel Ennoblement is caused by deposition of biomineralized manganic oxide on the metal surface. Figure 8.4 shows the distinctive ring-shaped morphology of the manganese-rich deposits formed in fresh river water. The rings are 10-20 μm in diameter, approximately 3 μm thick, and frequently contain clusters of individual bacterial cells within the 3-4 μm diameter central void. Figure 8.5 shows the microbial characteristics associated with the rings for biofilm formed on 316L SS in fresh river-water.

The photograph, obtained using epifluorescence microscopy, reveals sheathed cells characteristic of the *Leptothrix-Sphaerotilus* group and cell clusters within the rings characteristic of *Siderocapsa* bacteria. Both genera are known to deposit manganese, and in our experiments, manganese-oxidation was exhibited by separate cultures of both filamentous and sheath free cells isolated from Ennobled coupons. Manganese enrichment within the annular deposits is shown in figure 8.6.

The ring–bacterial cell taxonomy, in the presence of MnO_2, suggests the following mechanism as the basis for the characteristic subsurface pitting observed in MIC of SS: Ennobled potential due to cathodic MnO_2 depolarization, coupled with diminished redox potential caused by microbial respiration, increases the interfacial potential difference within the rings to a value exceeding the critical pitting potential (E_{pit}). This occurs before E_{pit} for metal exposed to bulk solution is reached and leads to preferential pit nucleation within the rings. Enhanced pit nucleation in turn increases the probability that stable pit growth will develop. The fixed MnO_2 cathode would initially prevent the pit from spreading but would support relatively large anodic currents, leading to the microscopic surface openings. Once stable pitting develops, active corrosion currents may consume the available MnO_2, removing the fixed cathode and allowing the surface openings to broaden. The combination of ferrous corrosion products and continued iron and manganese biomineralization around these sites would result in visible red-brown mounds. By this mechanism, MFOB can be expected to promote SS pitting even in fresh waters. The combined influence of MFOB and colonization succession by SRB would be potentially even more damaging, since the risk of pit nucleation would increase as SRB activity further decreases redox potential within the rings.

Evidence to support the above model can be obtained by considering the anodic current required to sustain SS pitting. The 'pit stability product' required for stable pit growth on 304 SS is 3 mA cm^{-1} [18]. For hemispherical pits constrained to the 3-4 μm diameter area within the rings (figure 8.4), this would correspond to about 5 μA. Figure 8.2 shows that Ennobled SS of a few cm^2 area would support this current at potentials that still exceed E_{pit} (-50 mV at 0.5N NaCl[19]), indicating that a greater density of metastable pits can be sustained by manganic oxide depolarization than by oxygen depolarization alone. The greater density, increases the probability that a metastable pit will stablilize. In addition to increasing the density of metastable pits, the ring shape would serve as a barrier to diffusion of cations from the metastable site, lowering the 'pit stability product' required to maintain the high cation anolyte concentrations required for pit growth.

The mechanism described above has some similarities to previous arguments relating SS pitting to manganese biofouling[1] but differs in a fundamental way, and, contrary to the previous discussions, is based on experimental evidence that manganese biofouling strongly shifts E_{corr} in the noble direction. In past discussions, the corrosive agents produced during MFOB biofouling are considered to be ferric and manganic chlorides. The argument assumes that metal ions produced during oxidation of the substratum necessitate accumulation of counter anions (typically chloride) at the metal surface to maintain charge neutrality. Chloride accumulation in the presence of MnO_2 presumably results in an aggressive manganic chloride solution. While this mechanism suggests that manganese biofouling intensifies attack once corrosion is initiated, it does not address the possible mechanism in which MnO_2 fosters corrosion by enhancing pit nucleation and sustaining greater metastable pit density.

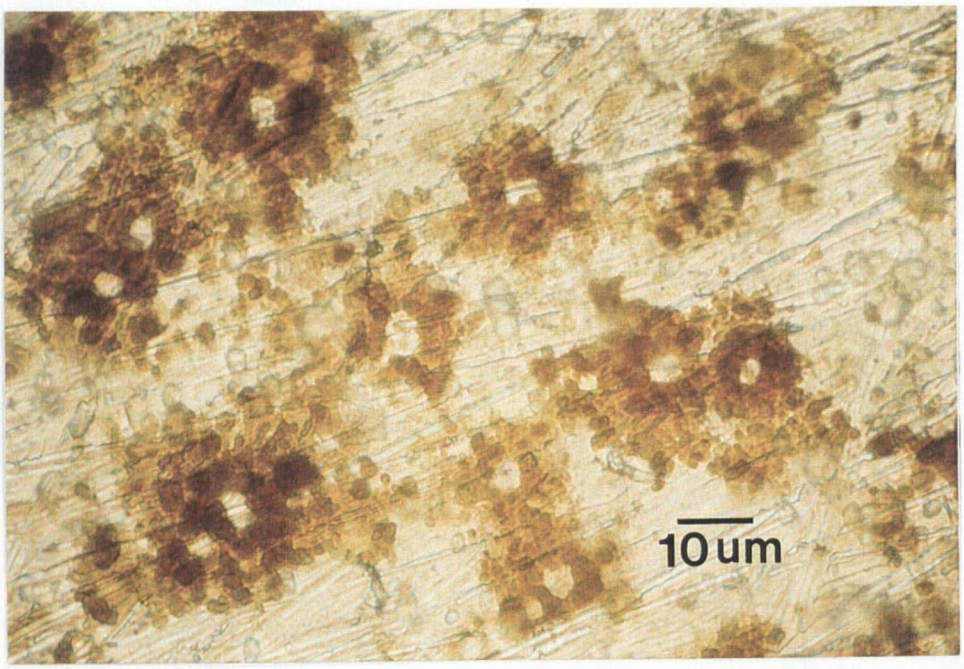

Figure 8.4. Reflected-light micrograph of annular deposits on 316L stainless steel coupon after 13 day *in situ* exposure to fresh river-water. Stainless steel substratum is visible outside the rings and within the central void.

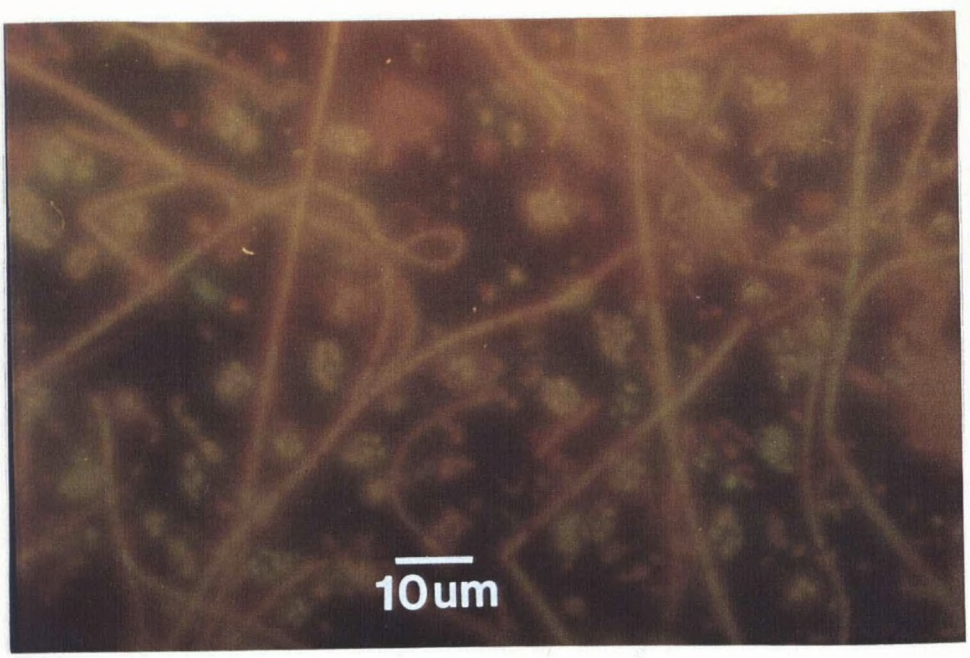

Figure 8.5. Epifluorescence micrograph of acridine-orange stained biofilm on 316L stainless steel after exposure to fresh river-water. Bacterial cells centrally located within annular deposits as well as sheathed filamentous bacteria can be seen.

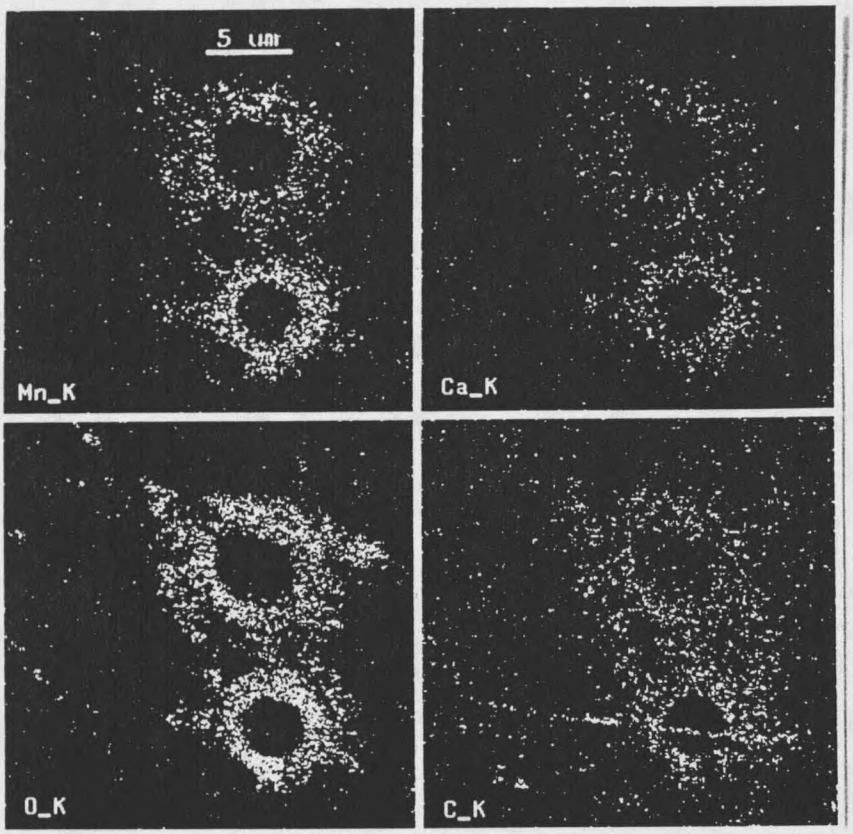

Figure 8.6. EDS maps of annular deposits on 316L stainless steel coupons confirming the presence of Mn, Ca, O, and C.

MnO_2 Induced Corrosion

To demonstrate that MnO_2 can induce corrosive attack of SS, chemically prepared MnO_2 paste[4] was applied to a 304L SS coupon, and the coupon was immersed in 0.05N NaCl solution carbonate buffered at pH 8.2, while E_{corr} was monitored and linear polarization resistance (R_p) was periodically measured. As shown in figure 8.7, E_{corr} exhibited a series of negative excursions that were accompanied by a sharp decrease in R_p. The behavior is interpreted as follows: 1) cathodic depolarization by MnO_2 elevates E_{corr} above E_{pit} (E_{pit} =

0.12V in 0.05N NaCl-pH 8.2, unpublished data); 2) increased corrosion current caused by pit initiation anodically depolarizes the electrode, with MnO_2 furnishing the cathodic current; 3) as E_{corr} falls below the protection potential (E_{prot}), anodic current drops, and E_{corr} again increases. The process is the same as for active-passive cycles with dissolved oxygen (DO) as the sole depolarizer, with the marked distinction that the elevated cathodic current supplied by MnO_2 (cf. Figure 8.2) requires a higher anodic current to polarize E_{corr} to E_{prot}. Thus more numerous or more active pits must form before repassivation can occur, increasing the risk of stable pit formation and localized damage.

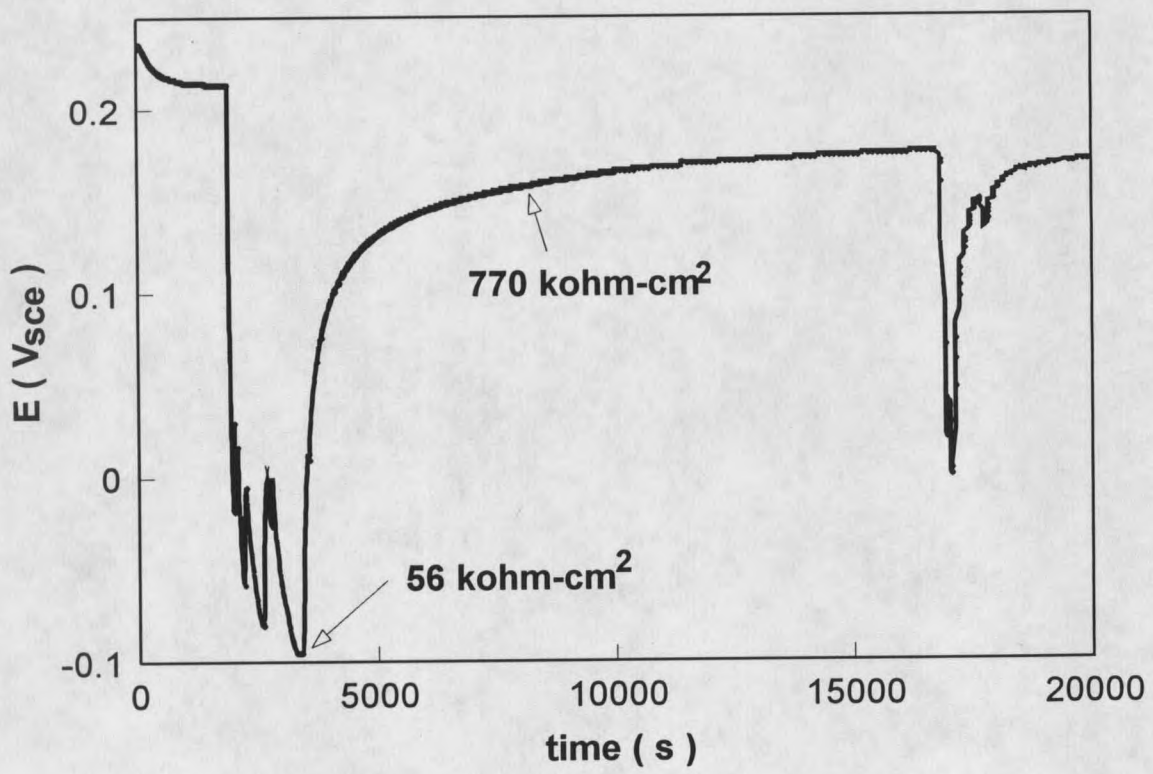

Figure 8.7. E_{corr} vs. time for MnO_2-paste coated 304L stainless steel coupon in 0.05N NaCl / pH 8.2. Polarization resistance at two points during exposure is shown.

Potential Scope of MFOB Related corrosion

In view of the proposed mechanism of microbially induced pitting of SS, the question arises, 'how pervasive is MFOB corrosion?' Only a few of the reports published since MIC of SS was first noted in the early 1970's[20] have included manganese analysis of the corrosion products[5,15,16,21]. Nevertheless, the widely acknowledged role of MFOB in tubercle formation[22-24] indicates that these bacteria are prevalent; and indeed these organisms are known to be broadly distributed in soils and natural waters[25-27]. While reports of MFOB related corrosion have most frequently implicated the freshwater genera *Siderocapsa*, *Gallionella*, and the filamentous bacteria *Leptothrix* and *Sphaerotilus*, a far broader range of organisms are known to deposit manganese. These include the bacterial genera *Bacillus*, *Pseudomonas*, and *Micrococcus*[28], numerous marine bacteria, and a variety of algae, yeast and fungi[26]. Schuett et al.[29] isolated forty-seven strains of manganese-oxidizing bacteria from manganese nodules, sediments, and seawater in the Pacific Ocean and the Mediterranean Sea; Moffett[30] demonstrated microbially-mediated oxidation of manganese(II) in seasonally anoxic coastal waters; and Cowen and Silva[31] established the presence of manganese-oxidizing bacteria and biomineralized manganese on macroparticulate material in the oceanic water column. Such reports underlie the pronouncement that "microorganisms are, either directly or indirectly, the major catalysts of manganese cycling in the natural environment"[27] and indicate that manganese biofouling can be expected under a variety of natural conditions.

The extent of corrosion caused by manganese biofouling has yet to be assessed. The ability of manganese deposits to depolarize SS is at least partially dependent on where the

deposit is located relative to the metal surface since the mineral must be within charge-transfer distance or must be embedded in electrically conductive material. Thus in our experience, adherent deposits such as those depicted in figure 8.4, are effective depolarizers, while deposits broadly distributed within a polysaccharide biofilm matrix may cause E_{corr} to shift only slightly, if at all. Furthermore, the extent of Ennoblement may be influenced by the rate of manganese deposition. That is, MnO_2 accumulation will reflect both the rate of biological and chemical deposition and the rate of removal by discharge through the metal corrosion current. We determined rates of cathodically active MnO_2 deposition between 0.57 and 3.1 mcoul cm^{-2} day^{-1} for 316L SS exposed to fresh river-water[9]. For a one-electron reduction according to equation 8.1, the cathodic material deposited at these rates would be discharged by between 6 and 36 nA cm^{-2} of anodic current. Initially, with E_{corr} near the pre-exposure value, anodic current will be balanced by DO reduction, allowing MnO_2 to accumulate; however as MnO_2 deposition shifts E_{corr} in the positive direction, more and more cathodic current will be supplied by MnO_2 reduction. Only metals with low corrosion currents (i.e. noble or passive metals) will allow MnO_2 to accumulate sufficiently to reach Ennobled potentials. MnO_2 accumulation will also depend on the nature and activity of the organisms causing deposition, and on the redox, chemical, and physical characteristics of the environment. As an example of the possible influence of physical conditions, we speculate that inhibition of Ennoblement, which has been observed for sunlight-irradiated seawater[32] may be caused by photo-inhibition of enzymatic manganese oxidation[33], that prevents MnO_2 deposition.

Manganese oxidation rates (biological plus chemical) have been determined in a number of natural environments[26] but these are typically reported as Mn(II) uptake rates

(moles liter^{-1} hour^{-1}.) It is difficult to relate these rates to deposition of cathodically active material since the surface area of the particulate material (on which the deposition is presumed to occur) is generally not known. Nevertheless, if all Mn(II) oxidation were to deposit MnO_2 on a metal surface placed in solution, the above studies suggest that deposition rates as high as 4000 nmoles day^{-1} per liter of solution may be encountered in some natural environments. This would have a very strong influence on the cathodic performance of the metal.

A better perception of the extent of potentially destructive manganese biofouling is gained by considering the reported instances of Ennoblement. In separate studies, the electrochemical behavior of passive metals exposed to fresh, estuarine, and marine waters at more than a dozen sites world-wide has been examined. In all but two of the reports, E_{corr} was observed to increase to values exceeding +300 mV at rates between five[34] and several hundred[9,35] mV day^{-1}. If these experiments are representative of the behavior of SS exposed to natural waters, then the risk of pit initiation due to manganese biofouling is significant.

MnO_2 and SRB: Chemistry within the Deposits

A possible symbiotic relationship between MFOB and SRB has been noted above. SRB are obligate anaerobes and under natural conditions, depend on the action of aerobic and facultative anaerobic microorganisms to generate oxygen depleted conditions. MFOB respiration coupled with a deposit morphology that impedes oxygen transport can reasonably be expected to provide such conditions, and this point has been raised repeatedly in the

literature[15,21,23]. In light of the chemical and electrochemical reactivity of MnO_2 however, a number of possible chemical aspects of MFOB/SRB symbiosis also bear consideration.

Hamilton[36] has noted the limited nutritional spectrum of SRB. The bacteria can utilize small organic acids and alcohols, but are generally unable to grow on carbohydrates or biopolymers. To quote further,

> "Although SRB are strict anaerobes, it has been noted that in sediment systems they demonstrate maximal activity within a few centimeters of the aerobic/anaerobic interface. Almost certainly this reflects nutrient input from the metabolic activities of other aerobic and facultative organisms also present but with greater biodegradative capability than the SRB, and the availability of biotic and abiotic oxidation of the produced sulphide to which the SRB are themselves sensitive."

Nutrient Production

Sunda and Kieber[37] have recently reported significant levels of pyruvate formation by MnO_2 oxidation of humic substances in natural waters. They speculate that manganese oxidation has evolved as a means by which abundant but biologically refractory humic and fulvic acids can be converted to low-molecular-weight biological substrates. They measured pyruvate formation rates of 10 nM h^{-1} for 2 mg L^{-1} fulvic acid in the presence of 55 mg L^{-1} of suspended MnO_2, and noted that total production of small organic substrates including alcohols and short chain organic acids is likely to be considerably greater. We previously measured MnO_2 biofouling rates greater than 1 μg cm^{-2} day^{-1} on 316L SS exposed to river-water[9]. The MnO_2 is contained almost completely within the annular deposits shown in figure 8.4, which numbered approximately 1600 rings mm^{-2} after 7 days exposure. From

these values, a mass of 44 ng MnO_2 per ring is calculated. Treating each ring as a tiny reaction vessel, and applying the following simplifying assumptions: 1) stagnant solution containing 2 mg L^{-1} fulvic acid permeates the roughly 15 μm diameter x 3 μm thick volume of the ring plus central void (volume of ring plus void, 5×10^{-13} L; substratum area beneath central void, 1.2×10^{-11} m^2), 2) all MnO_2 in a ring is accessible for reaction with the stagnant solution; 3) the 10 nM h^{-1} rate for 55 mg L^{-1} of MnO_2 can be extrapolated to the grossly larger MnO_2 weight to solution volume ratio within the rings; and 4) pyruvate removal by mass transfer can be ignored; a pyruvate production rate of 15 μM h^{-1} within the rings can be estimated. For a ring volume of 5×10^{-13} L, a production rate of 7.5×10^{-18} moles h^{-1} per ring is estimated. Characklis and Marshall[38] reported glucose removal rates of about 2.8×10^{-4} moles m^{-2} h^{-1} for a 10 μm thick mixed culture biofilm. Converting this to a pyruvate removal rate based on a pyruvate/glucose ATP ratio of 0.4 for aerobic metabolism, gives a value of 7×10^{-4} moles m^{-2} h^{-1}. For a biofilm area of 1.2×10^{-11} m^2, a pyruvate consumption rate of about 8×10^{-15} moles h^{-1} within each ring is calculated. Thus, pyruvate produced by MnO_2 oxidation of fulvic acid is estimated to furnish roughly one-tenth of one percent of the substrate demand within the rings, and as noted, pyruvate may represent only a small fraction of the total assimilable organic carbon produced during fulvic acid degradation. This coarse calculation provides a modest test of Sunda's hypothesis concerning the evolutionary selection of manganese biomineralization, and suggests that MFOB activity could generate modest levels of organic substrates for SRB growth.

Sulfide Removal

Sulfide is known to repress SRB growth[36,39] and standard culture technique for these organisms includes addition of ferrous iron that detoxifies the media by formation of FeS[39]. This same process may protect SRB during growth in the presence of active ferrous metal dissolution, as would occur during corrosion of mild steel. For SS in the passive state, however, ferrous iron production will be negligible, and the above mechanism of sulfide removal will not be operative. Under these conditions, other sulfide removal mechanisms may be important to SRB growth, and one such mechanism is sulfide removal by reaction with MnO_2.

MnO_2 is reduced by bisulfide ion in natural waters according to the reaction[40]:

$$\delta MnO_2 + HS^- + 3H^+ \Rightarrow Mn^{2+} + S^o + 2H_2O \qquad (8.3)$$

and MnO_2 may further oxidize elemental sulfur to sulfate[41]. Reaction 8.3 is rapid and quantitative, and provides a substantial removal mechanism for microbially produced sulfides in anoxic waters. The same process may be the primary mechanism controlling sulfide toxicity during initial SRB growth on passive SS, and so may promote pit nucleation by fostering SRB growth as described in the Mechanism of Pit Formation above.

Reactions with Corrosion Products

Once pit nucleation occurs within a ring, MnO_2 chemistry may continue to influence the corrosion process. Thermodynamically favored reactions such as 8.4 and 8.5, would serve

to oxidize ferrous corrosion products and deposit hydrous ferric oxides. Oxide accumulation near the pit nucleation site would serve as an added barrier to Cr^{3+} diffusion and so would promote the high concentration of this acidifying cation required for metastable pit growth. The result would be similar to porous cap formation that occurs in conventional pitting of SS when ferrous ion is oxidized by dissolved oxygen[24]. The role of MnO_2 in forming the barrier may be particularly important for processes occurring in the low oxygen conditions at the base of a biofilm where ferric oxide deposition might not otherwise occur.

$$Fe^{2+} + MnO_2 + 2OH^- \Rightarrow FeOOH + MnOOH \tag{8.4}$$

$$2Fe^{2+} + MnO_2 + 2OH^- \Rightarrow 2FeOOH + Mn^{2+} \tag{8.5}$$

In the presence of sulfides, an additional process may occur as insoluble FeS is oxidized by MnO_2 to produce SO_4^{2-}, and regenerate Fe^{2+} [41]. Fe^{2+} may then be oxidized further by reactions 8.4 and 8.5. The net result would be to shift the location of surface occlusions that form during the corrosion process. The actual influence of MnO_2 on the corrosion chemistry will very likely depend on the spatial relationship between the deposit and the nucleation site; near surface pH and oxygen gradients; the geometry of the ferrous ion plume emanating from the pit; counter-ion access; and whether SRB are present. Microbiological analysis coupled with micro-electrode measurements of DO, S^{2-}, redox potential, and pH within the rings before and after pit initiation would help clarify the actual pitting process.

Model for MFOB/SRB Induced Corrosion

The proposed chemical interactions between MnO_2 and SRB, together with the electrochemical effects already described, make it possible to propose an overall synergistic relationship between MFOB and SRB in promoting SS corrosion. The following model is put forth:

1) SS is colonized by heterotrophic MFOB which consume oxygen and produce MnO_2-rich deposits;
2) the deposits i) physically impede oxygen transport, allowing oxygen depleted conditions to develop; ii) oxidize natural polymeric substances to produce organic substrates suitable for SRB growth; and iii) elevate metal potential by depolarizing the cathodic process;
3) SRB colonization, which develops under the favorable growth conditions, lowers redox potential within the deposits by producing sulfides;
4) sulfide toxicity is controlled by oxidation at the MnO_2 deposits, furthering SRB growth;
5) the combined electrochemical effects of elevated metal potential and diminished redox potential raise the interfacial potential difference within the deposits above the critical pitting potential, causing pit nucleation;
6) elevated cathodic current density provided by the MnO_2 prevents repassivation of the nucleation sites and increases the probability of stable pit growth by supporting a greater density of metastable pits;
7) MnO_2 deposits impede diffusion of acidifying corrosion products, and so promote the high anolyte cation concentrations required for stable pit growth.

Figure 8.8 shows the overall nature of this process. While the key role of MnO_2 in SS Ennoblement has now been established, several of the steps in the model are based on theoretical arguments that clearly invite continued research.

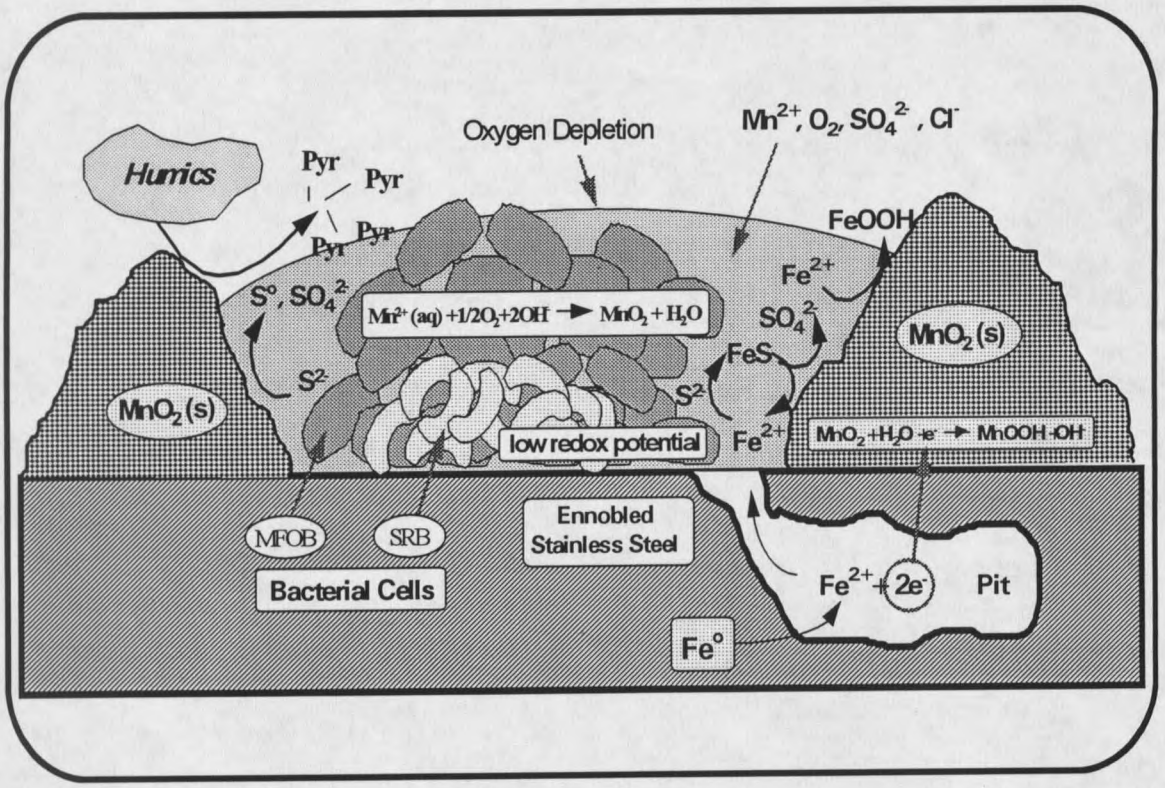

Figure 8.8. Proposed model of corrosion processes within biomineralized MnO_2 deposit containing SRB. MnO_2 depolarization shifts E_{corr} to values exceeding E_{pit} at local sites of diminished redox potential. Cross-section through annular ring is shown.

Concluding Remarks

Manganese biomineralization is a widely distributed process in natural waters. Results from recent experiments on Ennoblement have demonstrated that this process profoundly alters the electrochemical behavior of SS and suggest that biomineralized MnO_2 may be responsible for widely observed pitting corrosion of microbially colonized SS. It has been

shown that, at modest chloride concentrations, MnO_2 coated SS exhibits behavior typical of pit initiation, and it is suggested that an annular deposit morphology may compound the corrosive effect by serving as a barrier to oxygen penetration and cation removal. SRB succession within manganese biofouling deposits may intensify the corrosive effect of MnO_2 by diminishing redox potential; and both chemical and physical interactions between MnO_2 and SRB are expected to promote SRB succession. Defining the ecological and corrosion relationships between MOB and SRB will be an important next step in controlling microbially influenced corrosion of stainless steel.

References Cited

1. Duquette, D. and R. Ricker, (1986). Electrochemical Aspects of Microbially Induced Corrosion, in: Biologically Induced Corrosion, Dexter, S. C. ed., (NACE, Houston, TX), pp 121-130.

2. Linhardt, P.,(1994). Manganese-Oxidizing Bacteria and Pitting of Turbine Components Made of CrNi Steel in a Hydroelectric Power Plant. Werkst. Korr. **45**:79-83.

3. Tomashov, N. D., and G. P. Chernova, (1967). Passivity and Protection of Metals Against Corrosion, (Plenum Press, New York, NY) 208 pp.

4. Dickinson, W., F. Caccavo Jr. and Z. Lewandowski, (1996). The Ennoblement of Stainless Steel by Manganic Oxide Biofouling. Corr. Sci. **38**:1407-1422.

5. Tatnall, R., (1990). Case Histories: Biocorrosion, in: Biofouling and Biocorrosion in Industrial Water Systems. Flemming, H-C, and G. Geesey eds., (Springer-Verlag, New York, NY) pp. 165-168.

6. Kobrin, G., (1986). Reflections on Microbiologically Induced Corrosion of Stainless Steels in: Biologically Induced Corrosion, Dexter, S. C. ed., (NACE, Houston, TX) pp. 33-46.

7. Videla, H. A., and W. G. Characklis, (1992). Biofouling and Microbially Influenced Corrosion. Int. Biodeterior. Biodegrad. **29**:195-207.

8. Hamilton, W., and S. Maxwell, (1986). Biological and Corrosion Activities of Sulphate-Reducing Bacteria Within Natural Biofilms, in: Biologically Induced Corrosion, Dexter, S. C. ed., (NACE, Houston, TX), pp. 131-143.

9. Dickinson, W., and Z. Lewandowski, (1996). Manganese Biofouling of Stainless Steel: Deposition Rates and Influence on Corrosion Processes. CORROSION/96, paper no. 291, (NACE, Houston, TX).

10. Dickinson. W., and Z. Lewandowski, (1995). Electrochemical and Microelectrode Studies of Stainless Steel Ennoblement. CORROSION/95, paper no. 223, (NACE, Houston, TX).

11. Carpio, J., A. Parra, L. Martinez, M. Mondragon, and V. Castano, (1995). Scanning Electron Microscopy and Infrared Spectroscopic Studies of Marine Atmospheric Corrosion Products of Steel. CORROSION/95, paper no. 242, (NACE, Houston, TX).

12. Evans, U. and C. Taylor, (1972). Mechanism of Atmospheric Rusting. Corr. Sci. **12**:227-246.

13. Ramasubramanian, N., N. Preocanin, and R. D. Davidson, (1985). Analysis of Passive Films on Stainless Steel by Cyclic Voltammetry and Auger Spectroscopy. J. Electrochem. Soc. **132**:793-798.

14. Bates, J., D. Lubben, N. Dudney, and F. Hart, (1995). 5 Volt Plateau in $LiMn_2O_4$ Thin Films. J. Electrochem. Soc. **142**:l149-l151.

15. Kobrin, G., (1976). Corrosion by Microbiological Organisms in Natural Waters. Mat. Perform. **15**:38-43.

16. Stoecker, J., (1984). Guide for the Investigation of Microbiologically Induced Corrosion. Mat. Perform. **August**:48-55.

17. Dexter, S. C., (1995). Effect of Biofilms on Marine Corrosion of Passive Alloys, in: Bioextraction and Biodeterioration of Metals. Gaylarde, C., and H. Videla, eds., (Cambridge University Press, Cambridge, UK), pp. 129-168.

18. Pistorius, P. C. and G. T. Burstein, (1992). Growth of Corrosion Pits on Stainless Steel in Chloride Solution Containing Dilute Sulphate. Corr. Sci. **33**:1885-1897.

19. Uhlig, H. H., (1971). Corrosion and Corrosion Control. (John Wiley & Sons, New York, NY) 419 pp.

20. Stott, J., (1993). What Progress in the Understanding of Microbially Induced Corrosion Has Been Made in the Last 25 Years? A Personal Viewpoint. Corr. Sci. **35**:667-673.

21. Tatnall, R., (1981). Case Histories: Bacteria Induced Corrosion. Mat. Perform. **20**:41-48.

22. Miller, J. and A. Tiller, (1970). Microbial Corrosion of Buried and Immersed Metal, in: Microbial Aspects of Metallurgy. Miller, J. ed.,. (Elsevier, New York, NY), pp 61-106.

23. Tiller, A., and M. Corr, (1986). A Review of the European Research Effort on Microbial Corrosion Between 1950 and 1984, in: Biologically Induced Corrosion, Dexter, S. C. ed., (NACE, Houston, TX) pp. 8-29.

24. Jones, D.A., (1992). Principles and Prevention of Corrosion, (Macmillan Publishing Company, New York, NY) 568 pp.

25. Ghiorse, W. C., (1984). Biology of Iron- and Manganese-Depositing Bacteria. Ann. Rev. Microbiol. **38**:515-550.

26. Nealson, K., B. Tebo, and R. Rosson, (1988). Occurrence and Mechanisms of Microbial Oxidation of Manganese, in: Advances in Applied Microbiology, Vol. 33. Laskin, A. ed., (Academic Press, San Diego, CA), pp. 279-318.

27. Gounot, A.-M., (1994). Microbial Oxidation and Reduction of Manganese: Consequences in Groundwater and Applications. FEMS Microbiol. Rev. **14**:339-350.

28. Staley, J., (1989). Iron- and Manganese-Oxidizing and/or Depositing Bacteria. in: Bergey's Manual of Systematic Bacteriology, Vol. 3, Staley J. ed., (Williams and Wilkins, Baltimore, MD), pp. 1873-1874.

29. Schuett, C., L. J. Zelibor, and R. Colwell, (1986). Role of Bacterial Plasmids in Manganese Oxidation: Evidence for Plasmid-Encoded Heavy Metal Resistance. Geomicrobiol. J. **4**:389-406.

30. Moffett, J., (1994). A Radiotracer Study of Cerium and Manganese Uptake onto Suspended Particles in Chesapeake Bay. Geochim. Cosmochim. Acta **58**:695-703.

31. Cowen, J. P. and M. W. Silva, (1984). The Association of Iron and Manganese with Bacteria on Marine Macroparticulate Material. Science **224**:1340-1342.

32. Eashwar, M., S. Maruthamuthu, S. Palanichamy, and K. Balakrishnan, (1995). Sunlight Irradiation of Seawater Eliminates Ennoblement-Causation by Biofilms. Biofouling **8**:215-221.

33. Moffett, J., (1990). Microbially Mediated Cerium Oxidation in Seawater. Nature **345**:421-423.

34. Scotto, V., R. DiCintio, and G. Marcenaro, (1985). The Influence of Marine Aerobic Microbial Film on Stainless Steel Corrosion Behavior. Corr. Sci. **25**:185-194.

35. Motoda, S., Y. Suzuki, T. Shinohara, and S. Tsujikawa, (1990). The Effect of Marine Fouling on the Ennoblement of Electrode Potential for Stainless Steels. Corr. Sci. **31**:515-520.

36. Hamilton, W.A.,(1990). Sulphate-Reducing Bacteria and Their Role in Biocorrosion, in: Biofouling and Biocorrosion in Industrial Water Systems. Flemming, H-C, and G. Geesey eds., (Springer-Verlag, New York, NY), pp. 188-193

37. Sunda, W., and D. Kieber, (1994). Oxidation of Humic Substances by Manganese Oxides Yields Low-Molecular-Weight Organic Substrates. Nature **367**:62-64.

38. Characklis, W. G., and K.C. Marshall, (1990). Biofilms, (John Wiley & Sons, New York,

NY) 796 pp.

39. Brock, T., D. Smith, and M. Madigan, (1984). Biology of Microorganisms, (Prentice-Hall, Englewood Cliffs, NJ), 706 pp.

40. Burdige, D. and K. Nealson, (1986). Chemical and Microbiological Studies of Sulfide-Mediated Manganese Reduction. Geomicrobiol. J. **4**:361-387.

41. Aller, R. and P. Rude, (1988). Complete Oxidation of Solid Phase Sulfides by Manganese and Bacteria in Anoxic Marine Sediments. Geochim. Cosmochim. Acta **52**:751-765.

APPENDIX

Galvanostatic Pulse Circuit and Derivation of Equation 3.20

Equation 3.20 is based on a simple parallel combination of Faradaic resistance, R_p, and interfacial capacitance, C, as the model for the electrode-solution interface. Faradaic or polarization resistance is interpreted as the value of η_{act} / I_{app} near E_{corr}. This relationship is obtained for small values of $2.3\frac{\eta_{act}}{\beta}$ by making the substitutions:

$$e^{2.3\frac{\eta_{act}}{\beta_c}} = 1 + 2.3\frac{\eta_{act}}{\beta_c} \quad \text{and} \quad e^{-2.3\frac{\eta_{act}}{\beta_a}} = 1 - 2.3\frac{\eta_{act}}{\beta_a}$$

in equation 3.17 to give:

$$i_{meas} = i_{corr}\left(1 + 2.3\frac{\eta_{act}}{\beta_c}\right) - \left(1 - 2.3\frac{\eta_{act}}{\beta_a}\right) \tag{A.1}$$

Solving for $\frac{\eta_{act}}{i_{meas}}$ gives:

$$\frac{\eta_{act}}{i_{meas}} = R_p \qquad \text{with} \qquad R_p = \frac{\beta_a \beta_c}{2.3 i_{corr}(\beta_a + \beta_c)} \tag{A.2}$$

Figure A.1 depicts the circuit model for a constant current, I_{app}, applied to the electrode interface.

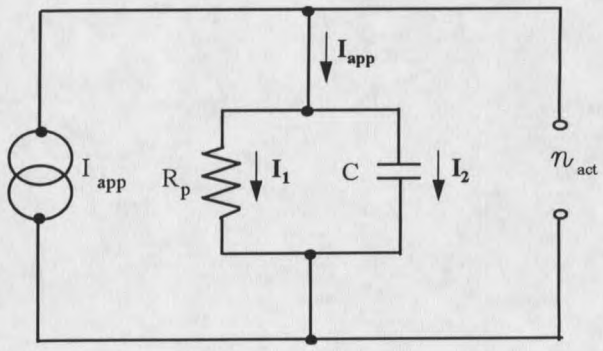

Figure A.1 Equivalent circuit for constant current applied to an electrode-solution interface

A physical interpretation of the circuit indicates that the applied current will charge the capacitance, increasing the voltage across the resistance until a steady-state potential is reached at which all applied current flows through the resistance. Analysis of the circuit allows the time dependent activation overvoltage, η_{act}, to be determined as a function of I_{app} and the component values R_p and C.

$$I_1 = \frac{\eta_{act}}{R_p}; \qquad I_2 = C\frac{d\eta_{act}}{dt}; \qquad I_{app} = I_1 + I_2;$$

$$I_{app} = \frac{\eta_{act}}{R_p} + C\frac{d\eta_{act}}{dt} \tag{A.3}$$

$$\frac{I_{app}}{C} = \frac{\eta_{act}}{R_pC} + \frac{d\eta_{act}}{dt} \tag{A.4}$$

apply the integrating factor, $e^{\frac{t}{R_pC}}$:

$$\frac{I_{app}}{C}e^{\frac{t}{R_pC}} = e^{\frac{t}{R_pC}}\left(\frac{\eta_{act}}{R_pC} + \frac{d\eta_{act}}{dt}\right) \tag{A.5}$$

taking the integral:

$$\frac{I_{app}}{C}\int e^{\frac{t}{R_pC}} = \int \frac{d}{dt}\left(\eta_{act}\, e^{\frac{t}{R_pC}}\right) \tag{A.6}$$

$$I_{app}R_p e^{\frac{t}{R_pC}} = \eta_{act}\, e^{\frac{t}{R_pC}} + D \tag{A.7}$$

dividing by $e^{\frac{t}{R_pC}}$:

$$I_{app}R_p = \eta_{act} + D\, e^{\frac{-t}{R_pC}} \tag{A.8}$$

at time zero, $\eta_{act} = 0$, so that $D = IR_p$

$$I_{app}R_p = \eta_{act} + I_{app}R_p\, e^{\frac{-t}{R_pC}} \tag{A.9}$$

$$\eta_{act} = I_{app}R_p\left(1 - e^{\frac{-t}{R_pC}}\right) \tag{A.10) \& (3.19}$$

η_{act} is recorded as a function of time and the constants R_p and C are obtained by non-linear regression of equation 3.20.

A circuit to supply I_{app} and measure η_{act} is shown in figure A.2. η_{act} corresponds to the change in interfacial potential difference between the working and reference electrodes caused by application of I_{app} (assuming negligible uncompensated solution resistance). The working electrode is at virtual ground, consequently the difference between the reference electrode potential at time t, and the reference electrode potential at time zero is numerically equal to η_{act}. This difference is obtained by adjusting the output of the x100 difference amplifier,

ADC524C, to zero before applying I_{app}, then recording the amplified signal as a cathodic value of I_{app} forces the potential measured by the reference electrode to become more positive. I_{app} was chosen to keep η_{act} below 10 mV, thereby assuring that the steady-state value of R_p (= $\frac{\eta_{act}}{I_{app}}$) is independent of η_{act}. Duration of the applied current was controlled either manually through the debounced switch, I_{hold}, or electronically through the 4538 monostable. The monostable was used to apply constant current for accurately measured times of the order of a few milliseconds, allowing capacitance to be determined by the relation $C = q / \eta_{act}$. (q is the charge generated by applying a constant current for a known duration). This approach was generally less reproducible than the galvanostatic technique and was not used. To make a measurement by the galvanostatic technique, logic low generated by I_{hold} is inverted to drive comparator 3 to the positive rail. This turns on the bidirectional VMOS switch and allows voltage follower 4, connected through either 1 kΩ or 1 MΩ, to source current to the summing amplifier 1A. All current applied to the summing point flows through the working electrode-counter electrode feedback path, producing the activation overvoltage, η_{act}, at the working electrode. Use of the source connected VMOS switch allows either anodic or cathodic current to be applied. Current source 2 was used as a separate polarizing current to polarize the working electrode to a preset potential before applying I_{app}. This allowed capacitance to be measured at various electrode potentials to determine if potential alone influenced capacitance.

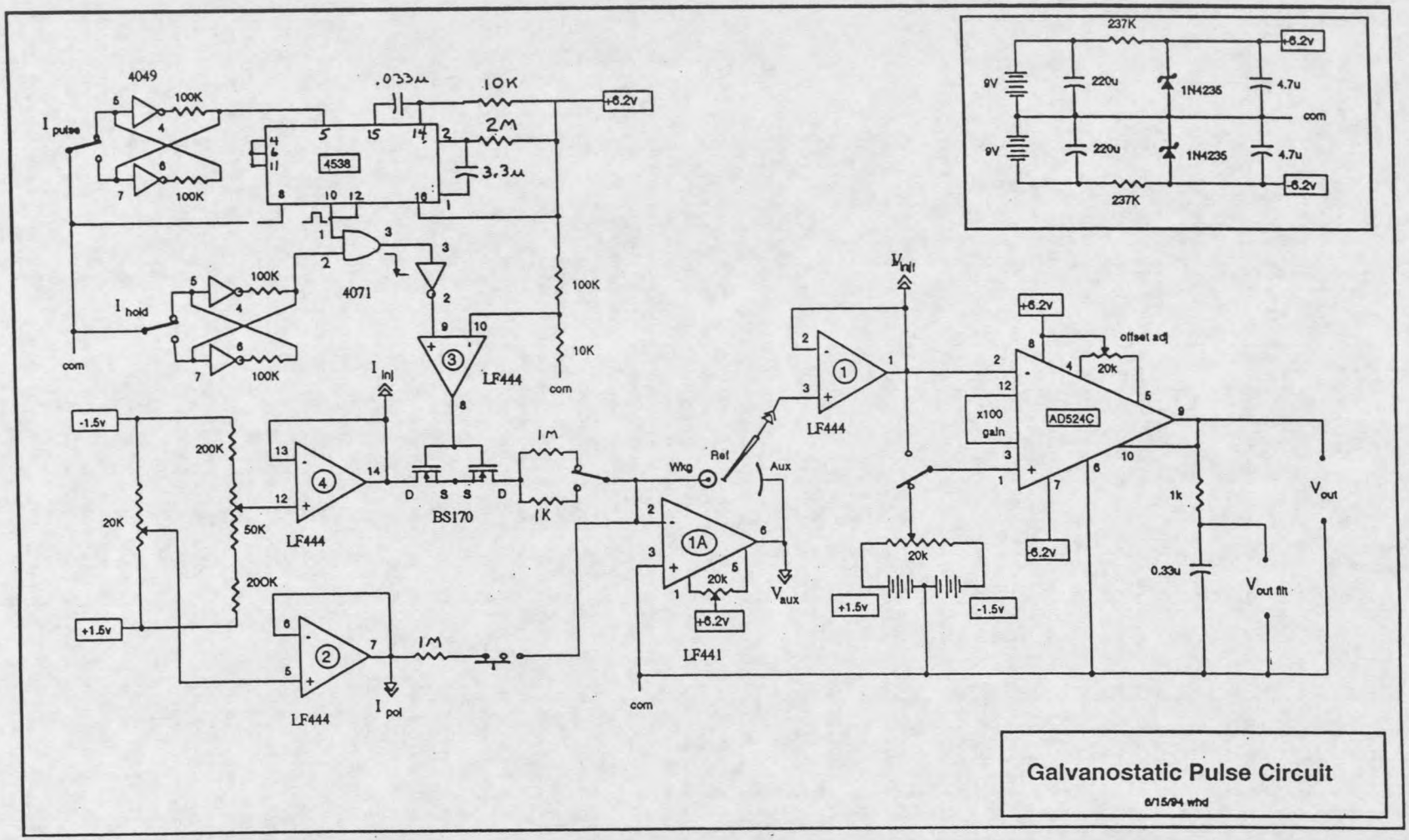

Figure A.2 Galvanostatic circuit used to assess capacitance according to equation 3.20